ESL-TR-88-76

CENTRIFUGE MODELING OF PROJECTILE PENETRATION IN GRANULAR SOILS

R.J. FRAGASZY, T.A. TAYLOR

WASHINGTON STATE UNIVERSITY
DEPARTMENT OF CIVIL AND
ENVIRONMENTAL ENGINEERING
PULLMAN WA 66164-2910

APRIL 1989

FINAL REPORT

JULY 1986 — OCTOBER 1988

ENGINEERING & SERVICES LABORATORY
AIR FORCE ENGINEERING & SERVICES CENTER
TYNDALL AIR FORCE BASE, FLORIDA 32403

NOTICE

PLEASE DO NOT REQUEST COPIES OF THIS REPORT FROM HQ AFESC/RD (ENGINEERING AND SERVICES LABORATORY). ADDITIONAL COPIES MAY BE PURCHASED FROM:

NATIONAL TECHNICAL INFORMATION SERVICE
5285 PORT ROYAL ROAD
SPRINGFIELD, VIRGINIA 22161

FEDERAL GOVERNMENT AGENCIES AND THEIR CONTRACTORS REGISTERED WITH DEFENSE TECHNICAL INFORMATION CENTER SHOULD DIRECT REQUESTS FOR COPIES OF THIS REPORT TO:

DEFENSE TECHNICAL INFORMATION CENTER
CAMERON STATION
ALEXANDRIA, VIRGINIA 22314

UNCLASSIFIED
SECURITY CLASSIFICATION OF THIS PAGE

REPORT DOCUMENTATION PAGE

Form Approved
OMB No. 0704-0188

1a. REPORT SECURITY CLASSIFICATION UNCLASSIFIED	1b. RESTRICTIVE MARKINGS
2a. SECURITY CLASSIFICATION AUTHORITY	3. DISTRIBUTION / AVAILABILITY OF REPORT Approved for public release Distribution unlimited
2b. DECLASSIFICATION / DOWNGRADING SCHEDULE	
4. PERFORMING ORGANIZATION REPORT NUMBER(S)	5. MONITORING ORGANIZATION REPORT NUMBER(S) ESL-TR-88-76
6a. NAME OF PERFORMING ORGANIZATION Washington State University Dept. of Civil & Envir. Engrg. 6b. OFFICE SYMBOL (If applicable)	7a. NAME OF MONITORING ORGANIZATION Air Force Engineering and Services Center
6c. ADDRESS (City, State, and ZIP Code) Pullman, WA 99164-2910	7b. ADDRESS (City, State, and ZIP Code) HQ AFESC/RDCS Tyndall AFB, FL 32403-6001
8a. NAME OF FUNDING / SPONSORING ORGANIZATION 8b. OFFICE SYMBOL (If applicable)	9. PROCUREMENT INSTRUMENT IDENTIFICATION NUMBER F08635-86-K-0279
8c. ADDRESS (City, State, and ZIP Code)	10. SOURCE OF FUNDING NUMBERS PROGRAM ELEMENT NO. 6.2 / PROJECT NO. 2673 / TASK NO 0065 / WORK UNIT ACCESSION NO N/A

11. TITLE (Include Security Classification)
Centrifuge Modeling of Projectile Penetration in Granular Soils

12. PERSONAL AUTHOR(S)
Fragaszy, Richard J. and Taylor, Teresa A.

13a. TYPE OF REPORT	13b. TIME COVERED	14. DATE OF REPORT (Year, Month, Day)	15. PAGE COUNT
Final	FROM 860701 TO 881001	APRIL 1989	141

16. SUPPLEMENTARY NOTATION
Availability of this report is specified on reverse of front cover.

17. COSATI CODES			18. SUBJECT TERMS (Continue on reverse if necessary and identify by block number)
FIELD	GROUP	SUB-GROUP	Sand, Dimensional Analysis, Pluviation, Projectiles, Scale Modeling, Penetration, Centrifuge

19. ABSTRACT (Continue on reverse if necessary and identify by block number)

Investigations of the projectile penetration phenomenon in granular soils have been impeded by the difficulty in adequately quantifying and characterizing soil targets, and by the inability to directly scale results of 1-g penetration tests to full-scale conditions. The former is largely due to the failure to adequately prepare and quantify laboratory test samples, and the inherent limitations involved with testing and quantifying in situ soils. The latter is associated with an incomplete understanding of the soil parameters involved in the projectile penetration event.

A series of laboratory tests on dry sands was conducted to assess the influence of confining pressure on projectile penetration depth, using a centrifuge to simulate full-scale stress levels in the soil targets. Projectiles were fired from a Thompson Contender pistol at impact velocities of approximately 305 meters/second into the rotating soil samples. Corresponding tests were conducted under 1-g conditions. A limited number of centrifuge and 1-g tests were conducted on moist samples. Most tests involved vertical impact angles; a few tests were conducted at other

20. DISTRIBUTION / AVAILABILITY OF ABSTRACT ☒ UNCLASSIFIED/UNLIMITED ☐ SAME AS RPT ☐ DTIC USERS	21. ABSTRACT SECURITY CLASSIFICATION UNCLASSIFIED
22a. NAME OF RESPONSIBLE INDIVIDUAL Steven T. Kuennen, 1Lt, USAF	22b. TELEPHONE (Include Area Code) (904) 283-4932 22c. OFFICE SYMBOL HQ AFESC/RDCM

DD Form 1473, JUN 86 — Previous editions are obsolete. — SECURITY CLASSIFICATION OF THIS PAGE
UNCLASSIFIED

19. ABSTRACT (continued)

than normal impact angles to illustrate the flexibility of the firing system design.

The targets were prepared using a pluviation technique that resulted in uniform, reproducible samples of known density; this sample preparation technique contributed to the reproducibility of penetration test results that was observed in the test program. Significant differences in projectile penetration depths were obtained for different soils and for the same soils prepared at different densities.

The penetration depths obtained in the test samples subjected to accelerated g-levels were compared to those obtained in corresponding 1-g tests. The test results indicate a gravity-dependence for the penetration event in granular soils. In addition, the magnitudes of penetration depths predicted by the centrifuge test results compare well to results from full-scale field tests. Thus, the centrifuge testing technique appears well-suited to further investigation of the penetration phenomenon in granular soils.

PREFACE

This report was prepared by Washington State University, Department of Civil and Environmental Engineering, Pullman, Washington, 99164-2910. Work was accomplished under Contract No. FO8635-86-K-0279, sponsored by Headquarters, Air Force Engineering and Services Center, Engineering and Services Laboratory (AFESC/RD), Tyndall Air Force Base, Florida.

Principal contributors to the report were: Dr. Richard J. Fragaszy, Associate Professor, Washington State University; and Dr. Teresa Taylor, Assistant Professor, University of Missouri-Columbia/Kansas City (formerly graduate student, Washington State University).

Work summarized in this report was performed between 1 July 1986 and 1 October 1988. Captain Paul L. Rosengren, Jr. and Lt. Steven T. Kuennen were AFESC/RDCS project officers.

This report has been reviewed by the Public Affairs Office (PA) and is releasable to the National Technical Information Service (NTIS). At NTIS, it will be available to the general public, including foreign nationals.

STEVEN T. KUENNEN, 1Lt., USAF
Project Officer

ROBERT J. MAJKA, Lt. Col., USAF
Chief, Engineering Research Division

WILLIAM S. STRICKLAND
Chief, Facilities Systems and Analysis Branch

LAWRENCE D. HOKANSON, Colonel, USAF
Director, Engineering and Services Laboratory

Accession For	
NTIS GRA&I	☒
DTIC TAB	☐
Unannounced	☐
Justification	
By	
Distribution/	
Availability Codes	
Dist	Avail and/or Special
A-1	

(The reverse of this page is blank)

TABLE OF CONTENTS

Page

APPENDIX

LIST OF FIGURES

LIST OF TABLES

LIST OF SYMBOLS

M	mass
v	velocity
t	time
c_{1-3}	constant
P	penetration depth
W	projectile weight
A	projectile area
K	soil constant (after Petry)
S	soil constant (after Young)
K	mass scaling factor
N	nose shape factor
g	acceleration due to gravity
V	velocity
δ_{lp}	locked plastic density
R	radius
δ_t	target density
Y	target yield strength
E	Young's modulus
E_t	strain-hardening modulus
e_i	elastic volumetric strain
v'	vertical acceleration
δ	mass density
C_D	drag coefficient
μ	dynamic viscosity
d	projectile diameter
N_{1-2}	dimensionless shape factors
σ_f	flow stress
M^*	total effective mass
z	embedment distance
W_b	buoyant weight
F_D	driving force
S_u	undrained shear strength
S_e	soil constant (after True)
N_c	bearing capacity factor
A_f	frontal area of projectile
r_a	adhesion reduction factor
S_t	soil sensitivity
A_s	side area of projectile
mm	millimeter
m	meter
s	second
cm	centimeter
kg	kilogram
Mg	megagram
a	centripetal acceleration
r	radial distance
a_t	total acceleration
ω	angular velocity of rotation

α_v vertical stress
Δ delta
r_s radial distance to soil surface
a_c coriolis acceleration
F_c coriolis force
C_v coefficient of consolidation
τ shear stress
γ unit weight
n modeling scale factor
L length
T time
F force
d penetration depth
β impact angle
s caliber
l length
r radius
α nose angle
S_{ult} ultimate stress of projectile
δ_p projectile density
π_{1-14} dimensionless parameters
D_{50} median grain size
D_r relative density
e void ratio
σ ultimate soil stress
D_{10} grain diameter, 10% passing
C_u coefficient of uniformity
C_c coefficient of curvature
r correlation coefficient
M projectile mass
F,S,H geometric distances, pluviator

(The reverse of this page is blank.)

SECTION I

INTRODUCTION

A. OBJECTIVE

The primary objective of this research is to determine the usefulness and validity of centrifuge modeling for investigation of projectile penetration in granular soils. In spite of its potential contributions to penetration research, centrifuge modeling has not been used to any significant extent for investigation of this phenomenon. This first objective requires the development of a technique to deliver projectiles at the desired velocity and impact angle to a rotating sample.

A second objective of the research is to generate depth of penetration data for vertical impact in soil with known engineering properties, standard classification, and controlled moisture conditions. This second objective includes developing a sample preparation method that results in reproducible test samples of appropriate size for centrifuge use, as well as development of techniques to saturate centrifuge test samples. Finally, the third major objective of the research is to compare the centrifuge test results to existing large-scale penetration data and to penetration depth predictions determined using existing penetration prediction equations.

B. BACKGROUND

The study of projectile penetration has a long history. The military has been interested in penetration research for active applications such as design of projectiles to maximize penetration into different materials, and for passive applications such as bunker design and spacing of earth-covered shelters to protect against bombs and artillery shells (References 1, 2 and 3). Industrial interest in projectile penetration has generally lagged behind military interest; however, recently the phenomenon of projectile penetration is being investigated for a range of non-military applications including remote soil exploration, seismic monitoring and surveying (Reference 4). Other land-based applications include soil exploration from the air and investigation of the properties of large earth structures such as dams (Reference 5). Projectile penetration is also assuming a significant role in the advancement of marine technology for such diverse uses as sea-ice thickness and water depth measurements, disposal of radioactive wastes in deep ocean sediments (Reference 4), estimating embedment depths of

salvageable objects, designing direct-embedment anchors and deep piles in seafloor soils, and improving coring equipment (Reference 5). Finally, the use of projectile penetration, in the form of subsurface probes, is even being investigated as a method for exploration of extraterrestrial geology (Reference 4).

Most penetration research to date has taken one of three major forms: (1) empirical predictions based on large-scale experiments; (2) depth predictions from standard equations of motion in which unknown coefficients are obtained experimentally using an instrumented projectile; and, (3) motion and depth predictions from constitutive equations for the target material. In addition to these major approaches, attempts at modeling the phenomenon using two dimensional finite difference codes or multidimensional wave codes have been made (References 7 and 8).

One of the major difficulties involved with penetration research is the inherent mathematical complexity associated with defining constitutive equations describing the target material, and with developing solutions to conservation equations describing projectile motion. This difficulty is particularly apparent when the target medium is soil. Attempts have been made to address this difficulty by developing empirical or semiempirical equations based on experimental data, or by evaluating unknown coefficients in standard equations of motion using experimentally obtained values (Reference 9). A drawback to this approach is that empirical correlations must be established for all soil types of interest (Reference 10).

Both full-scale field tests and 1-g laboratory tests have provided experimental data used in both of these approaches. However, a considerable amount of scatter exists in this experimental data base. Two of the major contributors to this scatter are: (1) lack of sample quantification, and (2) scale differences.

Lack of sample quantification is evident in the very general, qualitative soil descriptions that are provided for use in conjunction with various depth prediction equations (References 11, 12, and 3). These descriptions are used to determine what is frequently termed a soil penetrability index, which is recognized as one of the more significant parameters contributing to the magnitude of penetration obtained by various projectiles (Reference 9). Such indices, however, are not based on standard engineering properties or soil classifications, which makes an appropriate selection difficult, and also significantly limits the accuracy with which

existing penetration equations can be used to predict soil properties in applications such as remote soil exploration. Failure to adequately quantify soil characteristics in penetration experiments has been largely due to the inherent inability to define and control target material properties in full-scale tests, the limited range of test sites employed in full-scale tests, and the lack of understanding of soil behavior and consequent inadequate sample preparation and/or definition in the lab.

Scale differences between 1-g laboratory tests and full-scale field tests have been recognized by many researchers (References 13, 8, 14, and 15), yet comparatively few full-scale penetration tests have been conducted, primarily due to the large costs involved. A significant example of a scaling difference that appears important with respect to the problem of penetration into granular soils is the self-weight dependency of stress, and therefore strength distribution, in the soil. Although there is considerable evidence that this factor should be taken into account, some investigators have attempted to describe the penetration phenomenon on the basis of 1-g laboratory test data (References 16, 17, and 18). Thus, some of the scatter in the existing empirical data base appears to be related to attempts to directly compare 1-g test results to field conditions. Further contributing to the scatter in experimental penetration depth data are 1-g test results obtained by firing projectiles horizontally into soil (or by "firing" a target material into a projectile, termed reverse ballistics), again with little regard for consistency in potentially important test parameters (References 17, 19, 20, and 7).

C. APPROACH

Centrifuge modeling is a laboratory technique that lends itself to study of projectile penetration for two major reasons. First, as a laboratory technique it is less expensive than full-scale tests, and it is possible to readily quantify soil sample characteristics. Centrifuge testing clearly provides potential for development of a large experimental data pool based on specific, quantifiable soil properties. Second, stress levels in a prototype (full-scale or otherwise) may be duplicated in a model by the radial acceleration field in a centrifuge, thus eliminating a significant scaling difficulty involved in applying 1-g test results to the field.

Although it is not possible with centrifuge testing to achieve exact similitude between model and prototype, the range of test validity over which nonsimilar parameters are not significant can be identified by a testing technique called modeling-of-models. This technique can be used to determine the influence of boundary conditions, such as soil container size, as well as address important deviations from exact prototype-model similitude, for example grain size distribution differences. The technique involves testing a given prototype using scaled models at a number of different g-levels. Where similar test results are obtained at different g-levels, nonscaled parameters, such as grain size or sample container size, may be considered insignificant over the range of models tested.

This report is organized in the following manner. Section II presents a literature review of former work on projectile penetration. The detail of this review is necessitated by the lack of published work on the subject; the majority of the information presented has been obtained from reports with limited circulation rather than journal or conference publications. Section III presents a description of the centrifuge modeling technique and the results of a dimensional analysis used to design the centrifuge testing program. Section IV presents a description of the soils used in the study and the method of sample preparation. A description of the facilities and equipment used in the research is presented in Section V, along with a description of the test procedures. Test results, conclusions and recommendation are presented in Section VI. All test data and details of the equipment design are presented in six appendices.

SECTION II

PROJECTILE PENETRATION

A. BACKGROUND

1. Description of Phenomenon

Projectile penetration is defined as the entry of a moving object into some target material, where the object may be a projectile specifically designed for penetration, or one not designed for penetration. Penetration may involve: ricochet, where the traveling projectile is deflected from the target surface; perforation, where the projectile travels through and exits the target material; or embedment, where the projectile is stopped by and within the target material. The target material is described by its composition and is frequently classified by its thickness. Semi-inifinite targets, such as soil deposits, are those for which boundary effects do not influence the penetration process. Boundary effects play an increasingly important role for targets of thick, intermediate or thin classifications.

Ballistics researchers have variously classified the penetration phenomenon by the impact angle of incidence, the geometry and material properties of the projectile, the geometry and properties of the target material, and the initial velocity of the projectile (Reference 2). Angle of incidence for projectile impact can range from vertical to nearly horizontal. Projectile geometries (frequently described by length, diameter, nose shape and material composition) are similarly variable, but can generally be quantified with reasonable accuracy. Projectiles can be composite and can include such main materials as steel, brass, aluminum and tungsten, along with various synthetics in the form of coatings, nose tips, or fins.

Considerable information is available on the relative penetration depth as a function of projectile geometry and nose shape. Mumma and Randall (Reference 18) conducted an experimental test series to study projectile shape and design using seven geometrically different projectiles fired into an earth bank. They determined stability of trajectory for different projectile body shapes, optimum length to diameter (L/D) ratios, and nose shape-projectile body combinations contributing to greatest penetration depths (ogive-cylindrical). They

also determined that, for relatively small L/D ratios, fins do not appear to be necessary to ensure a straight trajectory within the target medium. Yankelevsky and Gluck (Reference 21) used analytical techniques to conclude that projectile nose shape has an increasingly greater effect as impact velocity increases, suggesting that penetration calculations in which this geometric parameter is represented by a single constant term are not valid for all velocities. Subsequent work (Reference 22) suggests that the optimal shape for earth penetration is a function of velocity, deceleration and target material.

The properties of target materials such as soil and rock, in contrast to relatively homogeneous materials such as steel and concrete, are not as easily quantified as projectile characteristics. This fact is particularly evident in reviewing the difficulties penetration researchers have encountered with developing appropriate soil models, either by experimental, analytical or numerical techniques. A parametric study performed by Wagner, Fulton and Kreyenhagen (Reference 23) using a two-dimensional finite difference code for projectile penetration indicated that factor of two changes in basic target properties (defined for this study in terms of parameters such as bulk modulus, friction, density, yield surface slope and unconfined compressive strength), led to changes of 5 to 50 percent in projectile decelerations. From this study, the most critical target properties for soils were determined to be the strength and frictional characteristics. Their study further concluded that the impact velocity, target medium, velocity regime and penetrator shape were the most significant variables involved in projectile penetration.

A two-dimensional finite-difference code was also used by Chabai, et al. (Reference 8) to systematically study the influence of different material properties on projectile motion and response during penetration. Their study concluded that the soil properties that appear to most greatly affect the penetration process are the shear strength, compressibility, friction coefficient and density.

In describing a penetration event, definition of the velocity regime is extremely important because the character of the penetration phenomenon varies significantly among different velocity ranges. The freefall range (0-25 meters/second) is defined as the range below the terminal velocity of free falling objects. Simple drop experiments are used to test penetration in this velocity range. Penetration within the subordnance range (25-500 meters/second) can

be tested using equipment such as pneumatic guns. Conventional guns, rocket launch methods and recoilless powder guns (Reference 8) are used to test projectile penetration in the higher nominal ordnance velocity range (500-1300 meters/second). The ultraordnance velocity range (1300-3000 meters/second) is associated with penetrators such as warhead fragments. The highest velocity range is the hypervelocity range (above 3000 meters/second), typified by penetrators such as meteorites and some shaped charges. Gas guns can fire projectiles at velocities in the hypervelocity region (Reference 2). The different elements involved in describing projectile penetration within the different velocity realms are discussed in more detail in Section III, with particular emphasis on the lower velocity regimes applicable to this research effort.

The variables involved in the penetration event are sometimes described using a ballistic phase diagram, or nomogram, which represents interrelationships of significant parameters in the penetration process. Ballistic phase diagrams can be experimentally determined for specific projectiles and targets; they are used frequently for design and behavioral studies (Reference 2). Parameters that can be used to develop the phase diagram include the final state of the projectile (described by such terms as intact, deformed or broken) and the projectile motion (often described by ricochet, embedment or perforation behavior). Other potentially useful parameters include ratios of the geometries of target and projectile. Ballistic limit curves define boundaries on the phase diagram between complete and partial penetration; thus, a ballistic phase diagram determined for a semi-infinite target medium, such as an in situ soil, will not have ballistic limit curves.

2. Historical Approach to Investigation

Experimental, analytical and numerical techniques have been used to understand and quantify the penetration phenomenon. In the 18th and 19th centuries, Robins (Reference 24), Euler (Reference 25), Poncelet (Reference 26), and Resal (Reference 27) expressed the resistive force to penetration as a polynomial velocity equation obtained from integration of Newton's basic equation of motion. All of the various solutions proposed by these investigators were special cases of the following equation:

$$M\,(dv/dt) = c_1 + c_2 v + c_3 v^2 \qquad (1)$$

Attempts to evaluate the constants in the above equation led to development of a number of specific equations, one of the more well known being that developed by Petry (Reference 28):

$$P = (W/A)\, k \log [\, 1 + (v^2/215{,}000) \,] \qquad (2)$$

In this equation, developed in English units, P is the penetration depth (feet), W is the projectile weight (pounds), A is the projectile cross-sectional area (in^2), v is the projectile velocity (feet/second), and the constant K (in^2/pound) is a term used to describe the "penetrability" of a soil. Very general values suggested for K ranged from 5.3 for a sandy soil, to 6.95 for a soil containing vegetation, to 10.6 for a clay soil.

Experimental attempts to evaluate the constants and refine these earliest penetration equations were continued by a number of investigators, such as Allen, Mayfield, and Morrison (References 29 and 30), Hakala (Reference 31), and Wang (Reference 32). These efforts, and those of most other investigators during this time period, were restricted to the nominal ordinance or lower velocity regimes.

The 1970s brought a number of significant advances in penetration research, including development of what continues to be one of the most widely used empirical relationships for predicting penetration depth, Young's Equation. The results of over 500 large-scale penetration tests were analyzed by Young (References 11, 33, 34, 35 and 36) in its development. Penetration depth is expressed as a function of the projectile geometry, impact velocity and mass, and of the target material, which is decribed by a single constant term, S. The relationship of these S values to the physical properties of the target material is unknown (Reference 37); consequently, the lack of certainty involved in both the establishment and the selection of the appropriate S value for a given target material is generally recognized as the most significant drawback to use of this empirical equation (References 33, 10 and 38). With accurate selection of the S value, the equation is claimed to provide penetration depth predictions within +/- 20 percent of actual depths obtained in full-scale tests (References 37 and 33). A pretest depth prediction reported by Hadala (Reference 39) found a 27 percent error in the maximum penetration prediction. True (Reference 10) determined that Young's equation typically underpredicted for soft soils, based on his investigations for saturated silts and clays. True attributed this apparent discrepancy to the fact that most of the penetration test data on which Young's

equation was based were collected from tests conducted in relatively hard soils and rocks.

Young's best-fit empirical relationship has been expressed both in the form of a nomogram, or ballistic-phase diagram (References 37 and 5), and in equation form. In equation form, the relationship for velocities less than 61 m/s is:

$$P = 2KSN\,(W/A)^{0.5}\,\ln(1 + 2V^2 \times 10^{-4}) \qquad (3)$$

in which

P = penetration depth (cm)
K = mass scaling factor (dimensionless)
S = soil constant (dimensionless)
N = nose shape factor (dimensionless)
W = projectile mass (kg)
A = projectile cross-sectional area (m^2)
V = velocity (m/s)

For velocities greater than or equal to 61 meters/second, the equation is:

$$P = 0.0117KSN\,(W/A)^{0.5}\,(V - 30.5) \qquad (4)$$

Values for the dimensionless terms were determined by replicating tests holding all parameters constant except the dimensionless term of interest. The mass scaling factor was introduced into the equations for projectiles with masses less than 27 kilograms to eliminate observed deviations for small projectiles from the penetration depths otherwise predicted by the empirical equation. Although the difficulty in scaling small projectiles was recognized and tentatively attributed to a mass scale effect, a theoretical basis for such an effect was not determined (Reference 33).

Values suggested by Young for the soil constant, S, are listed in Appendix A. According to Young (Reference 33) and Hadala (Reference 39), appropriate selection of this constant requires experience in earth penetration. This limitation to the use of Young's equation was also pointed out by Aitken, Swinzow and Farrell (Reference 38), along with the disadvantages that the equation requires conducting penetration tests on all target materials of interest to establish proper S values, and that the equation also requires determination of a mass scaling factor. Recommendations provided by Young for the dimensionless mass scaling factor, K, and values for the nose shape factor (alternatively, nose performance coefficient), N, are presented in Appendix A.

Although originally developed for a soil site that could be approximated as a single layer, a method for applying the empirical equation to layered targets was developed by Young (Reference 35). Hadala (Reference 39) presented an example of this method applied to a full-scale penetration test in Canadian glacial lake deposits.

A theory developed by Bishop, Hill, and Mott (Reference 40) and by Goodier (Reference 41), received renewed attention by Hanagud and Ross (Reference 42) and Bernard and Hanagud (Reference 43). This theory, termed the spherical cavity expansion theory (CET), involves solving for the pressure required to cause a spherical cavity to expand at a specified rate. The constitutive model for the target is that of an elastic work-hardening plastic, incompressible material (except at initiation of loading and along the plastic front), with a shear strength independent of the stress level. This last assumption, although reasonable for saturated, cohesive soils, is recognized as nonrealistic for granular materials (Reference 39). The target compressibility is approximated by a "locked plastic density", or "locked strain." These parameters are defined by a strain level at which the stress/strain curve becomes horizontal. The general solution involves both static and inertial resistance terms. Assumptions involved in applying the general solution to the projectile penetration problem include: a rigid and axisymmetric projectile, impact normal to the target surface, and action of only normal stresses on the projectile. Ross and Hanagud (Reference 44) present the CET-based equation for penetration as follows:

$$P = [(3W/4Ag_{\delta lp}\lambda_2) + (\lambda_1 R/2\lambda_2)] \ln [\, 1 + (2\lambda_2\delta_{lp}v^2/3\lambda_3) \,] \qquad (5)$$

The terms are defined in English units:

P = maximum penetration depth (ft)

W = projectile weight (lbs)

A = initial projected area of projectile (ft^2)

g = acceleration of gravity (ft/s^2)

δ_{lp} = locked plastic target density ($slugs/ft^3$)

R = projectile radius

$\lambda_1 = 1 - \lambda_4^{1/3}$

$\lambda_2 = 3/2 - (1 - \alpha_p)\lambda_4^{1/3} + 1/2\lambda_4^{4/3}$

$\lambda_3 = 4/9E(1-e^{-3\lambda_6}) - 2/3Y\ln\lambda_4 + 2/27\pi^2E_1 - 4/9E_l\lambda_5$

$\lambda_4 = 1 - \delta_i/\delta_{lp}(\exp(-3\lambda_6))$

$\alpha_p = 1 - \delta_i/\delta_{ip}$

$\lambda_5 = \sum_{n=1}^{\infty}(\lambda_4^n/n)$

v = impact velocity (ft/s)

$\lambda_6 = Y/2E - e_i/3$

δ_i = initial target density (slugs/ft^3)

Y = target yield strength (lb/ft^2)

E = Young's modulus for target, locked elastic region (lb/ft^2)

E_t = strain-hardening modulus for target, locked plastic region (lb/ft^2)

e_i = volumetric strain for target, elastic region

Bernard and Hanagud (Reference 43) reported maximum displacement predictions using the above equation within 25 percent of actual test measurements. According to Hadala (Reference 39), however, the equation produces more accurate predictions for rock penetration than for soil penetration.

The cylindrical CET theory employs the same consitutive model for the target material as the spherical CET theory, but instead of a spherical cavity, an infinitely long cavity is assumed to be expanding away from the penetrating projectile. The equation is similar in form to Equation (5) above, and is presented in detail by Norwood (Reference 45). One of the drawbacks to this theory is the less realistic description of penetrator nose shape that is employed in derivation of the equation.

In contrast to Young's empirical quantification of the target material, both of the CET theories attempt to express the characteristics of the target material in terms of measurable properties. As previously noted, however, the constitutive models utilized in the theories are not appropriate for granular soils. In addition, the equations are extremely cumbersome and do not readily lend themselves to simple hand solutions. The complex definitions of the input parameters provide considerable lattitude for error in appropriate determination of the parameters. This difficulty is augmented by the requirement that unconfined compression tests be properly run on representative undisturbed samples of the target material to obtain the input parameters. Even if this were easily accomplished, a very large data base would be needed to facilitate general use

of the equations for inaccessible target sites, where in situ samples could not readily be acquired for testing. These facts offset the advantage to the methods that no empirical constant is required. Aitken, Swinzow and Farrell (Reference 38) include, as a disadvantage, the assumption that target yield strength is independent of velocity and penetration depth, the inability of the methods to account for non-rigid impact, and the inability of the methods to account for different nose shapes. In spite of the comparative complexity of the CET equations, their use would appear to be justified if the predictions obtained from the equations provided significantly better results than other, more straightforward techniques. This does not appear to be the case (References 17, 39, 46, and 12).

Allen (Reference 47) presented a "viscoplastic" force law penetration equation:

$$-mv_a = (\delta AC_D/2)\, v^2 + 6\pi\mu\, (d/2)\, N_1 v + AN_2\sigma_f \qquad (6)$$

where

v_a = vertical acceleration
δ = mass density
A = projected frontal area of projectile
C_D = drag coefficient
μ = dynamic viscosity
d = projectile diameter
N_1 = dimensionless shape factor
N_2 = dimensionless shape factor
σ_f = flow stress of medium

For a workable solution to the penetration problem, the drag coefficient is ignored and the flow stress term is defined in terms of the maximum principle stress difference at a mean normal stress equal to a stagnation pressure defined by:

$$P_{stagnation} = [\, 1 + (6/R)\,]\, \delta v^2/2 \qquad (7)$$

where R is the Reynold's number, based on the projectile diameter. The constants N_1 and N_2 employed in the equation are taken from the nose shape coefficients used for Young's equation, the viscosity term is estimated from Young's S values. With the shared input values, the major difference between the two equations is that Allen's viscoplastic force law expresses penetration

depth as proportional to the projectile weight, while in Young's equation penetration depth is proportional to the square root of the projectile weight.

A differential area force law (DAFL) developed in 1974 by AVCO Corporation, Massachusetts and described by Henderson (Reference 20), assumes the local and normal shear stresses at a point on the surface of a penetrating projectile are functions of the instantaneous velocity of the projectile. Although still requiring computer solution, the method is far less complex and therefore requires less expenditure of computer resources than more complicated finite difference wave propagation code techniques (Reference 39). The DAFL approach essentially approximates resistance by the sum of the dynamic compressibility of the target media, the static penetration resistance, the resistance to flow and the surface effects. One of the difficulties with this approach is that there is no theoretical basis for combining the separate terms. In addition, nine separate target descriptors must be calculated or estimated; of these, only two relate to basic engineering properties. It should be noted, however, that the DAFL approach includes provisions for nonvertical impact angles, unlike many of the other penetration prediction techniques.

True (Reference 6) developed a penetration depth prediction equation specifically applicable to seafloor soils, based on the early penetration resistance force equation derived by Poncelet (Reference 26). True's two-part equation is:

$$M^* v\,(dv/dz) = W_b + F_D - F(v,z) \tag{8}$$

$$F(v,z) = S_u(z)\, S_{\dot{e}}\, [\, N_c A_f + (r/S_t) A_s\,] + 1/2 \delta_t C_D A_f v^2 \tag{9}$$

The component terms are:

M^* = total effective mass of penetrator
v = penetrator velocity
z = embedment distance
W_b = buoyant weight
F_D = driving force
S_u = undrained shear strength of soil
$S_{\dot{e}}$ = soil constant (3.7 for silt test soil)
N_c = bearing capacity factor
A_f = frontal area of penetrator
r_a = adhesion reduction factor
S_t = sensitivity of soil

A_s = side area of penetrator

δ_t = density of soil target

C_D = drag coefficient

An incremental form of the above equation can be used for hand computations.

Karnes, et al. (Reference 48) addressed the problem of subseabed disposal of radioactive wastes using penetrator emplacement, by comparing predicted penetration depths by Young's equation and by True's equation. Predicted values were contrasted to measured values for a series of large-scale penetration tests into nearly saturated seabed sediments (Reference 36). This comparison indicated an overprediction of actual penetration depths using True's model. The comparison is not particularly valid because the tests were performed by firing projectiles directly into sediments, without an overlying layer of water; thus, the upper portion of the sediments may not have been completely saturated. As pointed out by Karnes, et al. (Reference 48), however, the presence of water above the sediments would reduce the actual penetration depth by increasing the effective drag on the projectile.

With the advent of more powerful computers, detailed one-dimensional analytical models (Reference 49) and two-dimensional finite difference wavecodes (References 50, 51, 52, 53, 54, 55, 56, 57, 58, and 59) have been employed by numerous penetration researchers. Although a detailed review is beyond the scope of this research, one of the clear advantages to these techniques is the ability to systematically assess the relative influence of individual projectile and target properties. Such an assessment requires, however, a carefully controlled data base for projectile and soil properties, with the latter being the most difficult to achieve. This was recognized by Chaibai, et al. (Reference 8), who stated:

> "Unfortunately, no systematic set of penetration experiments has been performed for a soil target whose properties have been adequately modelled."

Although acknowledged for many years as a requirement for significant advances in penetration technology, the development of a data base comprised of well-documented actual penetration test results to use in conjunction with computer techniques continues to be of considerable importance.

B. EXPERIMENTAL INVESTIGATIONS

An early experimental program in projectile penetration was conducted by Allen, Mayfield and Morrison (Reference 29), to aid in the assessment of existing penetration depth prediction equations. Steel projectiles, 1.3 centimeters in diameter, were fired from a 0.5-caliber Browning® machine gun equipped with a smooth-bored barrel, at nominal ordnance velocities between 600 and 915 meters/second. The cone nose-shaped projectiles were fired horizontally into a target of medium-grained Monterey sand. By use of breakwire grids installed throughout the soil target, deceleration records of penetration were obtained. A nonlinear relationship between penetration depth and impact velocity was observed for the initial test series, with a critical impact velocity (thought to be associated with the velocity of sound in sand) defined at approximately 100 meters/second and considered a division between primarily elastic and primarily inelastic impact. Based on these results, different constants were determined for the basic polynomial velocity equation for velocities above and below the critical value. A second series of tests (Reference 30) essentially duplicated the first, with a modification to the sand target that allowed evacuation of air from the sample, and resulted in greater penetration depths.

Beginning in 1962, a program of large-scale penetration tests was conducted by Sandia Laboratories, Albuquerque, New Mexico. These tests are of considerable importance because they provide a large data base of full-scale field data; in addition, they provided the basis for development of Young's empirical equation, presented in the preceding section. The tests were complemented by both small-scale laboratory work and analytical/numerical studies. The penetration studies were conducted in a variety of different in situ soil and rock target materials. Soils included loess, gypsum, permafrost, stiff to soft clays, loose to dense sands, cemented sands and gravels. Rock types included sandstone, granite, welded tuff and dacite. In contrast to the lack of emphasis historically placed on quantifying target materials in penetration research, greater efforts were made to classify and describe the natural targets; these efforts were, however, constrained by the limitations inherent to sampling and measuring in situ natural geologic materials.

One of the earlier launch mechanisms used for the projectiles was that of freefall drop from an airplane or helicopter, with higher projectile velocities obtained by launching during aircraft diving (Reference 60). A rocket motor

penetrator system, described by Patterson (Reference 61), was used to fire a 295-kilogram penetrator at 783 meters/second into a dry lake playa. The projectile successfully penetrated to a depth of 57 meters.

Impact velocities between 18 and 840 meters/second were studied by Sandia, with measured penetration depths between 0.6 to over 61 meters. Considerable emphasis was placed on the structural performance and geometry of the projectile design required to maximize penetration, in keeping with the test program focus of earth-penetrating projectile design (as opposed to normal ballistic or protective design). Nose shapes were varied from flat to pointed, to study nose shape effects on penetration. Projectiles ranged from as small as 2.5 centimeters to as large as 46 centimeters in diameter. Projectile masses ranged between 2.3 kg to 2613 kilograms. Aerodynamic fins, which sheared off during penetration, and terradynamic fins, to stabilize the intratarget trajectory, were attached to the afterbody of the projectiles. The general projectile body shape was long and narrow, with a heavy forebody and hollow afterbody (Reference 37). Projectiles were instrumented with an accelerometer; a parachute-supported transmitter was trailed behind the projectile at sufficient distance to allow full projectile penetration prior to target impact by the transmitter. From the deceleration records, profiles of the target material were developed; reasonably successful attempts were made to correlate soil deceleration records to Standard Penetration (SPT) and cone penetration (CPT) data for the test site, laterally correlate soil strata across a site, and determine depth to bedrock (References 60, 18, and 5).

In 1974, Sandia developed a new launch mechanism that would allow high velocity testing of in situ soils. This system was known as the Davis Gun Penetrator Launch System, which contained a trailer-mounted recoilless solid propellant gun, with a 10.7-meter barrel length, and a 30.5-millimeter inner bore diameter (Reference 62). This gun could fire a 172-kilogram projectile at velocities up to 915 meters/second, or a 340-kilogram projectile at velocities up to 610 meters/second. Although this firing system increased the range of projectile sizes and velocities that could be tested, it had the disadvantage of a dual-projectile operating mechanism, in which two projectiles were simultaneously driven in opposite directions upon ignition of the propellant charge contained between the two, thus creating an "extra" projectile during testing.

In 1975, Hadala presented a review of an earth penetrating weapon program that had been sponsored by the Defense Nuclear Agency (DNA) during the preceding year, and conducted by Sandia. Pretest penetration depth predictions were made using Young's empirical formula, the spherical cavity expansion formula as presented by Ross and Hanagud (Reference 44), the cylindrical cavity expansion theory of Norwood (Reference 45), Allen's viscoplastic force law (Reference 47), and AVCO's differential area force law described by Henderson (Reference 20). The penetration tests involved a 181-kilogram projectile, 1.5 meters long with a 16.5-centimeter diameter ogive nose. The nominal impact velocity for all nine tests was 152 meters/second. The in situ target material was primarily glacial lacustrine deposits, consisting of thin layers of sand, silt and clay with a water table depth approximately nine meters below the ground surface. The top 1.2 to 1.5 meters of soil over part of the site consisted of disturbed backfill from prior ground leveling operations.

Comparison of the predicted values to the actual test results found that the differential area force law provided the best penetration depth prediction (within approximately 3 percent of the actual), but unrealistically large static resistance parameters were employed in obtaining this solution. Young's equation most closely matched the peak acceleration recorded for the projectile. As noted previously, Young's equation predicted the maximum penetration depth with a 27 percent underprediction error. The pretest predictions were performed for only one of the test shots. The test shots considered cumulatively reflected a near-linear relationship between velocity and penetration depth, and a weak relationship between penetration and the weight-to-area ratio of the projectile. None of the compared predictive techniques produced sufficiently good agreement with actual test results to justify its exclusive use.

Using small-scale models and higher impact velocities than could be obtained in the large-scale Sandia tests, Mumma and Randall (Reference 18) performed a series of penetration tests to further analyze projectile shape effects, as well as properties of the penetration phenomenon at higher impact velocities. A smooth-bored 57-millimeter diameter rifle was used to launch five different projectile sizes and shapes, fit to the bore dimensions with sabots (temporary projectile sleeves), at impact velocities of approximately 305 to 610 meters/second. A muzzle-mounted breakwire in sequence with foil switches mounted on the sabot stripper were initially used to actuate timed photographs of

the projectile flight. This system was subsequently replaced by flash X-rays. Projectiles were fired horizontally into an earth bank target, prepared by cutting into an existing natural bank, and into targets consisting of a concrete slab in front of the earth bank. An S number for the soil targets was estimated from dynamic cone penetrometer readings, using a formula suggested by Young (Reference 35). Foam castings were made of the projectile trajectories for the different projectile shapes and impact angles studied; this information was used in determining performance of the various projectile shapes.

Also in 1977, results from analytical and experimental penetration studies that were undertaken to assess soil overburden flight trajectories for detonation penetrator systems were reported (Reference 63). These vertical firing tests into sand were a continuation of a series begun in 1976 (Reference 64) that involved horizontal firing of projectiles into sand. Cylindrical projectiles, primarily flat-nosed, 0.02 meters in diameter with lengths ranging between 0.15 and 0.38 meters, were fired from a roof-mounted 20-millimeter gun aimed downward at the soil target. Velocities ranged between 50 and 400 meters/second. The target face of the soil sample was covered with an easily-penetrated fiberboard lid. Several flash X-ray units were used for each soil target to monitor the projectile during penetration. Dry test samples were prepared by slowly pouring sand into the sample container from an overhead crane. Wet test samples were prepared by separately mixing water and sand, then shoveling the mixture into the sample container and continuously adding water to the system as required to maintain a constant water level.

Results from these penetration tests were analyzed in several ways. Application of the classical force law developed by Poncelet (Reference 26) suggested that two velocity regimes existed, with the division between the two regimes occuring at a velocity of approximately 80 to 90 meters/second. Analysis of the constants in the force law, on the basis of both the previous horizontal firing test results (Reference 64) and the vertical firing test results (Reference 63), indicated no consistent difference between results from the two firing techniques; this conclusion was reached for the comparatively moderate penetration depths of less than 2.5 meters, obtained in this research.

The technique of dimensional analysis, discussed in detail in Section III, has also been used to define relationships between penetration parameters, in particular crater volume and penetration depth. Wang (Reference 16) used this

technique to interpret results from a laboratory study of right cylindrical projectiles dropped in the freefall velocity range into two densities of Ottawa silica sand. The steel-tipped hollow aluminum projectiles were filled with a mixture of sand and lead shot, then were guided in freefall by dropping through a smooth-walled pipe. Wang developed two independent dimensionless parameters involving penetration depth, projectile mass, impact velocity, static resistance per unit depth of the target material, and the coefficient of inertial resistance between projectile and target (the product of the soil density, the projectile cross-sectional area and the coefficient of restitution between the projectiles and the target). Although tumbling was observed to occur, the only consideration of variable projectile shape involved reduction of the values used for the coefficient of inertial resistance. From a least-squares fit of test data to the independent dimensionless parameters, Wang obtained two empirical expressions that indicated a nonlinear increase in penetration depth with increase in mass. He concluded that the main resistance to penetration into granular soils could be attributed to the increasing static resistance of soil with depth.

Advantages to use of soil as a protective barrier from penetration by artillery and mortar fragments prompted research by Rohani (Reference 17) at the U. S. Army Engineer Waterways Experiment Station (USAWES) in Vicksburg, Mississippi. Right circular cylindrical steel and brass projectiles were fired at velocities in the subordnance and nominal ordnance ranges, between 305 meters/second and 1524 meters/second. Targets were prepared from clay, loose sand and dense sand. A 35-caliber Remington® Model 660 bolt-action rifle was used to fire the projectiles, which were fitted with acrylic plastic sabots. Projectiles were fired horizontally through a thin cardboard front into the sand samples; the loose sand sample was prepared by pouring from a scoop, the dense sand sample by pouring from a scoop in lifts and then dropping the sample several times. Rohani noted a greater depth of penetration for the steel projectiles than for the brass over the range of velocities tested. Also noted in the test program was a decrease in the depth of penetration with increase in velocity for the steel projectiles, once some critical velocity value was reached. This trend was not observed for the brass projectiles; rather, the penetration depth remained essentially constant or slightly increased with increasing velocity. Rohani hypothesized that this behavior was likely a function of two phenomena. The first of these was the frontal enlargement (plastic deformation) of the steel

projectiles that was observed to occur at higher velocities. The second involved the constitutive properties of the soil; namely, that soil resistance to penetration increases with increasing velocity.

Research at USAWES continued with work by Butler (References 19 and 65), who used a 458-caliber low-velocity powder gun and a 22-caliber high-velocity powder gun to study projectiles impacting similarly prepared soil targets at velocities between 240 and 1280 meters/second. Like Rohani (Reference 17), Butler experienced difficulties with the separation of projectiles and sabots. Comparable to the results obtained by Rohani, a decrease in penetration depth with increase in velocity after some critical velocity was noted for the cylindrical projectiles fired into dense sand. Tests were conducted in an underground firing range, designed for horizontal firing of projectiles through a series of paper velocity screens into a soil target, with an ultrahigh velocity fragment stop situated behind the target. Deformation occurred in all projectiles at these velocities; the range of rigid penetration for steel projectiles was limited to velocities lower than approximately 760 meters/second on the basis of these results. Posttest grain size analyses were compared to pretest analyses to study communition of soil particles during penetration. Of particular significance is the conclusion reached by Butler that the penetration depth could be generally described as directly dependent on the projectile mass, and inversely dependent on the frontal cross-sectional area, possibly to some power.

The need for better design of direct embedment anchors prompted True's research on penetration into seafloor sediments (References 6 and 10), and development of Equations (8) and (9). Model tests were initially conducted in which a stud driver gun was used to fire aluminum and steel cylindrical projectiles downward through water into silt targets. Large-scale tests were also conducted in which 7.6-meter long, 1179-kilogram projectiles were lauched at free fall velocities into soft San Francisco Bay mud.

Forrestal and Grady (Reference 66) conducted tests using the technique of reverse ballistics, where a soil-filled projectile target is accelerated horizontally into a stationary instrumented penetrator. Use of the reverse ballistics technique allows measurement of the structural response of penetrators that would not be feasible with normal ballistics tests. The target material for these tests was a manufactured foundry core, consisting of silica sand mixed with binders and oven-fired, with resulting densities of 1.46 Megagrams/m^3. The tests are of

interest because of the test focus of obtaining acceleration-time records for different penetrator nose shapes.

Similar penetration experiments were conducted by Forrestal, et al. (Reference 67) using a gas-gun to fire projectiles at velocities between 200 and 1200 meters/second into foundry core samples with a density of 1.82 Megagrams/m^3. Three separate gas guns, with 64.5 millimeter, 102 millimeter and 178 millimeter bores were used, allowing analysis of potential boundary effects on the target and penetrator size combinations.

Reverse ballistics tests were also conducted by Setchell and Guzman (Reference 7). A compressed-gas gun was used to fire simulated soft sandstone targets into a stationary instrumented penetrator at velocities between 600 and 1200 meters/second. Acceleration records were obtained providing information on the variation in peak forces with impact velocity.

A number of investigators have conducted tests within the hypervelocity penetration regime. These tests have been primarily concerned with impact or explosive cratering. Hypervelocity penetration experiments were conducted by Braslau (Reference 68) using a light-gas gun to vertically fire aluminum spheres and plastic cylinders into dry quartz sand targets. At the test velocity of 6370 meters/second, an increase in soil density due to projectile impact was noted at the bottom of the crater, as well as some crushing of the sand particles. Heating of the soil target was determined to involve 26 percent of the initial kinetic energy of the projectile, with crater ejecta absorbing 53 percent. The crushing of sand particles was determined to absorb approximately 8 percent of the initial kinetic energy. The target strength was determined to be a critical factor in the final shape of the impact crater.

Some of the most significant recent work in hypervelocity impact has been performed by Schmidt (Reference 69) and Holsapple and Schmidt (Reference 70). Their theoretical derivation of scaling rules for explosive cratering indicated a strong gravity-dependence for crater size. This led to use of the centrifuge testing technique to investigate impact cratering. A rotor-mounted light gas gun was used to fire projectiles of materials such as polyethylene, nylon and aluminum, at impact velocities up to 2000 meters/second. Their derived scaling relationships for crater volume and radius were investigated experimentally for soil targets, primarily of Ottawa Flintshot sand. Their results indicated that the soil density and angle of internal friction were the most significant target

properties affecting crater size. Estimates of the energy involved in formation of Meteor Crater, Arizona, were calculated based on the results of these investigations.

C. SUMMARY

The analyses and investigative techniques described in the preceding sections provide a clear indication of the need for additional research in projectile penetration. Although many advances in understanding the penetration phenomenon have been made since the pioneering work of the 18th Century, many questions remain. The problem is complicated by the necessary integration of different scientific disciplines to analyze the interaction of the many separate variables involved in penetration, particularly when dealing with soil targets. The state of the art in soil penetration research is clearly less advanced than that for other more easily quantified target materials, such as metal, plastic and other synthetics. Fairly simple mathematical descriptions are available for such materials, because their behavior approximates that of homogeneous, isotropic solids with well-established constitutive relationships, a significant contrast to soils. The difficulty in understanding soil target behavior is augmented by the comparative nonavailability of technical literature. Much of the published information on projectile penetration in soil targets appears in research organization reports rather than in more accessible journals (and this lack of ready availability has undoubtedly affected research progress).

Although a fairly large data base of full-scale penetration tests in soils is available, the utility of this base is limited by the inaccuracies involved in the sample quantification. Indeed, to find a single full-scale test among published results that can be reasonably compared to a controlled series of laboratory tests is often impossible. From the laboratory investigations to date, the means for (and validity of) extrapolating small-scale penetration test results to full-scale results has not been established. Consideration of combined full-scale and laboratory test results shows that the specific influence of different geologic materials on penetration depth magnitudes has not been investigated in a comprehensive manner. This is due to: (1) an incomplete understanding of the complicated nature of this target material, (2) inadequate laboratory sample preparation techniques, and (3) inherent difficulties with testing and quantifying in

situ soils. A controlled investigative approach isolating different geologic material types appears essential.

Effects of the more easily quantifiable variables in the penetration process are better understood. Considerable experimental and analytical efforts have been directed towards analysis of the effects of penetrator nose shape, penetrator geometry and different velocity regimes. It appears that these variables may be accommodated with some confidence in penetration depth predictions.

The experimental, analytical and numerical techniques that have been utilized to study the penetration phenomenon have resulted in development of a large number of penetration depth predictive techniques of varying complexity, utility and accuracy. None, however, seem able to consistently provide the degree of confidence that might reasonably be desired in predicting penetration depths in soil targets. Recognition of this fact, and of some of the factors contributing to it, provided the motivation for the research described in the following chapters.

SECTION III

CENTRIFUGE TESTING TECHNIQUE

A. BACKGROUND

1. Principles of Centrifuge Operation

The use of scaled models to represent large structures, or prototypes, is common to many engineering fields. Testing in a 1-g environment, however, does not allow replication of the prototype stress levels in the model. Thus, where self-weight effects are significant, as in geotechnical structures, the resulting lack of model:prototype similitude jeopardizes the usefulness of physical modeling. If a scaled model is subjected to the artificial gravity field developed in a centrifuge environment, the effect is to make the model appear heavier. Comparable stress levels to those in the large-scale prototype can be induced in the model, and the effects of self-weight can be better simulated.

The main components of a typical centrifuge used for geotechnical testing are shown schematically in Figure 1. Rotation of opposing arms occurs about a central hub. Payload platforms are located at the end of one or both of the arms. The scaled test model is mounted to a payload platform and rotated at high rpm.

The acceleration field developed by the rotating motion of a centrifuge is dependent upon the orientation of the plane of rotation. If this orientation is horizontal with rotation occuring around a vertical axis (as shown in Figure 1), then the centripetal acceleration, a, acting at any point on this plane is represented by:

$$a = v^2/r \tag{10}$$

where v is the circular velocity and r is the radial distance from the center of rotation to the point on the plane of rotation. The total acceleration, a_t, acting at this point includes the centripetal acceleration and that resulting from the gravitational forces exerted by the earth's rotation:

$$a_t = (g^2 + a^2)^{1/2} \tag{11}$$

where g is the acceleration due to gravity. In the noninertial reference frame of the plane of rotation, the centripetal acceleration would be equivalent to the equal magnitude but oppositely directed centrifugal acceleration, acting radially outward. The associated pseudo force is termed the centrifugal force.

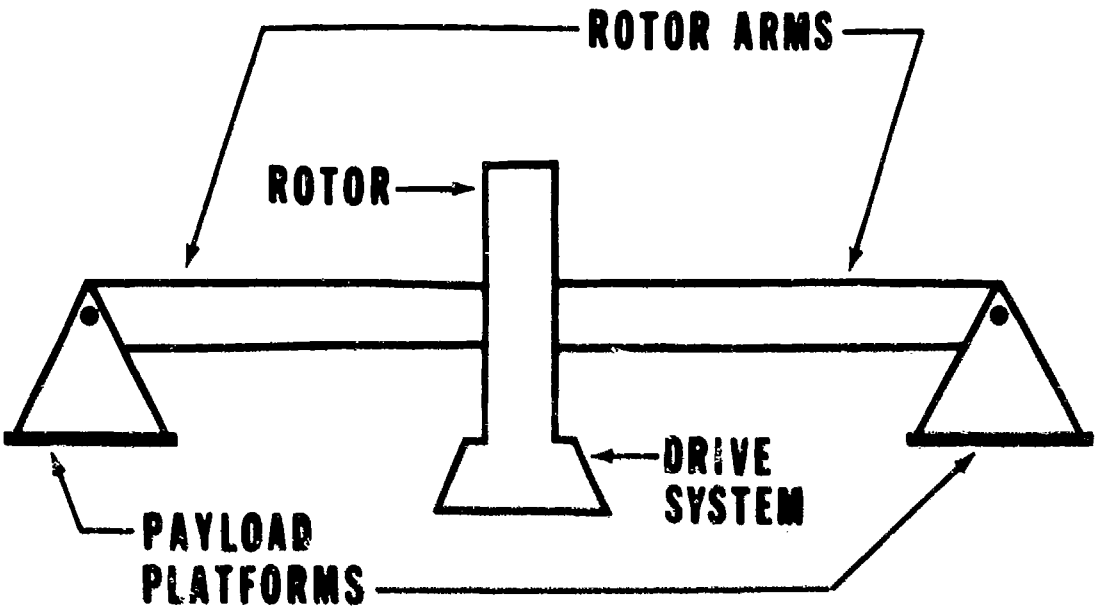

Figure 1. Centrifuge Schematic

For a centrifuge with radius R, the g level, G_R, acting at R is calculated as:

$$G_R = g\omega^2 R/g = \omega^2 R \quad (12)$$

where ω is the angular velocity of rotation. The g level, G_r, acting at any point r may be calculated by:

$$G_r = rG_R/R \quad (13)$$

For the equipotential surfaces describing equal force locations to be perpendicular to the direction of force in the rotating field, the surfaces must describe a parabolic shape. This is in opposition to the earth's gravitational force field which, at the centrifuge scale, is defined by horizontal equipotential surfaces. The inherent error associated with this discrepancy is expressed both in the dimensions and in the stress distribution in a soil model tested in a centrifuge. With respect to the model dimensions, all points in the soil model at different distances from the center of rotation ideally should rotate at the same angular velocity for the same scaling factor, a physical impossibility. The error can be minimized by limiting the ratio of the change in r throughout the model to the average r for the model, by decreasing the vertical dimensions of the model, or by testing with a larger radius centrifuge. With respect to the vertical stress profile in a soil model, the error associated with deviation from a linear stress variation in a uniform soil (Reference 71) can be quantified by:

$$\Delta\alpha_v/\alpha_v = \Delta r/2r_s \quad (14)$$

where α_v is the vertical stress and r_s is the radial distance to the soil surface. Again, the error can be minimized by varying the model or centrifuge dimensions to conform to desired limits.

Boundary effects due to friction between the soil and the walls of the sample bucket must also be considered,and a minimum width for particular test conditions must be determined. At the same time, the width of the model must be small with respect to the radius of the centrifuge to avoid inducing errors associated with the fan-shaped acceleration vector field (Reference 71).

Another potential source of error that may be significant in dynamic centrifuge testing is that associated with the coriolis force. An object moving within the plane of rotation is subjected to a coriolis force, which acts in a direction perpendicular to the velocity of the object (relative to the noninertial frame). This pseudoforce arises from the different angular velocities at different

locations on the plane of rotation, and is evidenced by an apparent sideways deflection of a moving object. The coriolis acceleration, a_c, is defined by

$$a_c = 2\omega v \tag{15}$$

and the coriolis force, F_c, is

$$F_c = 2M\omega v \tag{16}$$

A projectile fired radially into a rotating soil sample is subjected to the coriolis force. This affects both the impact location of the projectile on the sample surface, and the projectile trajectory through the soil. Because soil is compressible, horizontal deflection from the coriolis force can occur as the projectile travels through the soil, particularly in highly compressible soils. For the relatively incompressible granular soils of this research, the magnitude of this deflection is anticipated to be negligible. Additional discussion of the coriolis force is presented in Appendix B.

2. Centrifuge Use in Geotechnical Testing

The scaling laws generally applied in centrifuge modeling are listed in Table 1. Assuming the materials of model and prototype are the same, then the basic assumptions can be made that: 1) the length in the prototype, L, is equivalent to a reduced model length, L′, multipled by some scale factor, n; 2) the density, δ_t, velocity, v, and modulus, E, for model and prototype are the same; and 3) the coefficient of consolidation, C_v, dynamic viscosity, μ, and shear stress, τ, for model and prototype are the same. Thus,

$$L = nL' \tag{17}$$

$$\delta_t = \delta_t' \tag{18}$$

$$v = v' \tag{19}$$

where L represents any linear dimension. From these assumptions, other relationships can be obtained:

Area:	$A = L^2 = (nL')^2 = n^2A'$	(20)
Volume:	$V = L^3 = (nL')^3 = n^3V'$	(21)
Mass:	$M = \delta_t V = \delta_t'(nV)^3 = n^3M'$	(22)
Unit Weight:	$\gamma = \delta_t g = \delta_t' g'/n = \gamma'/n$	(23)

For dynamic events with no water involved:

Time:	$t = L/v = nL'/v' = nt'$	(24)

For hydrodynamic events, application of the consolidation equation results in:

Time:	$t = TH^2/C_v = T(nH')^2/C_v = n^2t'$	(25)

For viscous events, the velocity gradient or time rate of strain may be expressed:

$$dv/dt = \tau/\mu = \tau'/\mu' = dv'/dt' \quad (26)$$

Thus,

$$\text{Time:} \qquad t = t' \quad (27)$$

Table 1. SCALING RELATIONSHIPS

Quantity	Prototype:Model
Linear Dimension	n
Density	1
Velocity	1
Area	n^2
Volume	n^3
Mass	n^3
Unit Weight	1/n
Time:	
Dynamic Events	n
Hydrodynamic Events	n^2
Viscous Flow	1

The technique of modeling-of-models is frequently employed in centrifuge testing. It involves modeling the same prototype event at different g-levels. This technique allows a determination of the range of g-levels, if any, for which the scaling laws presented above appear to be valid for the particular model test configuration. This includes identification of size limitations and boundary effects. For the projectile penetration problem addressed in this research, modeling-of-models would involve testing various model projectile sizes at different g-levels, such that after application of the appropriate scaling relationships, the same full-scale penetrator would be modeled in all tests. If the same scaled penetration depth were observed, then the applicability of the scaling laws would be established for the range of projectile sizes, soil target and g-levels tested. With respect to size limitations and boundary conditions, it is evident that for a given sample size, a model projectile could be so large that boundary effects from the sample container would significantly influence the penetration process. Similarly, at the other end of the scale, a limiting bound to projectile size is imposed by the grain size of the target material. If the projectile

is too small, the scaled event would similate a projectile impacting boulders, rather than the soil target of interest.

B. PRELIMINARY ANALYSIS

1. Development of Soil Model

The penetration of a projectile into a soil medium can be separated into the surface penetration or impact phase, which involves the formation of a crater, and into the subcrater penetration phase. The depth of subcrater penetration can be as much as three orders of magnitude greater than the depth of the crater, depending on the shape of the projectile, and may be related to such soil properties as grain size distribution, density, degree of compaction, moisture content, and macrostructure (References 9 and 72).

When a projectile meets the soil, it is traveling at the maximum velocity experienced during the penetration event. During this impact phase, the nose of the projectile slices into the soil, creating a crater and surface soil particles break away from the penetrating projectile. Surface heave and cratering are free to occur along the stress free boundary of the initial soil surface. As the projectile penetrates the soil in the subcrater penetration phase, a free surface is also created behind the projectile in the form of a trailing tunnel.

As the projectile continues to penetrate the soil, it may still be traveling at a relatively high velocity. Penetration occurs largely due to the slicing action of the nose. For pointed penetrators, this slicing action shears and compresses a thin zone of soil around the nose, and imparts considerable lateral velocity to the soil particles in the vicinity of the projectile nose (Reference 60). The lateral velocity of the soil particles is greater than that of the projectile in the downward direction. The moving soil particles impact other soil particles, and similar movement occurs, resulting in the soil particles in the vicinity of the projectile being pushed away and compressed until they fail in shear. As the projectile passes, the stress on the the failed soil particles next to the penetrator path becomes zero, the soil dilates and slightly closes the tunnel created by the projectile (References 9, 72 and 8). For blunt penetrator shapes, target failure occurs over a more cylindrical or roughly conical surface. Although the transition in failure modes depends on penetrator shape, the relationship between projectile configuration and target properties is not well-established (Reference 2). Clearly the projectile impact angle influences the striking face of a projectile;

this can also be significant in determining whether penetration occurs in a blunt or piercing mode.

In summary, for this initial phase of subcrater penetration, the main soil resistance acts on the nose of the projectile, and there is very little skin friction acting on the body of the projectile during penetration. There will be some rebound of the soil particles after the projectile has passed and there has been time for elastic recovery to occur.

As the projectile decelerates to near-zero velocity during the secondary phase of subcrater penetration, the character of the penetration phenomenon changes. In the lower velocity regimes, the lateral velocity imparted to the soil particles by the penetrating projectile is small and impact behavior becomes plastic. The soil particles and the projectile reach the same velocity in the lateral direction; thus, the soil particles are not pushed away and remain in close contact with the projectile. This results in frictional forces and additional deceleration of the projectile. The friction continues to increase with the decrease in the velocity of the projectile. The terminal deceleration is the largest value of deceleration reached, and corresponds to development of the largest compressive force. Within higher velocity regimes, development of frictional forces may not occur. Some researchers explain this in terms of a phenomenon where the projectile is surrounded by a cavity created by flow separation of the soil particles around the moving projectile. Murff and Coyle (References 73 and 74) define the transition between nonseparation and separation by a critical velocity. Chabai, et al. (Reference 8) suggest that penetrator nose shape and target properties also influence whether or not separation of soil from the projectile surface will occur. There is evidence for lack of frictional resistance at high velocities from painted projectiles fired at high velocities that showed no removal of paint following penetration (Reference 72). Analytical calculations in which frictional forces have been assumed negligible have resulted in calculated forces at low velocities being less than those observed from penetration tests. Chabai, et al. (Reference 8) suggest that this may be due to the importance of friction at low velocities.

There is some evidence that separated soil particles may actually reattach to the projectile surface during the penetration event. This has been postulated based on striated erosion patterns on recovered projectiles. A possible explanation for this may involve deviation of the projectile from a straight

trajectory (Reference 8). Allen, Mayfield and Morrison (Reference 29) report the presence of a conical cap of crushed soil particles on the nose of recovered projectiles fired into sand targets.

After terminal deceleration of the projectile has been reached, the soil exhibits rebounding due to this compressive force which causes vibration between the soil and the projectile. The final stage in the subcrater penetration process is the point at which the projectile has lost all of its energy and comes to a complete rest.

2. Dimensional Analysis

Dimensional analysis is a method of reducing the separate variables describing a physical phenomenon to independent dimensionless groups of variables, termed "dimensionless parameters" or "pi terms". The ability to develop relationships between individual variables by dimensional analysis is particularly useful in analyzing complex physical phenomena where the governing equation relating the individual variables is unknown. In addition, dimensional analysis allows correlation of the results of model tests with full-scale, or prototype, conditions.

Of particular application for centrifuge modeling is the use of dimensional analysis for establishing the similarity requirements between model and prototype, as opposed to the alternative determination of these requirements from analysis of applicable differential equations. Coupled with results from experiments designed to verify similarity requirements, the method of dimensional analysis has the advantage of not relying on previously defined equations that may not adequately describe the relationships between different physical parameters (Reference 14).

The basic dimensions involved in most engineering problems are those of force (F), length (L), and time (T). Force is actually a derived unit that can be expressed in terms of the basic dimensions of mass, length, and time; however, by convention, force is generally used instead of mass in the process of dimensional analysis.

The number of dimensionless parameters that are required to correlate a given set of variables is generally equal to the number of individual variables minus the number of basic dimensions necessary to define the variables (Reference 75). In many cases, dimensional analysis can be simplified

by using known relationships between variables to reduce the initial number of independent variables that must be considered.

Pi terms can be divided or multiplied, modified by a constant, etc., without changing the basic similarity relationships specified by the term. Such manipulations have the effect of relating the phenomenon described by the pi term to a different standard. Examples of this are presented in Section Six.

The first step in dimensional analysis is to identify all of the separate variables of significance to the problem under consideration, and list these in a functional equation for the phenomenon of interest. Then, maintaining dimensional homogeneity throughout the equation, dimensions are systematically eliminated by algebraic or matrix manipulation. The largest sources of error in the method are the omission of significant variables in defining the functional equation, and the inclusion of unnecessary variables. Because different results can be obtained with selection of different parameters, careful problem definition is no less critical to a dimensional analysis approach to modeling than to other approaches.

The considerations addressed in the preliminary soil model developed in the preceding section, coupled with the discussion in Section II, provide a basis for analyzing the factors of significance in the interaction between a soil and a penetrating projectile. As noted previously, the velocity regime being investigated is one of the most significant considerations. A very significant break occurs in the penetration process between nominal ordnance and hypervelocity regimes. The low velocity regimes are typified by rigid projectile impact, that is, no significant projectile deformation. Projectile and target material characteristics are the most significant parameters affecting the penetration event. Projectile strength is significantly greater than dynamic impact pressures. At high velocities, material strengths of the projectile and target are significantly exceeded by impact pressures and thermal phenomena. Impact is viewed as fluid flow, and the rigidity and compressibility of the impacting bodies can be neglected (Reference 2). Between the two velocity extremes, a transitional region exists where mechanical and thermodynamic properties are both significant (Reference 76). Clearly, the divisions between the velocity regimes are not fixed, and depend upon the properties of the target and the projectile.

Appendix C provides a list of significant parameters for defining the penetration event in the transitional region for projectiles impacting material

targets such as steel, lead, concrete, etc. This list includes thermodynamic parameters including the temperature, specific heat and heat of fusion of the target material and projectile. A discussion of these high-velocity regime parameters and the resulting dimensional analysis for hypervelocity cratering experiments in soil targets is provided by Schmidt and Holsapple (Reference 77). Additional discussion and results of modeling tests performed to verify the pi terms established in their analysis are presented by Schmidt (Reference 69).

From the general list of Appendix C, the parameters of significance to the low velocity penetration regime investigated in this research were selected. These parameters are listed below in Table 2, along with additional parameters of potential significance for a dry, granular soil target.

Table 2. LOW VELOCITY PROJECTILE PENETRATION PARAMETERS

Variable	Symbol	Dimensions
Penetration depth	d	L
Impact angle	β	---
Impact velocity	v	L/T
Strain	ε	---
Projectile properties:		
Caliber	s	L
Length	l	L
Nose radius	r	L
Nose angle	α	---
Density	δ_p	FT^2/L^4
Ultimate stress	S_{ult}	F/L^2
Soil target properties:		
Density	δ_t	FT^2/L^4
Ultimate stress	σ	F/L^2
Median grain size	D_{50}	L
Friction angle	ϕ	---
Relative Density	D_r	---
Void ratio	e	---

Following the analysis of Baker, Westine and Dodge (Reference 76), pi terms involving the zero-dimension parameters can be established as follows:

$$\pi_1 = \beta \quad (28)$$

$$\pi_2 = \varepsilon \quad (29)$$

$$\pi_3 = \alpha \quad (30)$$

$$\pi_4 = \phi \quad (31)$$

$$\pi_5 = D_r \quad (32)$$

$$\pi_6 = e \quad (33)$$

Like dimension parameters can be combined to create additional pi groups:

$$\pi_7 = d/s \quad (34)$$

$$\pi_8 = l/s \quad (35)$$

$$\pi_9 = r/s \quad (36)$$

$$\pi_{10} = D_{50}/s \quad (37)$$

$$\pi_{11} = \delta_p/\delta_t \quad (38)$$

$$\pi_{12} = S_{ult}/\sigma \quad (39)$$

The remaining parameters can be combined to create:

$$\pi_{13} = \delta_t v^2/\sigma \quad (40)$$

Geometric similarity between model and prototype is described by pi terms 1, 3, 4, 5, 6, 7, 8, 9 and 10. π_{11} is a density ratio; π_2 and π_{12} relate the constitutive similarity requirements. π_{10}, which relates the median grain diameter to the arbitrarily chosen standard of projectile caliber, is a statement of one of the inherent limitations to modeling soils. Obviously, the implied necessity for grain size scaling imposes limits on the range of prototype events that can successfully be replicated in a model study, in either a l-g laboratory or elevated g centrifuge environment. Nevertheless, the ability to experimentally determine validity limits for modeling in soils has been documented by a number of researchers (References 13 and 78). Schmidt and Holsapple (Reference 77) have successfully performed small-scale centrifuge cratering experiments in sands that very closely replicate the actual prototype events of massive cratering in similar soils from both explosions and meteorites. Their conclusion is generally summarized:

> "It is recognized that the behavior of the soil is complex and requires complex constitutive equations. Thus it is probable that similarity will not be achieved unless the same soil is used for similar experiments. With this restriction... similarity is possible assuming only that the constitutive equations describing the soil are independent of the scale factors for size and time."

π_{13} is essentially an energy ratio for the target material, but an equivalent ratio is equally applicable for the projectile because of the constitutive similarity requirements defined by π_2 and π_{12}. π_{13} is clearly the most significant

term for describing penetration in the low velocity regime, because it is essentially a function of the geometric, density and constitutive similarity requirements of the other pi terms. The exact nature of the functional relationship, however, must be determined experimentally. For a dry granular soil target, the parameter σ in π_{13} (and in π_{12}) is defined as the body stress, $\delta_t gz$, or total vertical stress, where g is the acceleration due to gravity and z is the depth below the soil surface. For the constitutive similarity requirements expressed by π_{12} and π_2 to be maintained between model and prototype (which would realistically require the same soil for both model and prototype due to the complexity of the constitutive relationship for a soil target), a reduction in z would require an increase in g. Thus, for a small-scale model where the linear dimension of z is scaled by some arbitrary factor, a similarly scaled increase in g would be necessary for model similitude, i.e., the body force must be scaled as the reciprocal of size. A rigorous analysis of body forces in the thermomechanical response of soil (high-velocity impact region) made by Schmidt and Holsapple (Reference 77) resulted in development of a comparable gravity-scaled dimensionless parameter for crater size.

It is clear that gravity appears to be a significant factor in both the design and the interpretation of projectile penetration tests in granular soils. Thus, on the basis of the dimensional analysis, the ability to vary g-level, such as by use of a centrifuge, appears to be requisite to thorough investigation of the penetration phenomenon in granular soils. To provide experimental verification of this for a particular pi group would require conducting tests over a range of g levels to determine the value of the dependent variable of penetration depth. In addition to gravity, the soil and projectile parameters involved in defining the independent pi values for each pi group would be varied but in such a way that pi values would be equivalent for different tests. If the same value for the dependent variable were determined from each of the tests, then the functional relation described by these variables would be valid. Potential similarity violations due to particle size effects and boundary conditions can be evaluated in this manner. Lack of similarity in test results may indicate that the variables described by the independent pi values are not sufficient to describe the penetration phenomenon, and may suggest a need to develop additional independent pi values.

Conversely, the number of variables hypothesized for a given functional relationship can also be decreased on the basis of experimental evidence, if fewer independent variables are shown to be adequate to explain the results. With respect to the 13 pi terms developed above, it has already been suggested that, at least within bounds that can be determined experimentally, π_{10} is likely a superfluous term. Other pi terms, particularly the zero dimension terms describing soil properties, may have little, if any, significance in the penetration event. Thus, the use of dimensional analysis should be combined with parametric experimental studies to refine and confirm an initially hypothesized functional relationship. Quantification of the actual relationships defined between the experimentally-derived values for the dependent variable and the various independent π values can then be used to calculate actual scaling rules for use in nonsimilar experiments.

SECTION IV

SAMPLE PREPARATION

A. SOIL DESCRIPTION

Four different soils were used in the penetration test program. Ottawa Flintshot and Ottawa F58 sands were ordered from Ottawa Industrial Sand Company, Illinois, and shipped to the centrifuge facility located at Tyndall Air Force Base (AFB), Florida. A third sand, Florida beach sand, was obtained locally in the field and cleaned and dried in the laboratory. All three of these sands are uniform silica sands; the Ottawa sands are 99.8 percent pure SiO_2. A fourth soil blend was created by mixing Ottawa sands and ASTM No. 8 sand to achieve a nearly well-graded soil.

Grain size distribution curves for the four test sands are presented in Figure 2. As shown, the grain size distributions for the Ottawa F58 sand and the Florida Beach sand are similar. The major difference between the two sands is that the particle shape of the Ottawa sands is subrounded, while the Florida Beach sand is subangular. The Ottawa Flintshot sand is defined as a medium sand and the Ottawa F58 and Florida Beach sands are defined as fine sands by the Unified Soil Classification System. The soil blend is composed of coarse, medium and fine sand particles in subrounded, subangular and angular shapes. Relevant soil parameters for the four test soils are listed in Table 3.

TABLE 3. SOIL PARAMETERS FOR TEST SOILS

Soil Type	D_{10}(mm)	D_{50}(mm)	C_u	C_c
Ottawa Flintshot	0.5	0.56	1.16	1.00
Ottawa F58	0.15	0.23	1.67	1.01
Florida Beach	0.17	0.24	1.53	0.95
Soil Blend	0.17	0.75	6.47	0.66

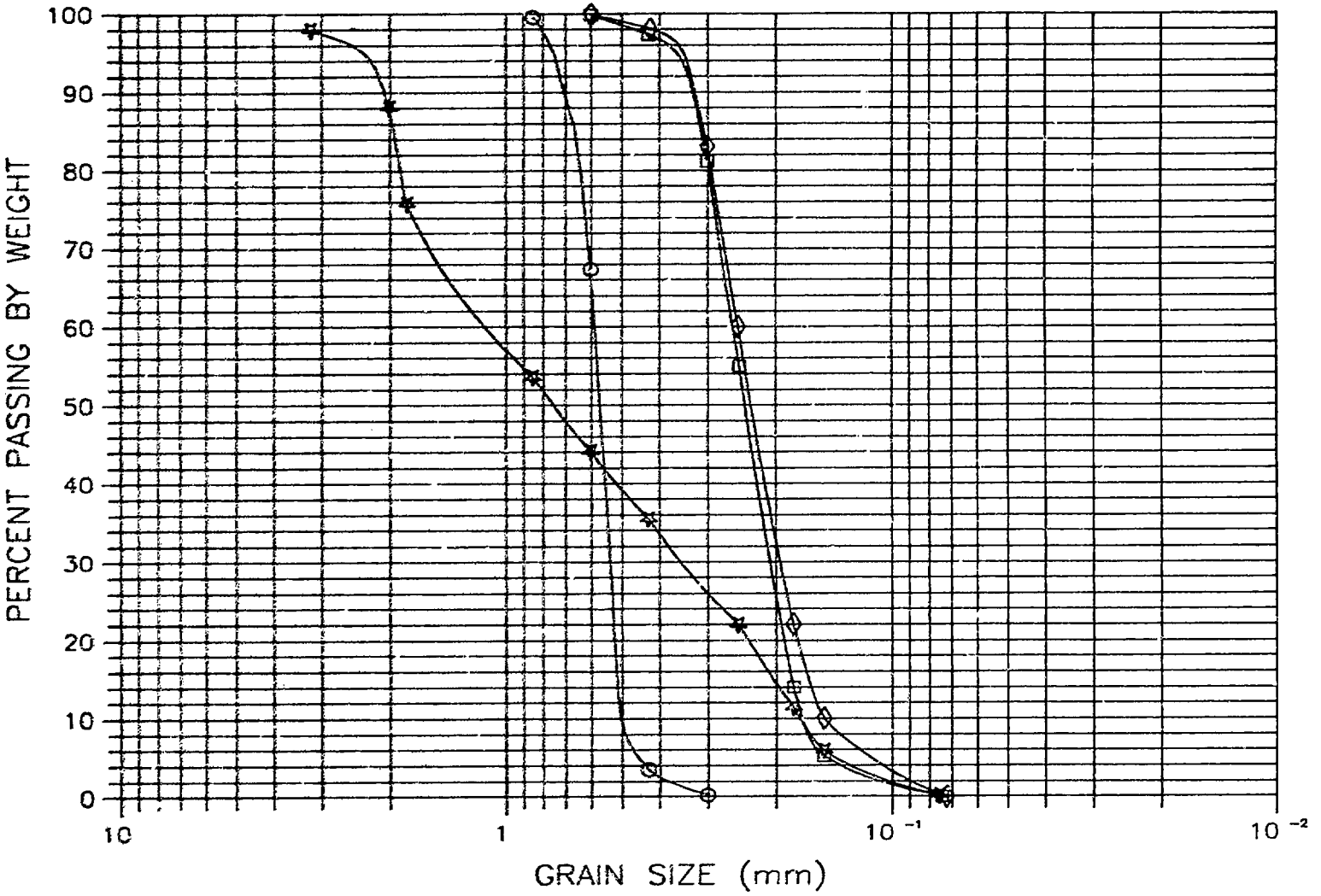

Figure 2. Grain Size Distribution Curves

B. PLUVIATOR DESIGN

1. Background

The technique of pluviation (controlled dropping or "raining") of sand particles through air has been recognized as a sample preparation method that simulates the soil fabrics formed by natural sedimentation processes, results in relatively homogeneous laboratory specimens, and can successfully produce a range of relative densities (Reference 79). Obtaining and reproducing these features among different samples are typically the major goals for laboratory preparation of dry sand samples.

The general technique involves dropping sand in a regulated manner, over heights dictated by the soil properties and sample requirements, into a calibrated sample container. A removable sample collar is frequently used during pluviation, with excess soil being trimmed off after collar removal. The sample surface is then leveled in some manner, usually by planing with a straight edge or smoothing with a piston-shaped tool, to obtain a sample of precisely known volume. Kildalen and Stenhamar (Reference 80) used a vacuum tube fixed at a predetermined height to remove extra sand from pluviated simple shear test samples. Final leveling was accomplished using a lightly greased piston carefully touched to the trimmed sample surface.

A special requirement for sample preparation unique to the goals of this research was to be able to prepare dense samples sufficiently level through pluviation alone, such that the need for any surface trimming or rearrangement of surface soil particles was eliminated. The actual height of the sample (within approximate bounds) was not critical. The requirement for a level surface in the dense samples, without use of smoothing techniques, was necessary to allow accurate investigation of shallow penetration depths (frequently less than 25 millimeters in the soil model), and to prevent scale-generated emphasis of surface disturbance arising from the scaling laws associated with centrifuge modeling. For example, 2.5 millimeters of "disturbed" surface soil in a soil sample would translate into 0.25 meters of disturbed soil in the corresponding prototype at 100 g's. This problem was not expected to be of significance for loose samples, because greater penetration depths were anticipated.

Although the basic pluviation technique for sample preparation is the same, a number of different types of sand rainers have been constructed

(References 81, 79 and 80), and studies have been made of the specific influence of different components and geometry of these rainers on the sample properties. A recent in-depth study by Eid (Reference 81) provided the basis for the soil pluviator used to form the 0.46-meter diameter centrifuge test samples of this research. This pluviator is shown schematically in Figure 3.

The major components of the sand rainer are: a sand bin to hold the sand to be used in sample formation; a perforated plate and shutter to start and stop the sand flow (in the form of jets) from the bin; a diffuser (sieve system) to transform the falling sand jets into a uniform rain; and a sample bucket to collect the sand in its final configuration.

The geometrical relationships among the major components can be defined by the distances F, S and H, shown in Figure 3. F is defined as the distance between the perforated plate and the top sieve in the diffuser; S is the distance between the top and bottom sieves in the diffuser, and H is the distance between the bottom diffuser sieve and the sample surface, which decreases as the sample is formed if the diffuser is kept stationary throughout sample formation.

In addition to these major components and their geometrical relationships, other potential variables in a sand rainer system have been studied to determine their effects on the resulting soil sample. These variables include the size, spacing and number of holes in the perforated plate, the size of the sieve openings and the number of sieves in the diffuser, the height of sand in the storage bin, and the mean particle diameter of the sand. The effect of maintaining a constant H distance as the sample is created has also been studied. This is accomplished by use of a moving diffuser system that allows a constant H value to be maintained throughout sample preparation, while the distance F is decreased (assuming the sand bin is held in a fixed position). Eid (Reference 81) determined that the more complicated moving diffuser arrangement produces samples with slightly more homogeneous soil structures than a fixed diffuser configuration, based on cone penetration test data. Eid theorized that air trapped in front of the falling sand in a fixed diffuser system may contribute to sample inhomogeneity.

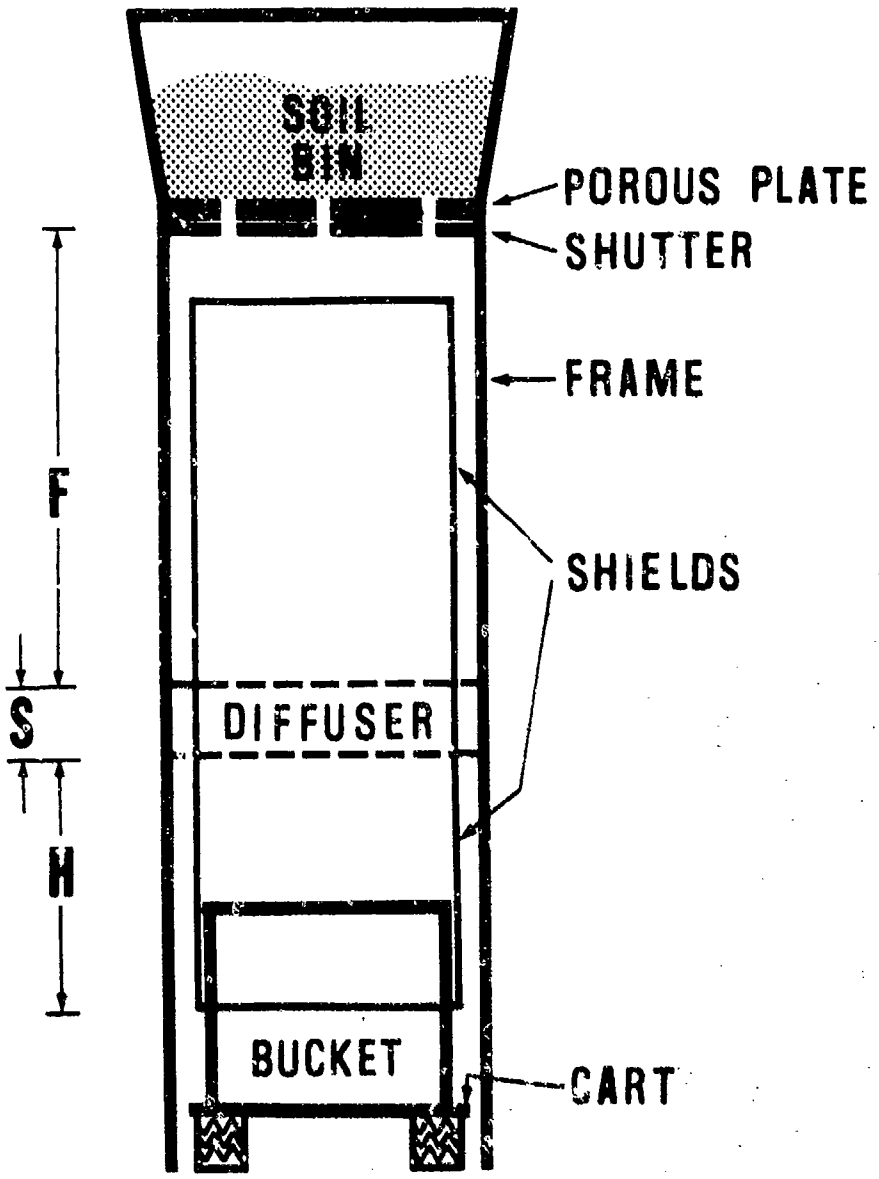

Figure 3. Schematic of Pluviator

Eid performed a comprehensive study, using Monterey sands, of the interaction of the above variables. He presented results of tests on a large number of samples in terms of "conditional" and "unconditional" parameters. Eid defined the significant conditional parameters as the distances F, S and H; variation of these distances did not affect the sample properties provided certain conditions were met, i.e. as long as the F and H distances were greater than the minimum distances ("critical" values) necessary for the sand rain to reach terminal velocity, there was no change in the relative density of the resulting sample with variation in these parameters. Thus, the minimum F and H distances were considered functions of the mean particle diameters of the sand. Similarly, by testing a wide range of grain size distributions in different Monterey sands, Eid determined that as long as the S distance was a minimum of approximately 10 centimeters for a two-sieve diffuser, there was no significant variation in the resulting sample relative density. These results were in agreement with conclusions suggested by Rad and Tumay (Reference 80) on the basis of tests performed using a single grain size distribution of Monterey sand.

Eid defined the significant unconditional parameters to be the number and size of holes in the perforated plate, and the size of openings in the diffuser sieves. Height of sand in the storage bin, constant H distance, and the number of sieves in the diffuser were not considered to be significant variables under the conditions set for the F, S and H distances. Differences in relative density for any soil could be achieved by varying only the unconditional parameters, once the minimum F and H distances were established for the sample soil. In agreement with Rad and Tumay (Reference 80), Eid concluded that higher relative densities could be obtained by decreasing the sieve opening size (subject to a minimum size opening requirement sufficient to prevent sand accumulation on the diffuser), and/or by decreasing the porosity of the perforated plate and shutter (thereby decreasing the intensity of deposition).

The critical H and F values for a particular soil are established experimentally. Samples are prepared over a range of H values for different F values, and the critical H value is chosen as the minimum value at which essentially no further increase in sample density is seen. It would be expected that the largest critical H value would correspond to relatively low F values. Using the critical H value determined in this manner, the distance F can then be varied and a critical value selected by the same criterion.

2. Construction and Testing

The pluviator constructed for this research is pictured in Figure 4. The basic frame was built using 1.8 meter length standard framing studs arranged in an open circular pattern with an interior diameter of approximately 0.6 meters to accomodate the 0.46 meter diameter sample buckets. Metal supports were added to the top front of the frame to provide added stability at the open end of the circle. Plywood was used to make the circular frame supports, interchangeable shutter plates and diffuser sieve mounts. A circular aluminum tub with the center bottom portion removed was used as the sand storage bin.

6.35 millimeter wire mesh was attached to the two diffuser sieve mounts, which were separated by threaded rod to allow adjustment of the S distance and use of different-sized sieves. Ropes anchored to the top of the diffuser were fed through side-mounted pulleys attached to the outside of the frame just below the shutter plate. Aluminum window tracking was installed on the interior of alternate studs and at corresponding locations on the exterior of the diffuser mounts. This provided a method of channeling the diffuser within the frame, preventing rotation but allowing variation in the position of the diffuser assembly (i.e. variation in relative F and H distances). Samples could also be prepared while maintaining a constant H distance by using the pulley system to lift the diffuser as the samples were formed.

Interchangeable circular perforated plates were machined from steel plate. Holes were drilled in the face of the plates to achieve the desired porosities. Eyebolts were threaded into the perimeter of the plates at all stud locations. The plates were mounted by rotating the eyebolts into slots in the studs and bolting in place. The plywood shutter plates, cut with hole patterns corresponding to those of the porous plates, were slid onto angle brackets mounted on the interior of the frame; flow of sand was initiated by pushing the shutter plates inward to align the holes with those in the porous plates.

The interchangeable circular steel plates proved to be very cumbersome and were subsequently replaced with lightweight machined nylon plates. The original plywood shutters were also replaced with shutters cut from particle board. These new shutters were water sealed and covered with Formica® to offset the problems with humidity-induced warping that affected the original plywood shutters. Although the warping problem was effectively eliminated with these new shutters, exact hole alignment when opening the

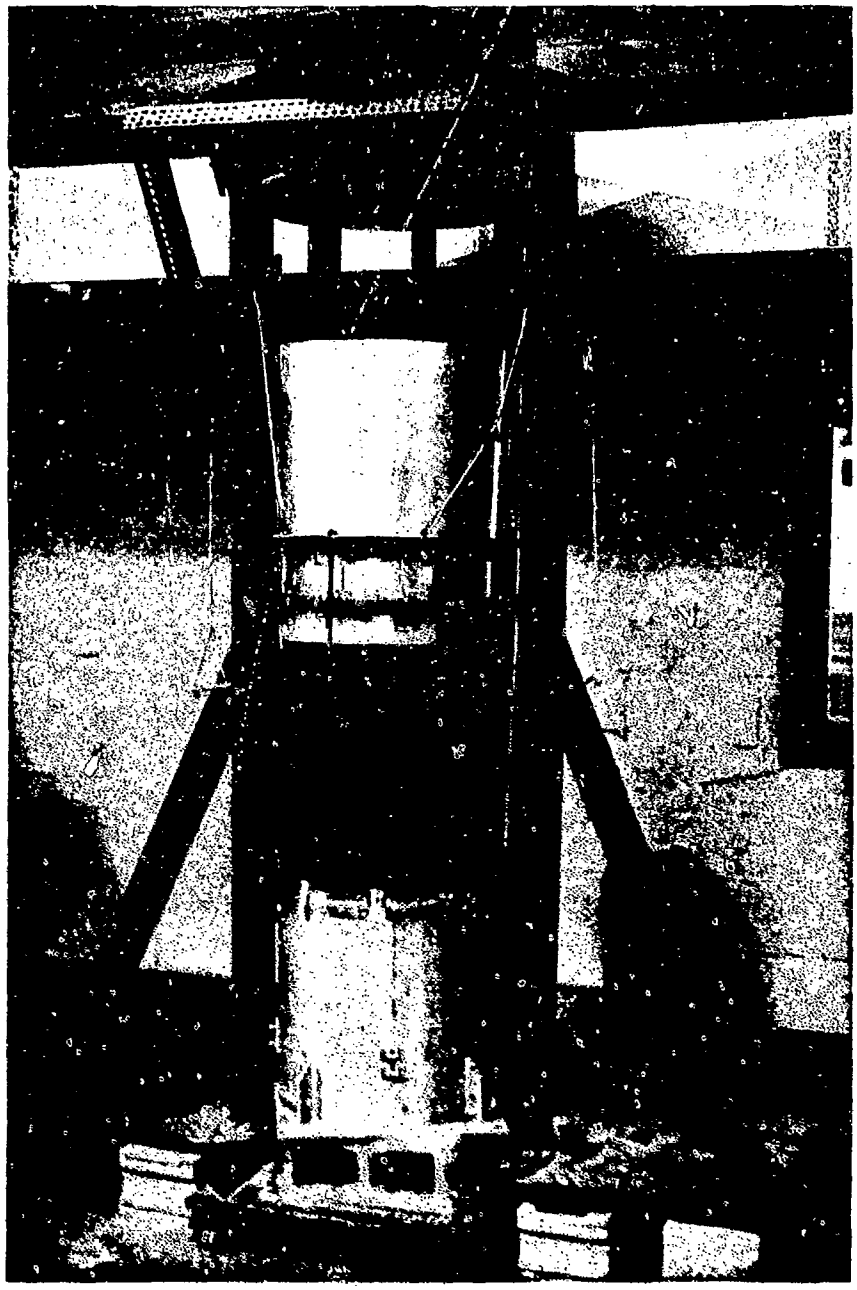

Figure 4. Soil Pluviator Used for Centrifuge Test Samples

interchangeable shutters was frequently difficult to achieve. This difficulty was solved by using a solid sheet of 1.6 millimeter thick aluminum, with handle cutouts on one end. The shutter was mounted in a fixed position approximately 3.2 millimeter below the porous plate. The aluminum sheet was slid between the porous plate and a plywood support ring prior to putting sand in the storage bin. Flow of sand was initiated by rapidly pulling the aluminum sheet out from between the porous plate and shutter. Rad and Tumay (Reference 79) used a similar technique with a plastic sheet to start the flow of sand in their pluviator system.

During initial work on the pluviator, wind-induced bending of sand jets during sample formation was observed. Aluminum sheeting was used to fashion tubular protective shields to guard against the effects of wind currents. Shields were attached at the top and bottom of the diffuser. The bottom shield was designed to closely fit around the outside perimeter of the sample bucket. Figure 5 illustrates a sample being prepared with the protective shields in place.

The circular sample buckets were constructed of 1.27 centimeter thick aluminum. A 0.26 square meter base plate was welded to the bottom of the bucket, and reinforcing flanges were welded to the outside of the bucket at each corner of the base plate. Lifting holes for securing the completed bucket to a crane hook were drilled in the reinforcing flanges. The bucket was designed with a 14 centimeter standard height, to which up to an additional 31 centimeters height could be added using machined collars that bolted into four flanges welded to the exterior walls of the main bucket.

A wheeled cart was used to position the sample bucket within the pluviator, and to remove the completed sample from the pluviator with minimal disturbance to the soil. The base of the wheeled cart could be raised to allow manipulation of the F and H distances, with the maximum distances defined by the lowest position of the cart.

An initial series of tests was conducted to assess the performance of the pluviator, the levelness of the samples, and the uniformity and reproducibility of the samples at different F and H distances and with different porous plates. Results of the tests performed by Eid (Reference 81) on Monterey sand were used to provide an initial approximation to the minimum F and H distances required for the Ottawa sand. An F distance was initially fixed and samples were prepared at different H distances. This allowed determination of

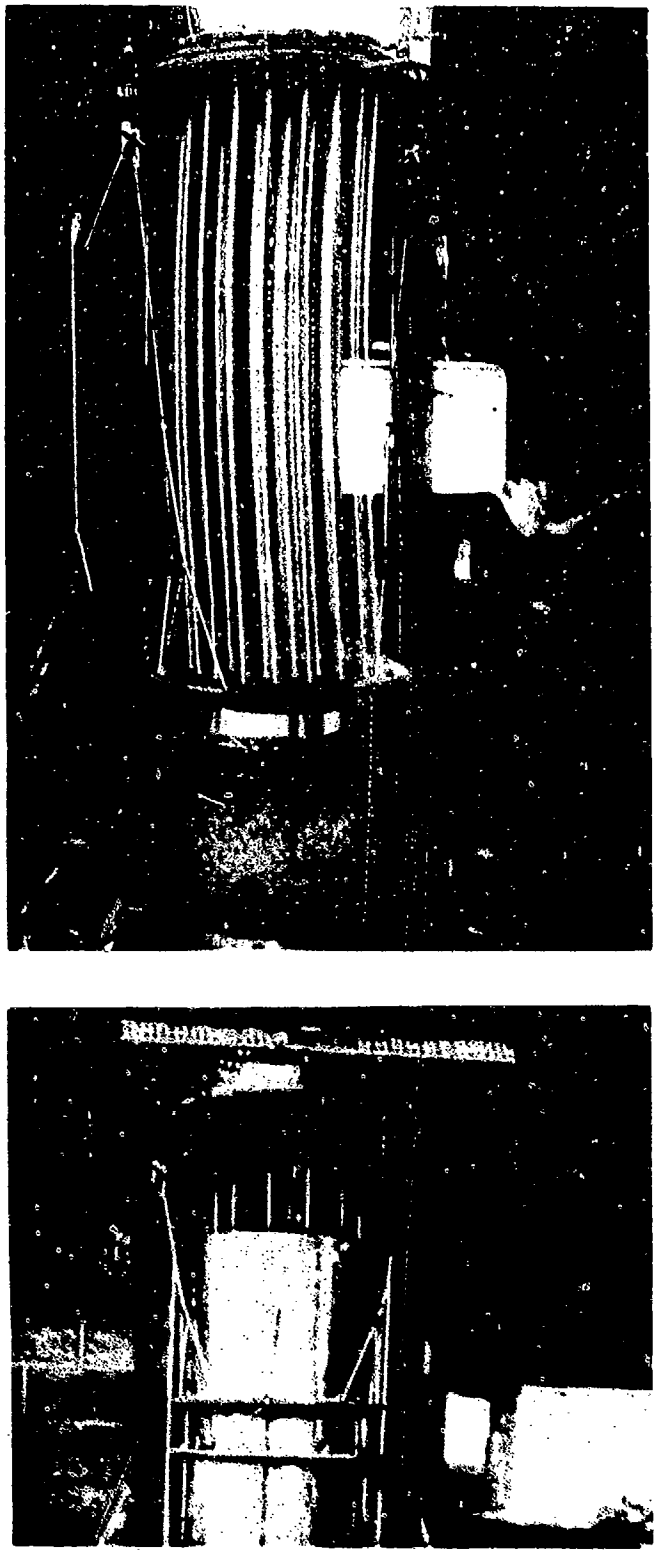

Figure 5. Sample Formation with Protective Shields In Place

the minimum H distance for the particular F value. The process was repeated for different F values until a minimum F distance was also established.

To test the uniformity of the samples, samples were prepared to different heights, while keeping all other test parameters constant, by pluviating the soil in both single and multiple lifts to the desired height. Density of the sample was determined after deposition of each successive soil layer, and for the completed soil sample. No specific controls were enforced for moisture content, but because of the high humidity at the centrifuge site, moisture contents were taken frequently--of the bulk soil prior to pluviation, and of the completed test sample at several locations within the test sample. Even under the most humid conditions, the moisture content was negligible, generally less than 0.1 percent and in no case greater than 0.3 percent. No variation in water content with sample depth was observed for the pluviated samples.

Kildalen and Stenhamar (Reference 80) used bubble levels and frame-mounted leveling screws to vertically level their sand rainer. Similar leveling of the pluviator frame alone was inadequate to obtain the level sample surfaces desired for the dense samples. It was necessary to level the individual component parts of the rainer with respect to each other and with respect to the wheeled cart holding the sample container. This was accomplished using a hand level and leveling wedges to position both the components of the pluviator and the sample bucket prior to each test.

3. Test Results

The initial trial tests indicated that samples could successfully and reproducibly be prepared at different densities with the constructed sand rainer. Further, no density variation with sample height was noted in the test samples. Trimming or other postsample formation leveling techniques were not required if proper care was taken in preparing the pluviator for tests.

Table 4 presents the properties of actual centrifuge samples prepared using the sand rainer, at an average density of 1.79 Megagrams/meter^3. An approximate sample height range sufficient to accommodate the anticipated projectile penetration depth without end effects was chosen for each test, and a sample was prepared accordingly. As shown in the table, samples were easily prepared within the desired range. Surface variations in elevation were measured with a profilometer accurate to 1

Table 4. RESULTS FOR CENTRIFUGE TEST SAMPLES PREPARED WITH OTTAWA FLINTSHOT SAND AT AVERAGE DENSITY OF 1.786 Mg/m³.

Desired Sample Ht. Range (cm)	Average Sample Ht. (cm)	Sample Density (Mg/m³)	Maximum Surface Variation (cm)
10.2 to 12.7	11.2	1.786	0.00
12.7 to 15.2	14.0	1.787	1.27
12.7 to 15.2	13.5	1.784	1.27
12.7 to 15.2	14.5	1.786	1.78
12.7 to 15.2	14.2	1.776	0.51
12.7 to 15.2	14.2	1.784	1.02
12.7 to 15.2	14.0	1.778	0.76
12.7 to 15.2	14.0	1.787	1.02
12.7 to 15.2	14.0	1.784	0.76
12.7 to 15.2	14.7	1.795	2.03
12.7 to 15.2	13.5	1.784	1.02
12.7 to 15.2	14.2	1.789	1.78
12.7 to 15.2	14.5	1.802	1.78
12.7 to 15.2	13.7	1.778	0.76
12.7 to 15.2	14.5	1.789	0.51
12.7 to 15.2	15.2	1.783	1.02
12.7 to 15.2	15.0	1.775	1.27
12.7 to 15.2	14.5	1.786	1.27
12.7 to 15.2	14.7	1.786	0.25
12.7 to 15.2	14.2	1.789	0.51
12.7 to 15.2	15.2	1.778	0.76
12.7 to 15.2	14.7	1.789	0.76
14.0 to 16.5	16.0	1.786	0.25
14.0 to 16.5	14.7	1.786	0.76
14.0 to 16.5	15.0	1.786	1.02
14.0 to 16.5	14.5	1.783	1.02
14.0 to 16.5	14.7	1.786	0.51
14.0 to 16.5	15.7	1.784	0.76
14.0 to 16.5	15.5	1.803	1.02
14.0 to 16.5	15.5	1.775	1.02
14.0 to 15.2	14.2	1.784	0.51
14.0 to 15.2	14.2	1.789	0.76
15.2 to 17.8	16.5	1.786	1.02
15.2 to 17.8	16.8	1.797	1.02
15.2 to 17.8	16.8	1.783	0.25
15.2 to 17.8	17.8	1.786	1.27
28.0 to 30.5	29.5	1.791	3.81
28.0 to 30.5	29.2	1.791	3.05

millimeter. The maximum measurements listed in Table 4 were typically caused by sample edge imperfections at opposite sides of the sample that resulted from leaks in the aluminum protective shields. The central portions of the samples, the regions into which projectiles were fired, were generally level within less than 1 millimeter. Figures 6 and 7 depict typical centrifuge test samples. The interiors of the sample buckets are ruled to illustrate levelness of the sample surfaces.

In accord with the conclusions reached by previous investigators (References 79 and 81), it was found that the most significant variations in density were obtained by varying the porosity of the perforated plate. Figure 8 illustrates the density variation that was obtained for Ottawa Flintshot sand, as well as the variation reported by Rad and Tumay (Reference 79) and Eid (Reference 81). It is clear from this figure that not only are the ranges of actual density values different, the observed decrease in density with increase in plate porosity varies significantly with soil type. Since all of the soils represented in this figure are uniform soils comprised of subrounded grains, actual grain size may influence the soil density/plate porosity relationship. A clear trend is not evident, however. The Ottawa Flintshot sand (D_{50} = 0.56) is a larger-grained sand than the two Monterey sands, which have fairly comparable grain size distributions. The mean particle diameter for Monterey #0 Sand is 0.36, while that for Monterey #0/30 sand is 0.45. It appears that selection of an actual plate porosity value for a given soil density must be determined experimentally for individual soils in the absence of a clear understanding of the relationship between plate porosity and soil type.

Figure 9 illustrates the variation in soil density with F distance obtained in this research for different test sands, as well as the variation reported by different investigators (References 79, 81 and 80). Very comparable trends are seen for the results of this research and the results reported by Eid. Rad and Tumay reported essentially no increase in soil density with increase in F distance over the four F distances they tested, although it appears likely from comparison to other results shown on Figure 9 that had they tested at smaller F distances they would have produced lower soil densities; in other words, the critical F distance for Monterey #0 sand is probably something less than 0.51 meters. Kildalen and Stenhamar's results actually showed a decrease in soil density with increase in F distance. The reason for this is not clear.

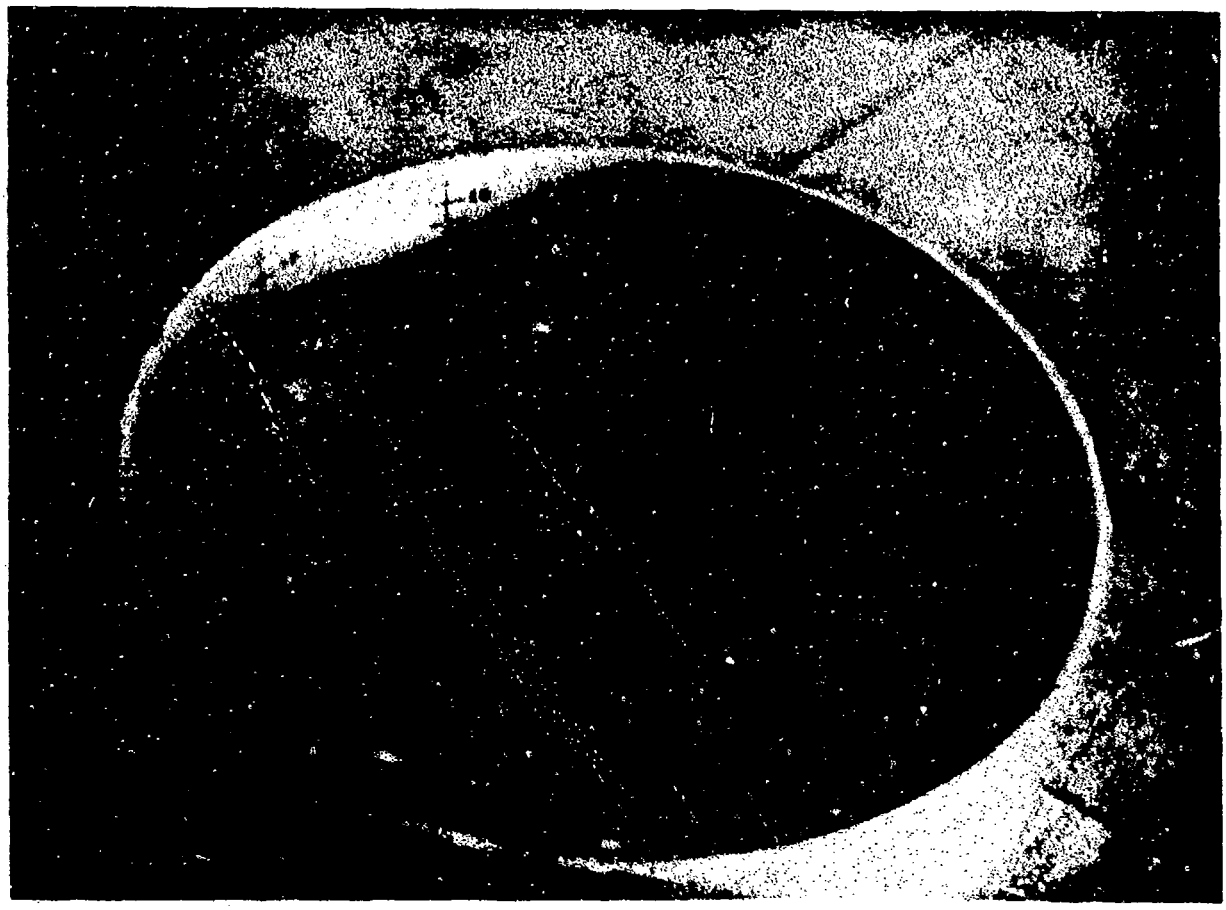

Figure 6. Typical 15 cm Centrifuge Sample Illustrating Levelness of Sample Surface

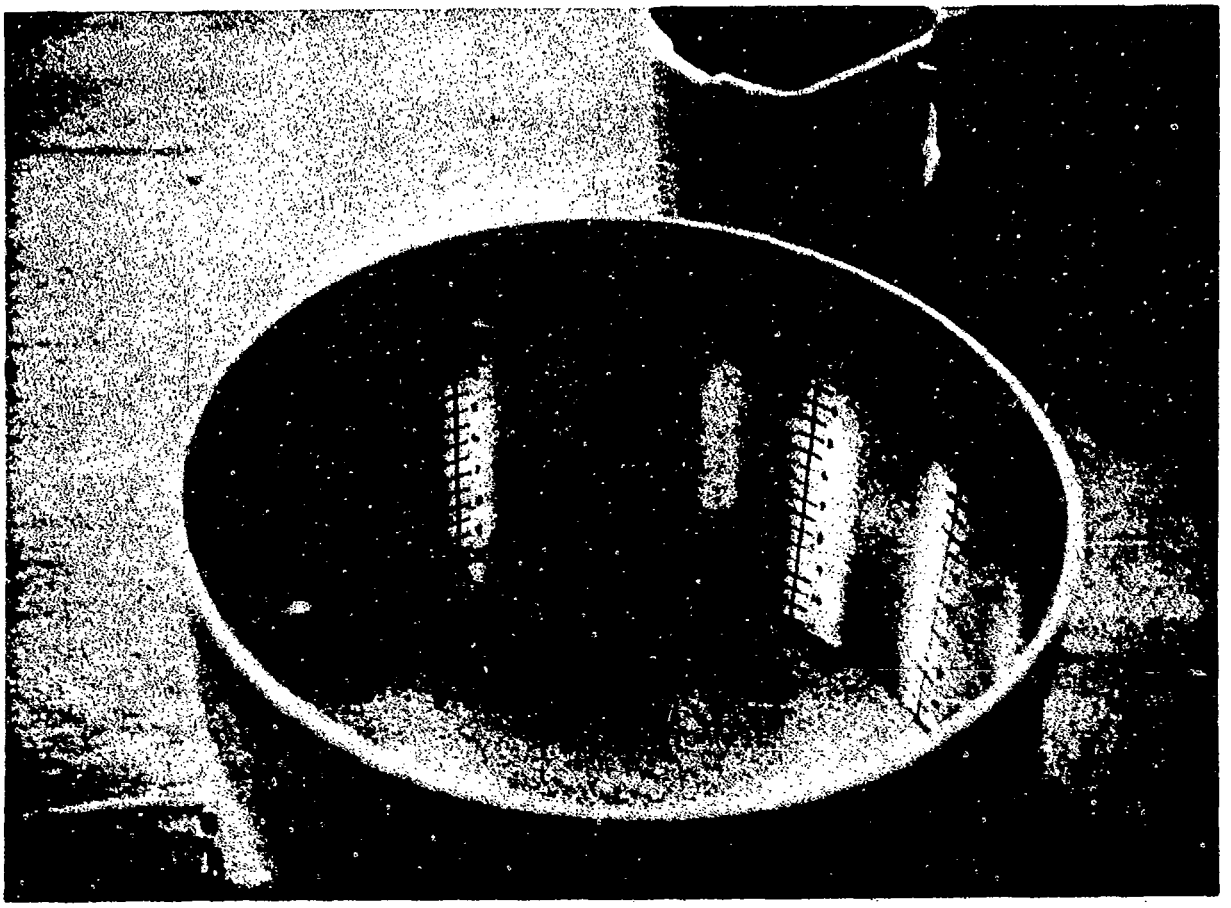

Figure 7. Typical 16.8 cm Centrifuge Sample Illustrating Levelness of Sample Surface

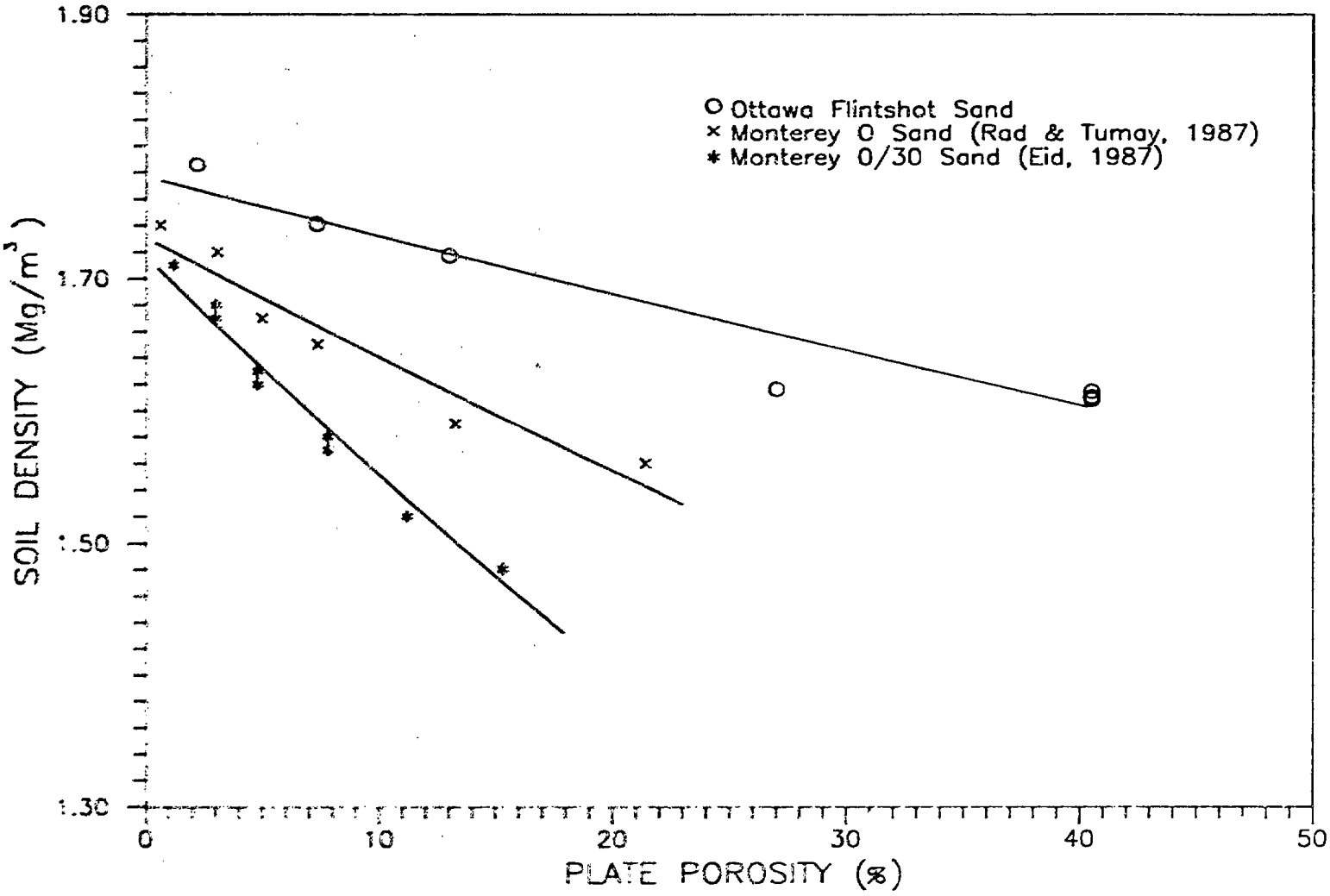

Figure 8. Plate Porosity vs. Soil Density for Different Sands

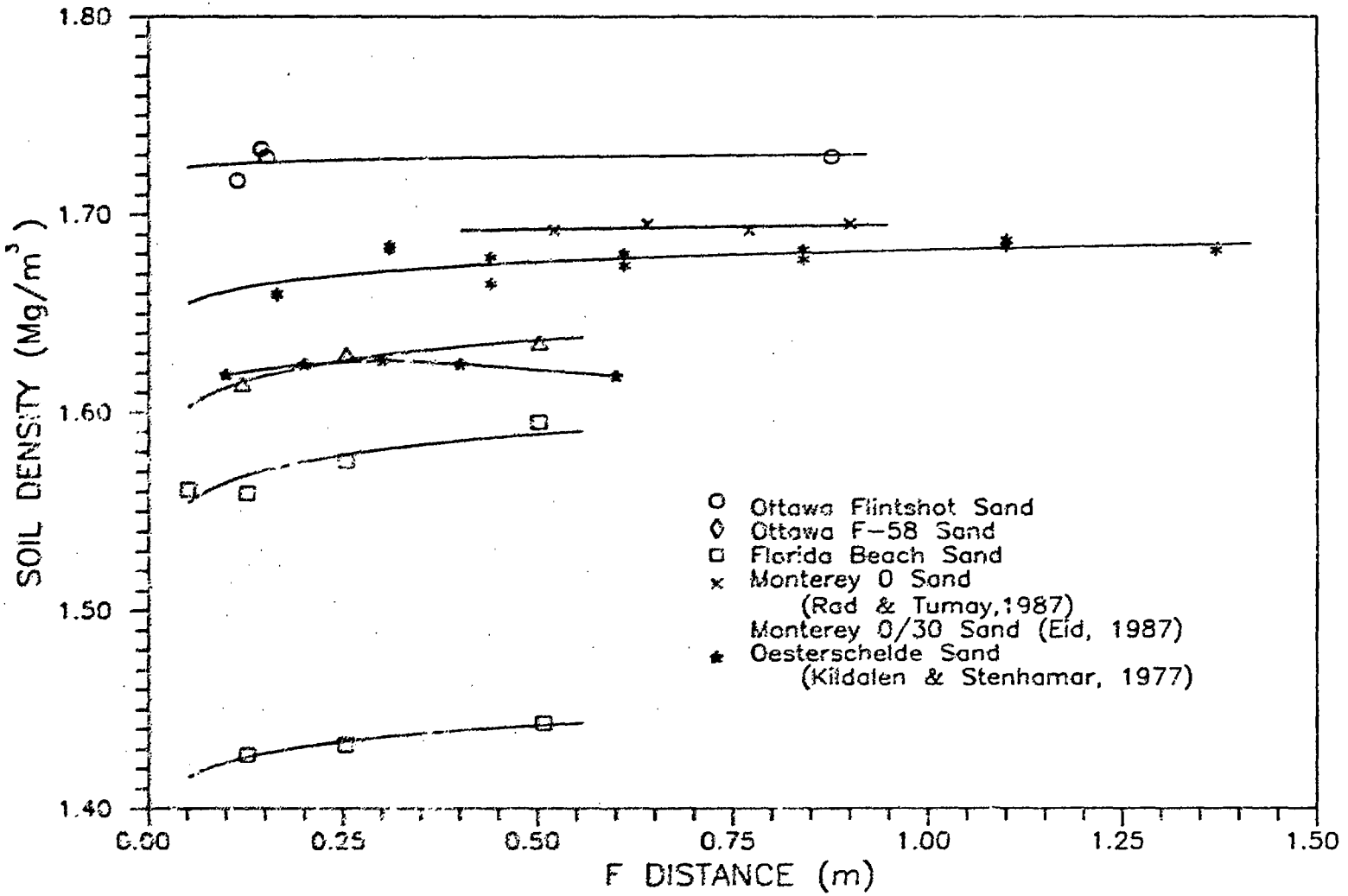

Figure 9. F vs. Soil Density for Different Sands

Figure 10 illustrates the relationship between soil density and H distance obtained for Ottawa Flintshot sand at different plate porosities over the range of F distances shown in the preceding figure. The lower magnitudes of soil density that can be obtained with higher plate porosities is also well illustrated in this figure. Figure 11 provides a comparison of soil density vs. H distance for Ottawa Flintshot sand and Florida Beach sand at the same plate porosity of 2.2 percent at an F distance of 0.51 meters. This figure also illustrates the soil density variation with H distance for Ottawa F58 sand at a plate porosity of 27 percent and an F distance of 0.15 meters. Figure 12 provides a comparison between the 2.2 percent porosity curve of Figure 11, and the cumulative results for Monterey #0 sand over the range of F values tested by Eid (1987) at a constant plate porosity. In all three figures, the increase in soil density with increase in H distance reported by Eid is evident. Less clear is the selection of a critical H value, as all of the curves exhibit some degree of continued increase in soil density with increase in H over the complete range of H values tested. A comparison of the curves for Ottawa Flintshot sand and Florida Beach sand in Figure 11 illustrates the different magnitudes of density obtained for different soils using an identical pluviator configuration.

C. PREPARATION OF MOIST SAMPLES

The centrifuge bucket used in the saturated tests was modified by attaching brass fitting and 0.64 centimeter tubing at four eqaully spaced locations just above the base of the bucket. Filters were placed inside the bucket at each of the four openings. A lid was constructed of 1.27-centimeter thick aluminum, with a rubber gasket placed around the edge to afford a better seal with the centrifuge bucket.

The moist samples were prepared from samples pluviated as described in the preceding sections. Water was used to prepare the test samples for testing under 1-g conditions as well as at elevated g levels. Although glycerin had been planned for use in the saturated centrifuge test samples (to allow proper modeling of pore water dissipation rate at g levels greater than one), acquisition problems prevented this. Consequently, a limited number of centrifuge tests were conducted on nearly saturated test samples, and these samples were prepared using water.

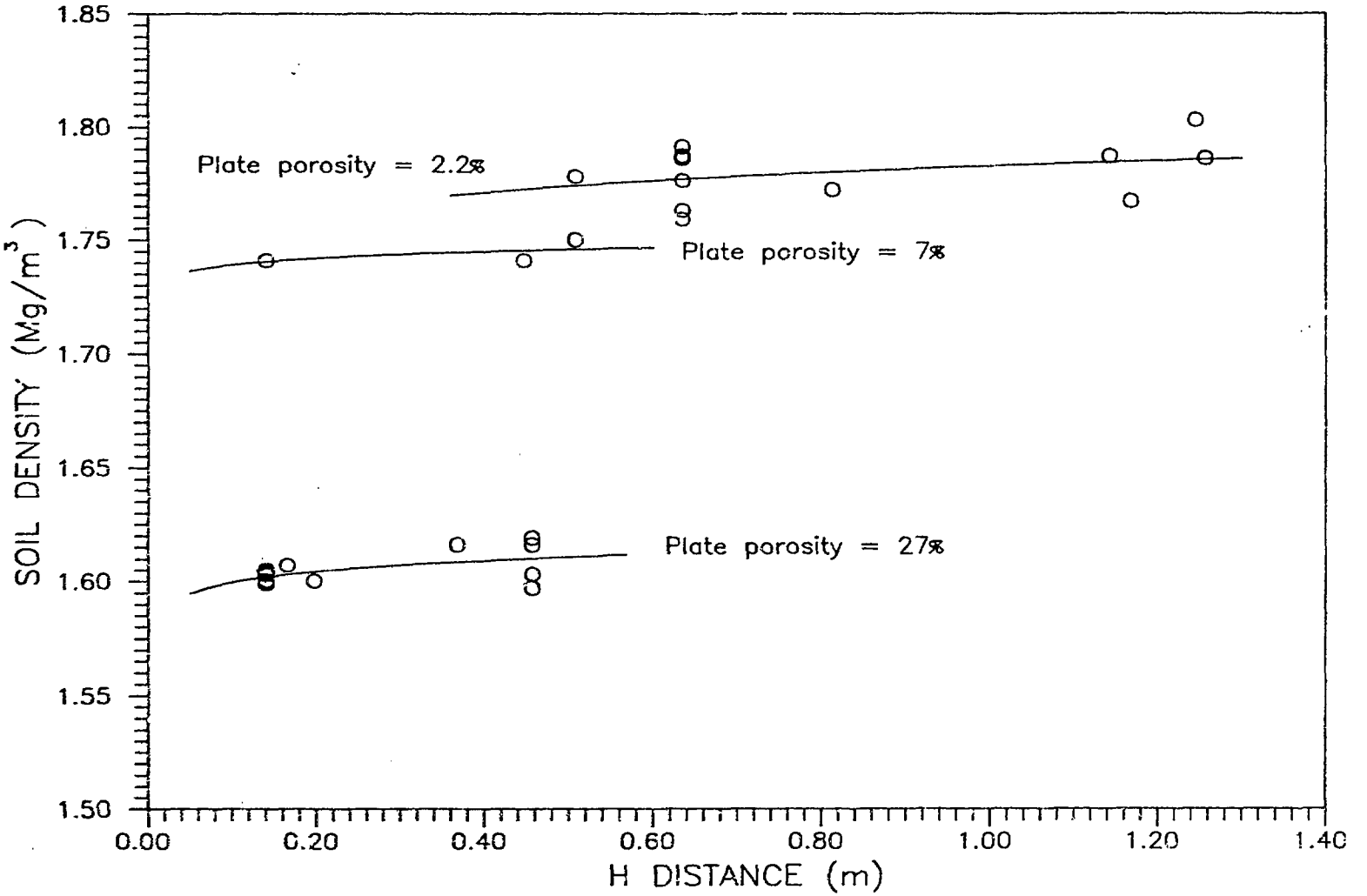

Figure 10. H vs. Soil Density for Ottawa Flintshot Sand

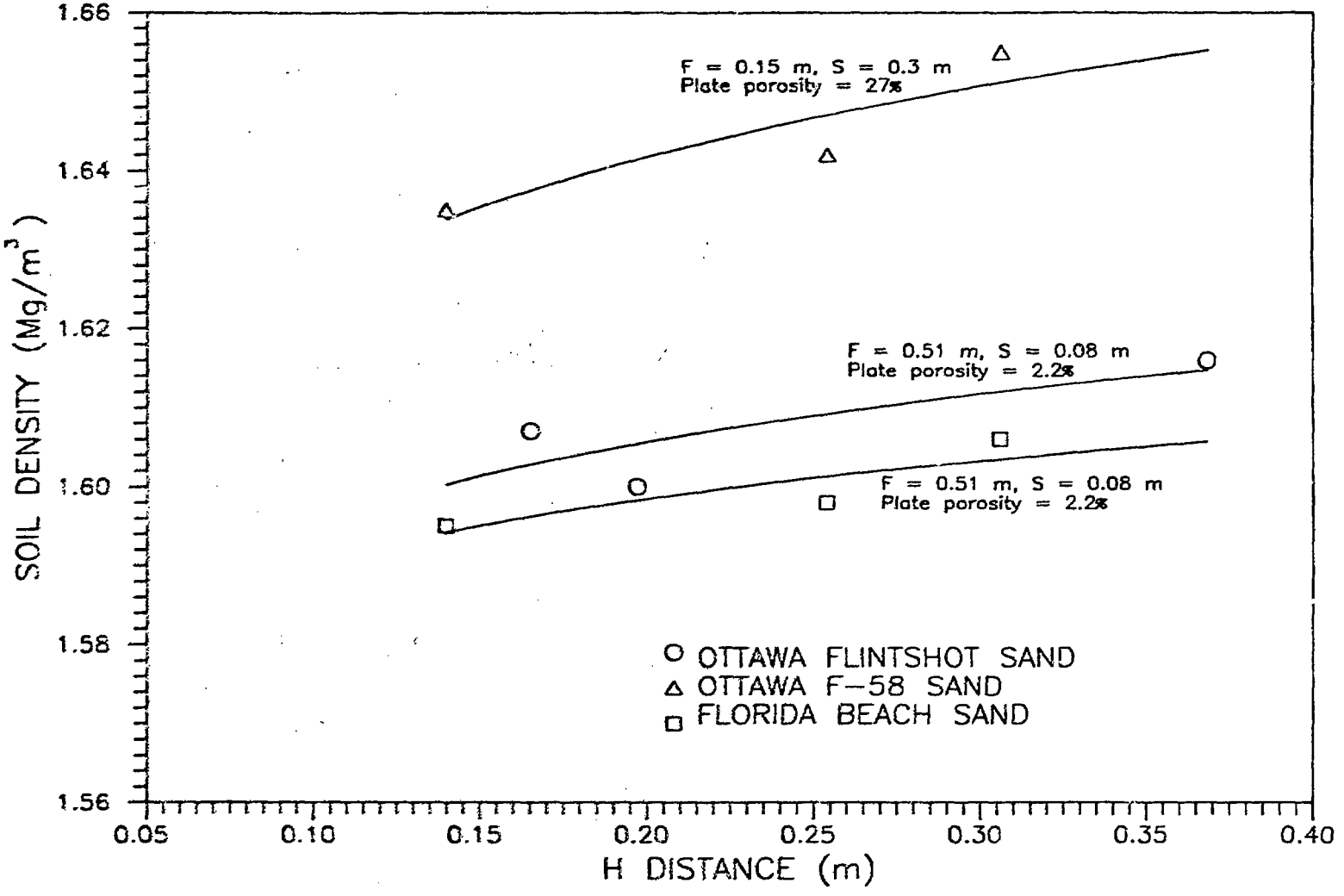

Figure 11. H vs. Soil Density for Different Test Sands

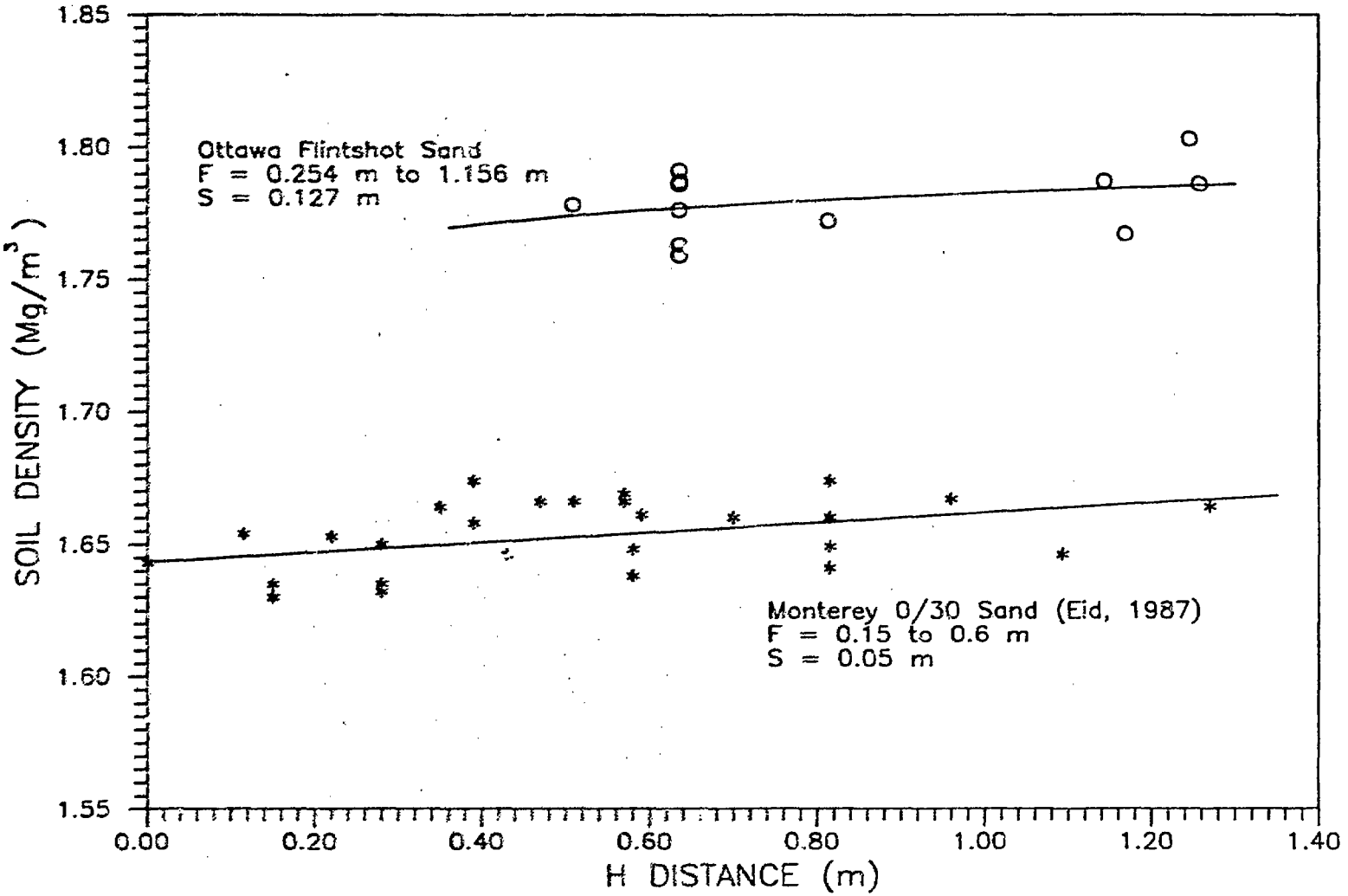

Figure 12. H vs. Soil Density for Ottawa Flintshot and Monterey 0/30 Sand

Several techniques were employed in attempting to saturate the samples. Although 100 percent saturation could not be achieved, nearly saturated samples were successfully produced. A vacuum was initially drawn from the top of the pluviated sample through a fitting attached to the bucket lid, with water pulled in through the bottom. This technique was ineffective because sand was pulled into the system along with the water, and because the soil in the vicinity of the water intake valves was disturbed. To alleviate the first difficulty, an aluminum collar was placed on top of the sample bucket, leaving a significant air space between the top of the sample and the vacuum port. To alleviate the second difficulty, the rate at which water was allowed to enter the sample was reduced; however, sample disturbance of the soil around the intake valves still occurred. A third technique employed for saturation abandoned the top evacuation system in favor of a split manifold system. The bucket lid was sealed to the bucket and both vacuum and water lines were routed into the bottom of the bucket. After drawing as much vacuum as possible, water was allowed to slowly enter the system, over a period of approximately twelve hours. Although nearly saturated samples appeared to be produced with this technique, sample disturbance above the intake ports still occurred. This problem was augmented by the extremely loose pluviated samples that were prepared for this series of tests.

The samples used to illustrate effects of capillarity were prepared by wetting the sample through one of the above techniques, and then allowing the sample to drain.

SECTION V

FACILITIES, EQUIPMENT AND TEST PROCEDURES

A. CENTRIFUGE FACILITY

Testing was conducted at the Air Force Engineering and Services Center (AFESC) centrifuge facility at Tyndall AFB. This facility operates a 15 g-ton capacity centrifuge (Figure 13), with a maximum payload of 136 kilograms at a maximum acceleration of 100 g's, and an ultimate payload of 227 kilograms at up to 60 g's. A hydraulic drive system is used to operate the centrifuge.

The centrifuge is housed inside a 4.9-meter diameter, 2.1-meter high, 0.23-meter thick reinforced concrete structure (Figure 14). The interior of the structure is painted with epoxy paint to make these surfaces as smooth as possible, thereby minimizing power consumption during centrifuge operation. Twelve equally spaced, sequentially numbered vertical lines are painted on the interior walls of the centrifuge housing to enable the position of the centrifuge to be determined via video from a separate control room. Access to the centrifuge is provided by removable ladders through two hatches in the steel roof. The hatch doors are equipped with safety interlock switches that prevent operation of the centrifuge while the doors are open. A rotating red warning light is mounted in a prominent position above the centrifuge housing, and is automatically activated whenever the centrifuge is operated.

The Model E-185 centrifuge was manufactured by Genisco, Inc. of California. It was originally installed at Kirtland AFB, Albuquerque, New Mexico and used for testing avionics and mechanical payloads at g-levels encountered during flight. In 1981 the centrifuge was modified for studying blast parameters in soil. This modification was undertaken to allow the cradle-type payload platforms to operate freely in a "swing mode" during centrifuge operation. In 1986 the modified centrifuge was shipped to Tyndall AFB, where efforts to update and improve instrumentation are underway.

The 1.83 meter radius centrifuge is classified as a small centrifuge. The 0.58 square meter payload platforms are attached to two symmetrical cantilever arms. These arms are integrated with an automatic dynamic balancing system that vertically adjusts placement of the arms during centrifuge operation. Limit switches activate automatic shutdown if balance cannot be obtained within the

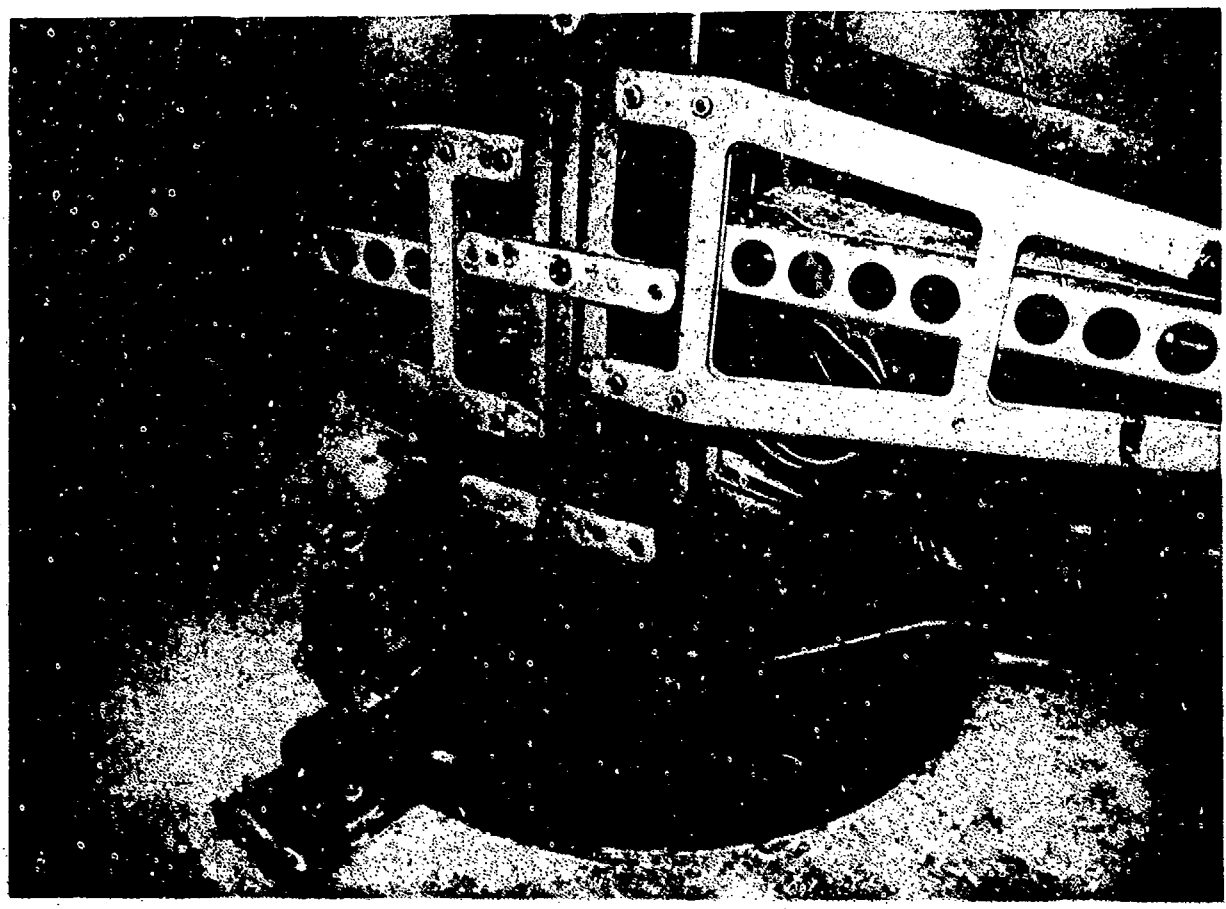

Figure 13. Tyndall AFB Centrifuge

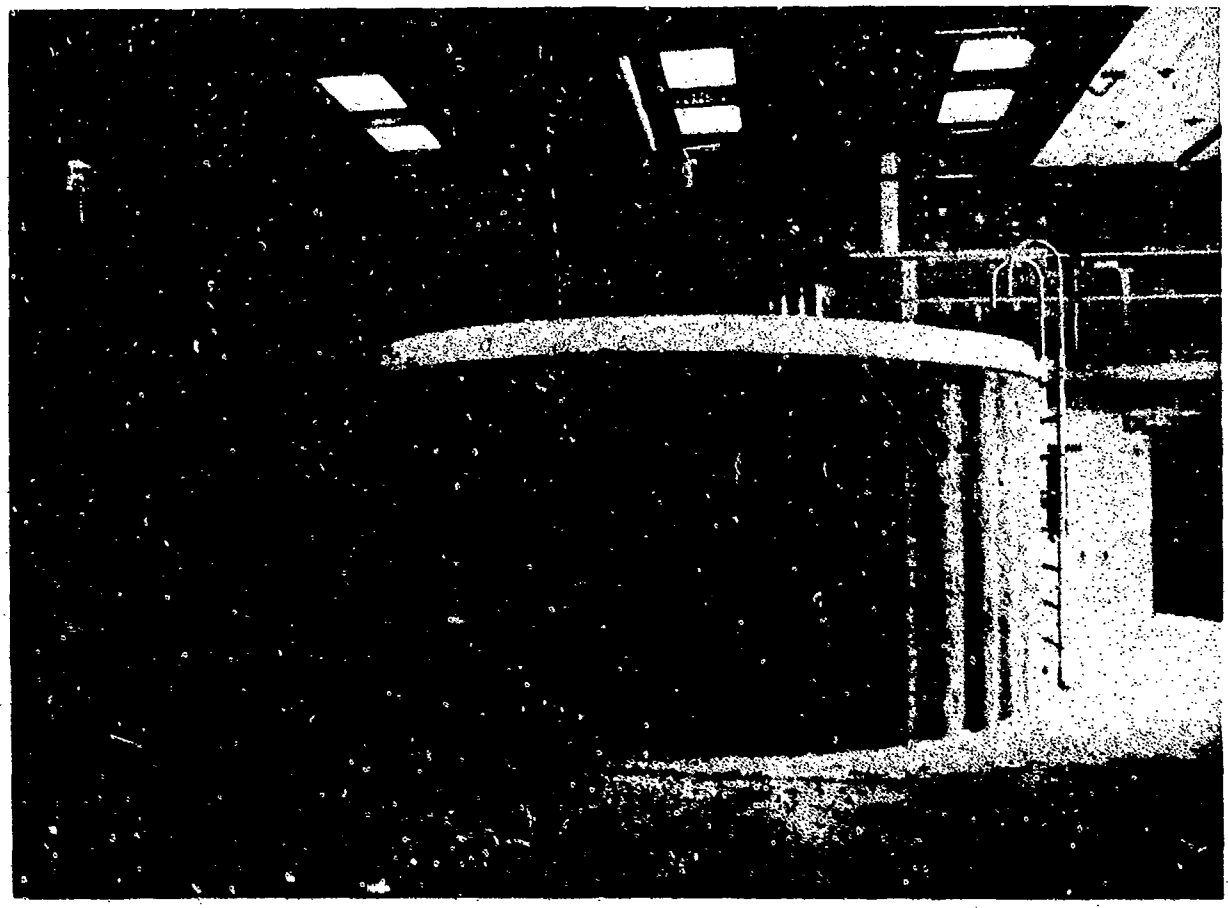

Figure 14. Tyndall AFB Centrifuge Housing

0.3-meter travel limitations of the self-balancing mechanism. In addition to the swing mode operation, the payload platforms may be locked into horizontal or other intermediate positions for testing.

The centrifuge is operated from the separate control room. A video monitor and recorder, connected to a video camera mounted on the hub of the centrifuge, is used to monitor events inside the centrifuge housing during testing. Twenty-eight slip rings are available for instrumentation exchange between the centrifuge and the control room.

Four key-operated safety switches on a control console must be unlocked before the centrifuge can be operated. A manually operated handwheel is used to vary rotor speed by increasing or decreasing hydraulic pressure. Rpm are displayed on a digital monitor. An emergency stop button can be used to quickly stop rotation if rapid termination of testing is necessary. A forward-reverse switch can be used to choose direction of rotation. Balance and payload platform verticality indicator lights are also located on the control console; these lights will illuminate if the self-balancing mechanism is activated during rotation to reestablish dynamic balance, and whenever the payload platform has rotated into a vertical position. Limit indicator lights will illuminate if static balance of the centrifuge arms is not achieved before attempting to operate the centrifuge; operation is prevented until the rotor arms are satisfactorially adjusted. A static overload warning switch will be activated if the maximum static load is exceeded during test set-up.

B. FIRING ASSEMBLY

1. Gun Selection, Modification and Mounting

A Thompson/Center Arms Contender® bull-barrel model pistol was used as the firing mechanism for the penetration tests. The single shot, break open action pistol is a unique handgun in that its frame accomodates interchangeable barrels that are chambered for a variety of cartridges. This feature allows a single gun to be used to fire a variety of projectile sizes without the use of sabots.

The bull barrel model was selected because the outer diameter of the barrels, unlike that of other types of barrels, is identical for all calibers. This allows the same centrifuge mounting arrangement to be used for all calibers.

Barrels in 22, 30, 35 and 44 caliber, chambered for 222 Remington, 30/30 Winchester, 35 Remington and 44 Remington Magnum cartridges were used in the tests.

Gun barrels are designed to serve a dual purpose. A fired projectile is accelerated as it travels down the entire length of the barrel. At the same time, interior riffling induces a spin on the projectile which helps to stabilize it during flight after exiting the gun barrel. Acceleration of the projectile within the gun barrel was not necessary to achieve the velocities of interest for the projectiles used in this research. Consequently, the barrels were modified by shortening the standard 25 centimeter and 36 centimeter lengths to approximately 18 centimeters, to lessen effects of g-forces on the free end of the barrels and to reduce the weight of the gun assembly. Similarly, the stabilization of projectile trajectory was not a concern for the projectiles used in this research. Therefore, the barrels were smooth-bored to remove interior riffling and eliminate induced spin. To ensure the legality of these modifications, approval was obtained from the United States Department of the Treasury Bureau of Alcohol, Tobacco and Firearms in accordance with the National Firearms Act, per the research organization provisions of the Federal Register Rules and Regulations for Commerce in Firearms and Ammunition.

The design of the AFESC centrifuge is such that the pistol could not easily be mounted on the rotor hub; instead, the pistol had to be mounted at some distance along the rotor arm of the centrifuge, away from the center of rotation. As a consequence of the g-forces to which the pistol would be subjected in this location, and because of the need to control the angle of impact for these tests, special mounting arrangements were designed. The modified pistol was attached to an aluminum swivel plate assembly. This swivel plate assembly allows positioning of the gun barrel at angles up to 35 degrees from the radial direction of the centrifuge. The gun plate assembly is pictured in Figure 15.

Four 2.5 centimeter diameter gears were attached to the bottom of the lower plate on machined axles. These gears were designed to ride along racks mounted to the rotor arm platform of the centrifuge. The network of rackgears was designed to minimize modification to the rotor arm platform of the centrifuge, but at the same time allow for very flexible positioning of the gun. The rack gears were mounted parallel to the radial direction of the centrifuge together

Figure 15. Gun Plate Assembly

with a series of three parallel aluminum tiebars and three perpendicular slotted aluminum crossbars. The gun assembly can be moved radially by simply rolling back and forth along the rack gears. After moving the gun assembly to the desired radial location, it is fixed in place using specially designed clamps on each side of the gun plate.

Nine screws attach the tiebars directly to the the rotor arm platform. Loosening these screws allows the rack gear network to be slid in a direction perpendicular to the radial direction of the centrifuge. This provision, coupled with the radial movement allowed by the rack gears and the angular positioning of the gun barrel allowed by the upper swivel plate, permits variable positioning and aiming of the gun.

This necessary freedom of movement is a consequence of the g-forces to which the gun would be subjected as a result of mounting it on the rotor arm platform. Angle of projectile impact was a function of the radial position of the gun along the rotor arm platform, the eccentricity of the gun with respect to the center line of the rotor arm platform, the angle of the gun barrel, the velocity of the projectile, and the g-level at the sample surface. A computer program (Appendix D) was used to iteratively solve the equations of motion to determine the angle of the barrel and the eccentric mounting of the gun with respect to the center line of the rotor arm, for a given velocity, g-level and position of the gun along the radius of the centrifuge. A sensitivity analysis of the iteration increment in gun angle was performed, and the value used in the iterative process was chosen to provide solutions with accuracies comparable to those that can be obtained in the mechanical positioning of the gun. The effect of drag was ignored in the calculations, as the projectile path would be extremely short (less than 0.9 meters). Tests proved this omission justified. Figures 16 and 17 present gun angle and eccentric mounting requirements, respectively, for different g-levels.

2. Triggering

The initial design of the gun assembly included a solenoid mounted on the upper plate in conjunction with an eccentric aluminum mechanical arm that was positioned to contact the gun trigger. The solenoid was wired through slip rings to a portable D.C. power unit in the centrifuge control room. A push button on the power unit remotely activated triggering by applying current to the

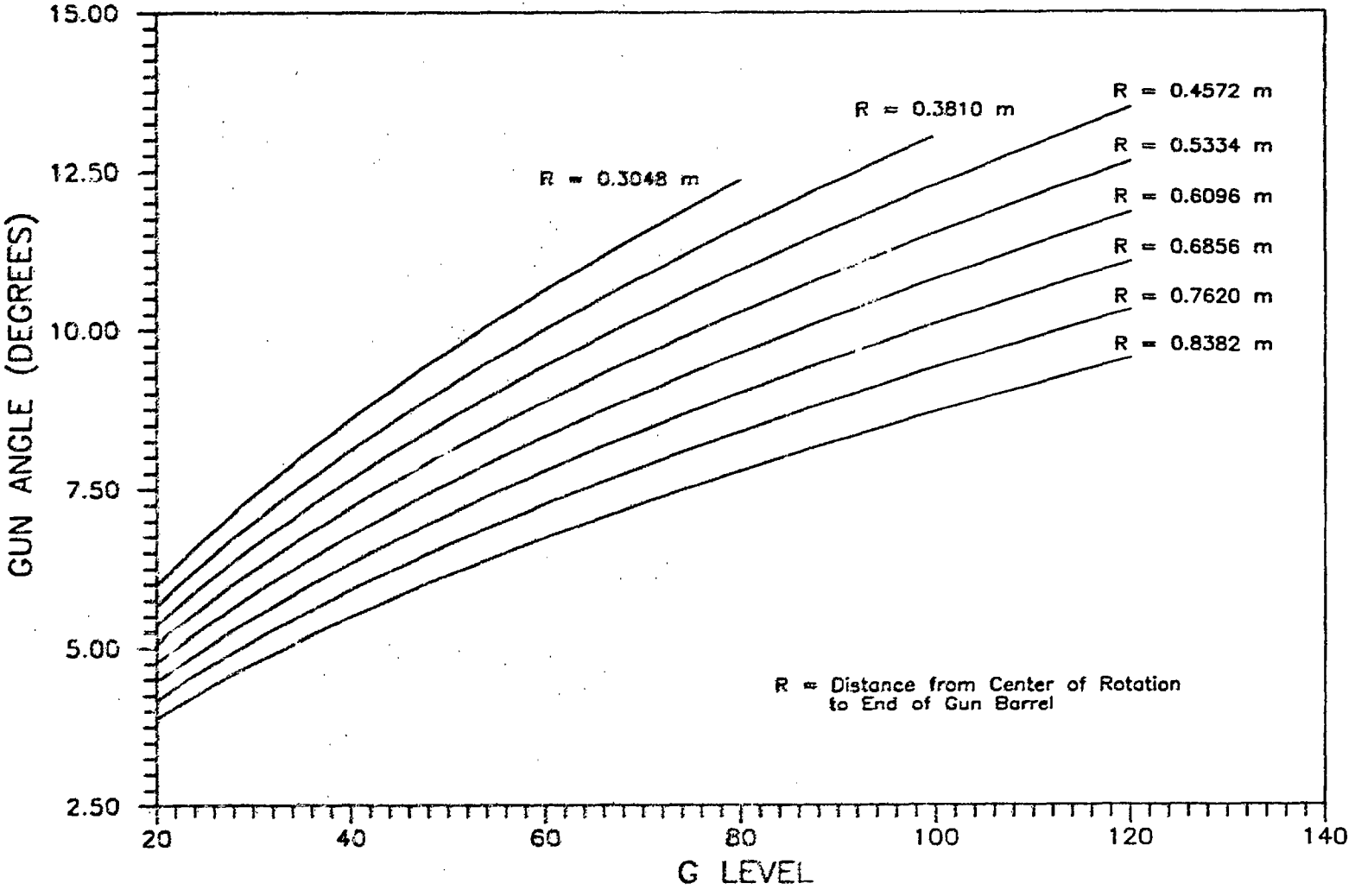

Figure 16. G-level vs. Gun Angle for Projectile Velocity = 305 m/s

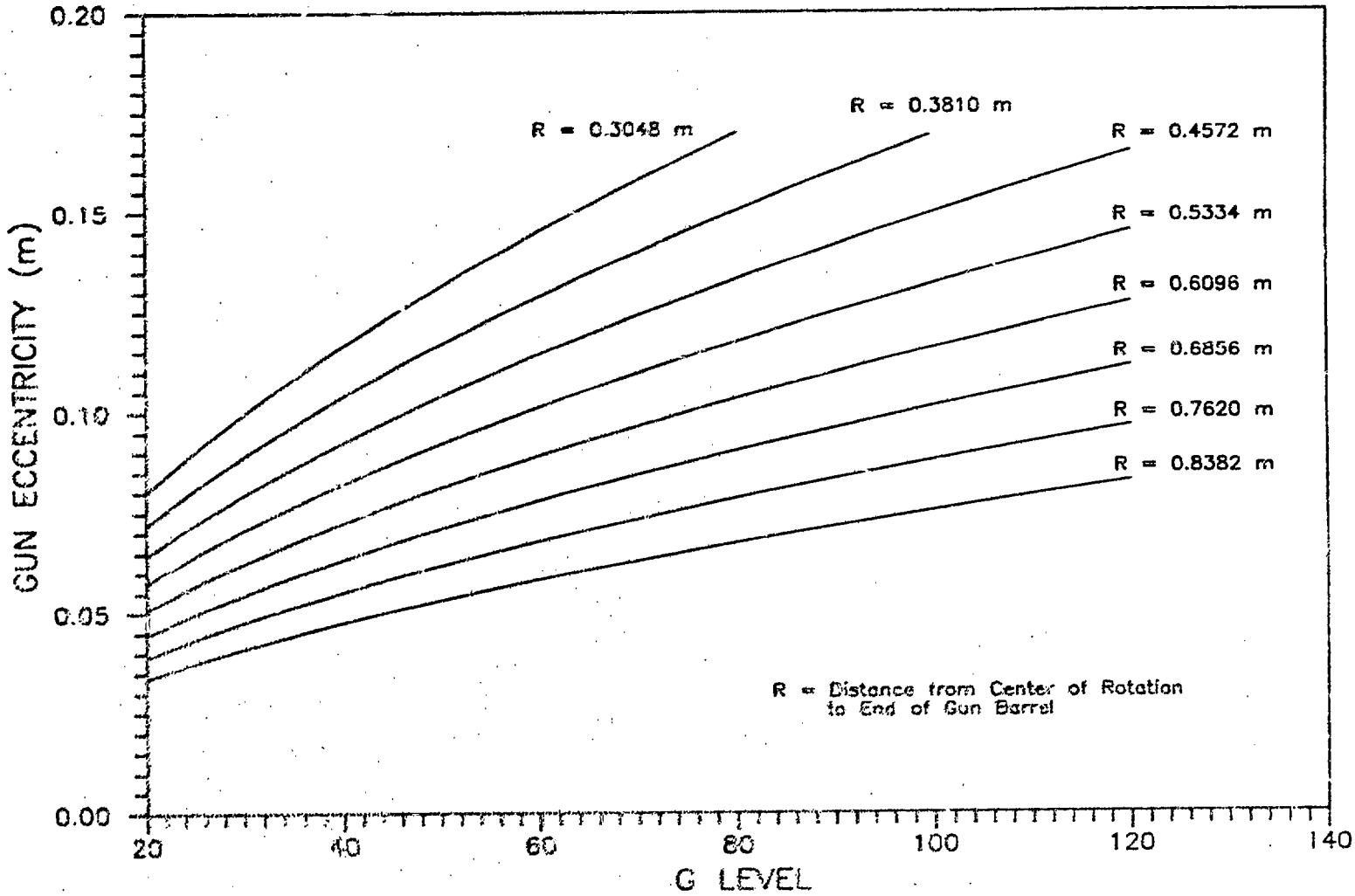

Figure 17. G-level vs. Gun Eccentricity for Projectile Velocity = 305 m/s

solenoid, causing the solenoid piston to pull in, the eccentric arm to rotate and the trigger to be depressed.

With this triggering configuration, the solenoid piston was mounted nearly parallel to the radial direction of the centrifuge and movement of the solenoid piston would potentially be augmented by the g-forces acting in this direction, promoting the potential for pretriggering. During centrifuge shakedown testing, pretriggering occurred at 50 g's. A new solenoid/arm mechanism was subsequently devised that positioned the solenoid with the piston action essentially opposing that of the g-forces. With this arrangement, although the dangerous potential for pretriggering was eliminated, it was impossible to trigger the gun at g levels greater than 60.

A new remote triggering system was developed, which used two small, high-torque servomotors mounted in tandem behind the gun. A thin, low-mass rod was mounted to the motors and extended forward to the gun trigger. A small metal cup, welded to the end of the rod and conforming to the curve of the trigger, is used to depress the trigger. Upon activating the motors using the D.C. power source in the control room, the rod is pulled back, bringing the metal cup in contact with the trigger. As power supply to the motors continues, the rod and metal cup are pulled back farther, depressing the trigger. This firing system, unlike the solenoid system which produces triggering virtually simultaneous with push-button power activation, requires approximately 2 seconds for the rod to be pulled a sufficient distance to trigger the gun. This delay had no impact on the centrifuge tests. The servomotor triggering arrangement permitted remote triggering at all g-levels up to 100 (the maximum capability of the centrifuge) with no potential for pretriggering. In addition, the servomotor system was considerably safer then the solenoid system during the loading and cocking of the gun, because the metal cup used to depress the trigger was not actually in contact with the trigger until the servomotors were activated remotely from the control room.

3. Projectiles and Reloading

As previously discussed, the importance of projectile shape has been documented by a number of investigators. Therefore, tests for this research were designed to keep this penetration parameter constant by using equidimensional projectiles. Standard spheres of nylon, polyvinyl chloride (PVC),

aluminum and brass in 6.35, 7.94, 9.53 and 11.11 millimeter diameters were used. A small seating collar was machined around the perimeter of the spheres at diameters of 5.69 millimeters for the 6.35 millimeters spheres, 7.82 millimeters for the 7.94 millimeters spheres, 9.09 millimeters for the 9.53 spheres, and 10.92 millimeters for the 11.11 millimeters spheres. The collars machined at these diameters corresponded respectively to 22, 30, 35 and 44 caliber dimensions. This technique maintained a nearly spherical shape for the projectiles, but allowed the projectiles to be seated adequately in standard center-fire Winchester® brass cartridge cases.

Cannister-grade, fast-burning Hercules Bullseye® smokeless pistol powder was used to load the cartridges. A fast-burning powder was selected because of the small loads anticipated and the possibility of erratic burning and excessively high chamber pressures being generated by use of a slow-burning powder in conjunction with light loads. A standard RCBS® reloading press, with seating and resizing dies for all four calibers was used. The reloading press was mounted on a portable plywood stand to allow easy reloading, both in the field and at the centrifuge site (Figure 18).

Reloading began with inspection of the brass cases for such defects as neck cracks, expanded primer pockets or bulges in the case. Cases were then measured with a micrometer to make certain the lengths were less than the specified maximums and did not require trimming. A burring tool was used to slighily bevel the inside of the neck of the cases to be used with nylon and PVC projectiles. This was done to avoid shaving material from the projectiles when pressing them into the brass case during seating. Next, the cases were lubricated, using a lube pad for the exterior of the cases and a neck brush for the interior of the cases. The cases were then resized using standard resizing dies. This process redimensioned the cases to properly seat the bullet and to allow proper fit of the cartridge in the gun chamber. This step also removed spent primers and exposed the primer pockets for light cleaning with a primer pocket brush prior to seating the primers into the primer pocket. The appropriate powder charge was then carefully weighed on a reloading scale and poured through a funnel into the primed case. The final step was to seat the projectile into the charged case using the seating die. Because of the non-standard shape of the projectiles, this step required extremely careful positioning

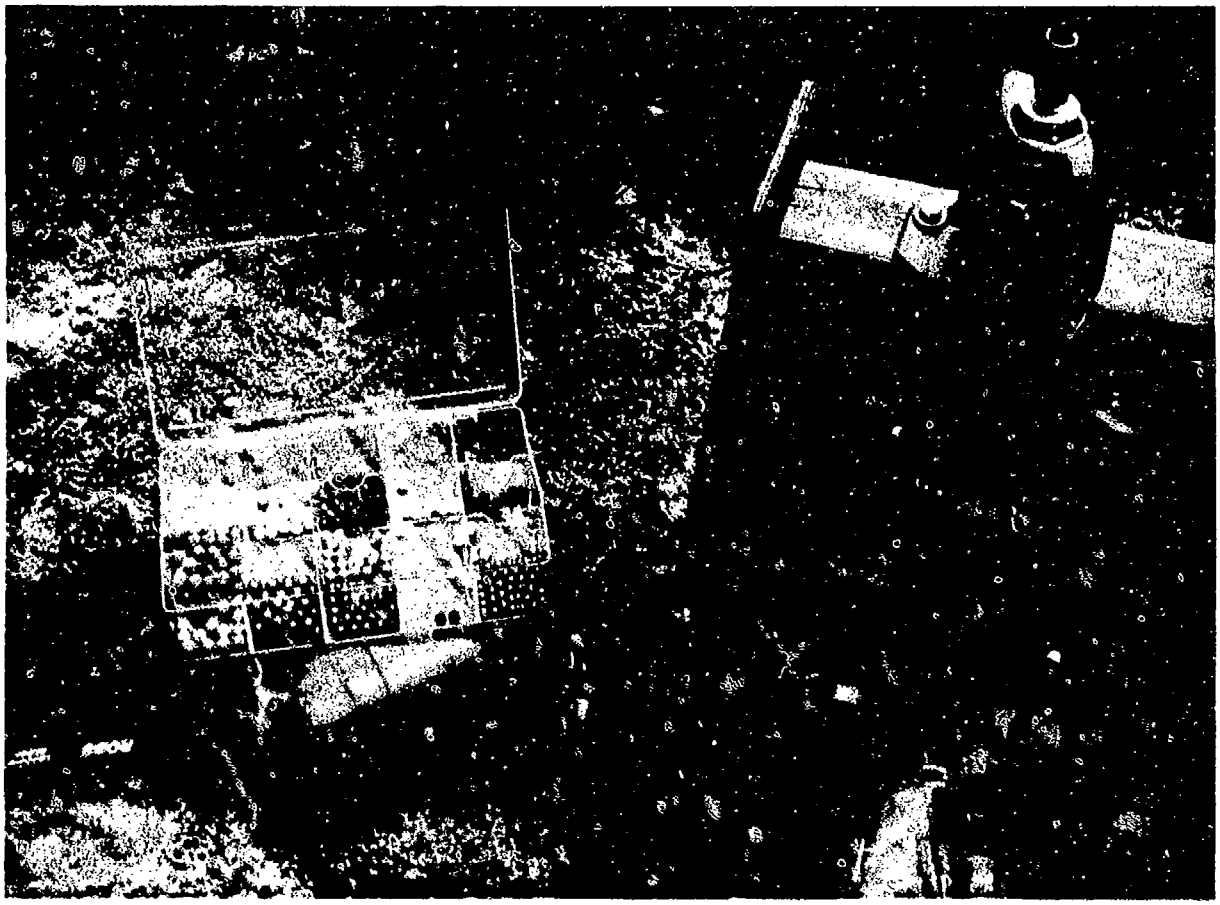

Figure 18. Reloading Equipment and Supplies

of the projectile on the mouth of the case before manipulating the loading press arm.

No information was available on quantities of powder necessary to obtain the velocities of interest (approximately 305 meters per second, compared to typical velocities around 670 meters per second for commercially marketed ammunition) for the nonstandard projectiles. Thus, it was necessary to use trial and error to determine appropriate charges. This process involved beginning with extremely small charges, and gradually building up the charge in very small increments. As the increase in velocity with amount of powder does not follow a linear relationship, extrapolation could not be used. Significant increases in velocity could suddenly occur with very slight increases in charge. Similarly, it was possible to achieve decreases in velocity with increases in quantity of powder depending on the internal pressures generated as a function of such variables as air space within the cartridge. After each trial shot, measured velocity, quantity of charge, projectile material and seating depth were recorded for each caliber. The condition of the case and the spent primer were inspected to assess performance and integrity, and were checked for indications of excessive pressure. Quantities of unburned powder were noted and adjustments to the charges made accordingly. The resulting powder charges determined were very small, typically 1.6 to 7 grains (0.1 to 0.45 grams). These low charges frequently resulted in a small amount of primer set-back (expulsion from the primer pocket) upon firing, but not enough to create any difficulties with cartridge extraction from the chamber.

To help obtain more consistent velocities at these small loads, polyester fiber fill was used in the 222 Remington, 30/30 Winchester and 35 Remington cartridges to contain the powder near the primer. In addition, cases were primed with CCI® Magnum primers, which produce a longer burning, hotter flame than standard primers. These primers were used in an effort to compensate for the considerable amount of air space in the loaded cartridges due to the very low charges, and for the accumulation of powder away from the primer when the cartridge was loaded into the centrifuge-mounted gun. Proper seating of the primers into the primer pocket was extremely critical to avoid misfires and promote consistent primer performance.

Because of the limited contact area between the sides of the projectile and the walls of the brass cases, friction (seating depth) was generally

not as significant a factor in projectile speed as it would be for typical bullet shapes; however, the projectiles were all seated to depths that maximized the contact area of the machined seating collar. This was done to ensure a better fit between the projectile and the case, such that the gas pressure-generated expansion of the forward portion of the case upon firing formed a sufficiently tight seal in the cartridge chamber to prevent rearward escape of gases. The most significant variable affecting velocity was generally the quantity of powder. For some projectile material/case combinations, velocity was essentially generated by explosion of the primer alone.

C. PRELIMINARY TESTS

1. Velocity Determination Tests

Velocities were determined using an Oehler Research, Inc. Model 33 digital chronograph with two photosensitive velocity detectors. Over 200 preliminary velocity determination tests were conducted to establish the required amounts of charge and fiber fill for each projectile material and caliber. These tests were conducted outdoors by firing horizontally across the chronograph detectors into sand bags. The gun was held in position by mounting it on the swivel plate assembly and attaching the assembly to a folding stool by means of a bar clamp. Because of the loading uncertainties involved in the trial velocity determination tests, the gun was triggered remotely by pulling a string attached to the trigger.

The reproducibility of velocities obtained through these tests was generally within 3 percent (6 to 10 meters per second). Because of this excellent reproducibility, and space and lighting limitations on the centrifuge, projectile velocity in the centrifuge tests was determined by charge size. The validity of this approacg was substantiated during testing, as discussed in Section VI.

2. 1-g Tests

The ability to control velocity was further assessed during a series of 1-g tests conducted before centrifuge testing. These tests were conducted at measured projectile velocities between approximately 150 and 315 meters per second. The tests were used to supplement the velocity determination test data and the pluviator test data, and to determine a "safe" sample height prior to

centrifuge testing. The primary goal of the tests was to establish a basis for comparison between 1-g and higher g penetration test data. If a difference was observed between 1-g and centrifuge data for the same test event (for example, a 44-caliber brass projectile fired at 305 meters/second under both 1-g and elevated g conditions), then some degree of gravity dependence for the penetration event would be suggested.

A simple wood box-shaped frame (Figure 19) to hold the gun assembly in a vertical position was constructed. The gun assembly was attached to the frame with the bar clamp used in the velocity determination tests. The chronograph detectors were mounted to the frame in line with the end of the gun barrel. A floodlamp was aimed at the chronograph detectors to provide adequate lighting for the indoor tests. Prepared samples were wheeled on the sample carts into the frame and positioned beneath the gun. As in the velocity determination tests, the modified gun was triggered remotely using a string attached to the trigger.

Final penetration depths were measured using a profilometer designed to rest along the top of the sample buckets for dry test samples, the impact crater was carefully excavated by hand until the top surface of the fired projectile was exposed. A profilometer rod was extended to the top of the projectile, and the distance between the initial soil surface level and the projectile location was measured to an accuracy of +/- 1 millimeter. This process was repeated three times for all tests, with the profilometer reinitialized and repositioned on the sample bucket before each measurement. The projectile was then carefully extracted, the impact surface was noted, and the appropriate projectile dimension was added to the measurement obtained from the profilometer to produce the final penetration depth.

For moist test samples, the same procedure was followed except, prior to excavating the impact crater, a release valve was opened at the base of the centrifuge bucket and water was allowed to drain from the sample. This created capillary tension in the sample, imparting additional strength to the soil and stability to the water, thus allowing easy excavation to the top of the projectile without fear of disturbance.

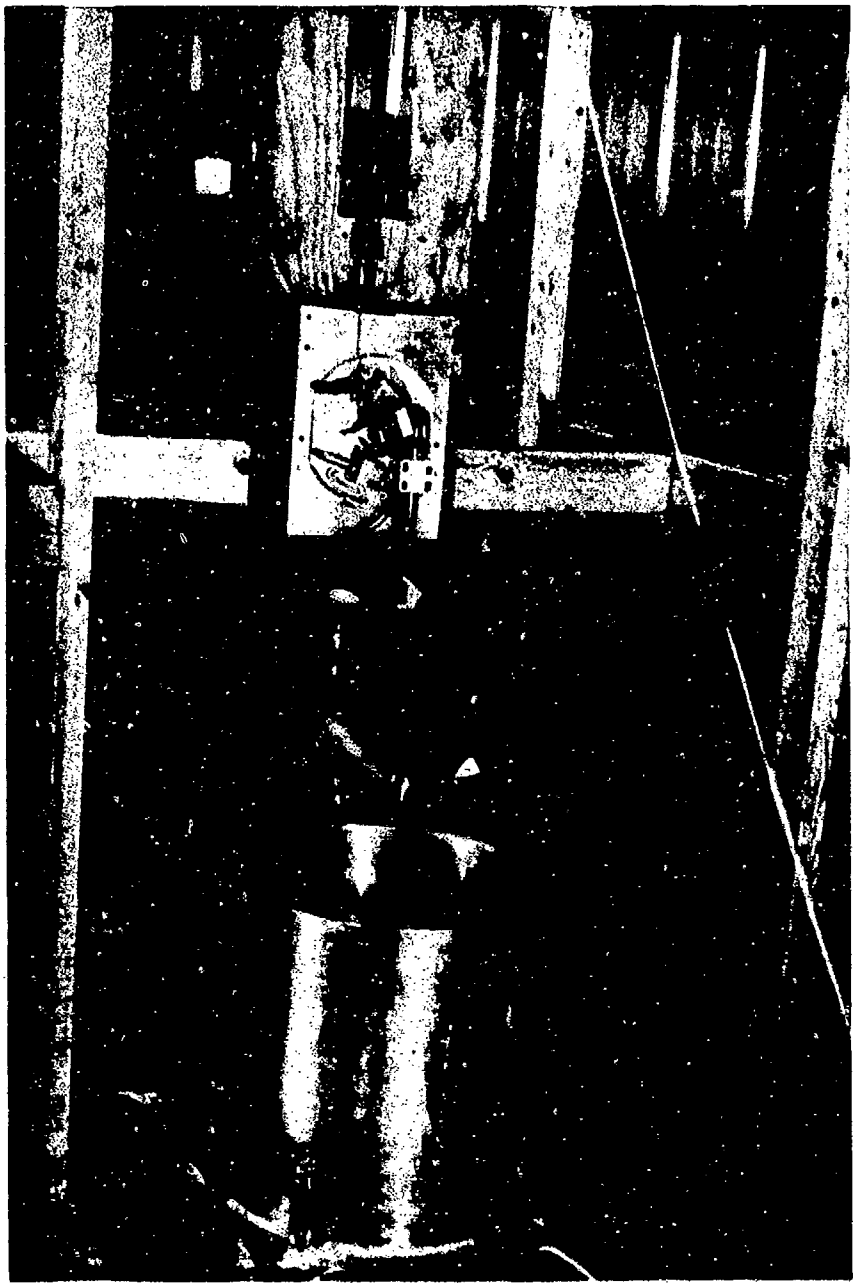

Figure 19. 1-g Test Frame

D. PENETRATION TEST PREPARATION

1. Safety

The safe operation of a centrifuge requires provisions to ensure that the unit cannot be started while anyone is inside the centrifuge housing. For the Tyndall AFB centrifuge, these provisions included the hatch door interlock switches, an emergency stop button inside the centrifuge housing, and the four key-operated safety switches. Test procedure mandated that anyone entering the centrifuge housing carry one of the four switch keys, thus preventing accidental operation of the centrifuge.

The firing of projectiles during centrifuge operation presented additional safety considerations unique to this research. A special test plan documenting storage, transportation, handling and use of the gun and reloading materials, as well as test safety precautions, was submitted for approval to the AFESC Test Safety Office, Weapons Safety Officer and Lab Director in advance of the centrifuge tests. This test plan also included misfire and failure to trigger procedures. In addition to the test plan, it was required that expertise in reloading and knowledge of potential reloading hazards be demonstrated to the gunnery sergeant before testing could begin.

2. Centrifuge Preparation

Several modifications to the centrifuge were made for this research. These included: reversing the raised pattern aluminum rotor arm platforms, to expose smooth surfaces for easier mounting of equipment along the rotor arms; replacing a steel horizontal cross bar in the rotor arms with an aluminum bar of equal dimensions, to reduce the mass of the rotor arms and compensate for the planned equipment addition to the rotor arms; reducing the number and size of mounting holes in the new cross bar from those contained in the old bar to maximize the vertical cross section and increase structural integrity under anticipated loadings; and, relocating electrical leads from the rotor arm platform surfaces to the faces of the cross bars, to increase the available mounting area on the rotor arm platform.

Before operating the centrifuge with the above modifications and the gun assembly mounted to the rotor arm platform, structural calculations were

performed to assess the safety of the centrifuge at the maximum g-level of 100 g's. These calculations are included as Appendix E.

The test equipment configuration required two sets of counterweights to be constructed. The first of these was a "dummy" gun assembly, attached to the opposite rotor arm platform to balance the actual gun assembly mounted on the test arm. This counterweight assembly consisted of aluminum blocks of mass and size designed such that the composite center of mass approximately corresponded to the center of mass of the genuine gun and plate assembly. The aluminum blocks were bolted together, and could be realigned in different configurations as necessary to compensate for any changes in the gun assembly. Locater bolt holes were placed at 0.051-meter spacings lengthwise and crosswise in the counterweight assembly. Three aluminum bars, essentially counterparts of the three aluminum tiebars in the gun mount system, were bolted to the surface of the rotor arm platform. Threaded holes along the tops of these bars, corresponding to the locater holes, allowed the counterweights to be positioned at variable locations both radially and crosswise on the rotor arm platform, to compensate for different radial and eccentric mounting positions of the actual gun assembly.

The second set of counterweights required for the projectile penetration test configuration was designed to compensate for the eccentric mounting of the sample bucket. Because the center of the gun barrel was approximately 0.09 meters above the surface of the rotor arm platform, the sample bucket had to be positioned a similar distance above the center line of the payload platform for projectile impact to occur in the center of the sample bucket. To reduce the quantity of counterweights required and expedite testing, the sample bucket was actually positioned just 0.073 meters above the center line, resulting in a slightly above-center projectile impact. The counterweights were prepared with masses ranging from 0.113 kilograms to 9.072 kilograms. The weights were designed with variable length and thickness but constant width, to facilitate balance calculations that would otherwise be complicated by the variable soil sample weights.

3. Centrifuge Shakedown Tests

Because the Tyndall AFB centrifuge was newly installed at the time of this research, and because of some of the previously discussed potential

safety hazards associated with this research, a series of shakedown tests was performed on the centrifuge. The tests were planned to assess the capabilities and performance of the centrifuge at g levels up to 60, with the mounted equipment and payloads designed for the penetration tests. Such items as video camera angle, payload platform verticality and performance of the self-balancing motor under heavy payloads were assessed. The tests were also designed to identify difficulties with the remote triggering system and with achieving on-target projectile delivery.

The shakedown test sequence began by mounting the firing assembly and rotor arm counterweights with no payload to check structural integrity of all equipment modifications and additions at high g levels. Spent cartridges were placed inside the gun to test the remote triggering mechanism. After remote triggering proved successful, the spent cartridges were replaced with primed cartridges. The primed cartridges made a loud noise on firing and allowed the time of triggering to be determined. Crumpled paper balls placed in the end of the gun barrel were used to visually observe the firing event. These tests proved the potential for pretriggering by the solenoid triggering system, as previously discussed.

The next series of tests assessed the performance of the fully loaded payload platform in swing mode, the sample and sample bucket, and the payload platform eccentric weights. These tests included assessment of the self-balancing mechanism operation with heavy payloads and the sensitivity of the payload platform verticality indicator light. The gun was not loaded for any of these tests.

Use of a primed cartridge and paper ball indicated that triggering could not be accomplished with the solenoid triggering mechanisms at g levels greater than 60. An initial test fire with a loaded cartridge was performed, using a light 30-caliber nylon projectile and a sample height determined on the basis of 1-g test results. The projectile impact occured in the upper righthand quadrant of the vertical sample bucket. This impact location was suggestive of turbulence problems, which had been anticipated due to the open hydraulic line access port in the centrifuge housing. This opening was sealed with spray foam prior to the next series of tests.

The next tests involved firing 30-caliber projectiles of all four material types. The centrifuge was operated at the planned g-level for

approximately one minute prior to firing to allow time for the air inside the centrifuge housing to stabilize at that g level. On-target delivery for these shots was achieved. The first series of low g centrifuge tests were conducted on the basis of the shakedown tests performed to this point.

The final series of shakedown tests was performed after the first series of centrifuge tests were completed. These tests were conducted in a similar manner to the previous shakedown tests and involved assessing the integrity of the system at g levels up to 100. The performance of the servomotor triggering system was tested and proved successful at these g levels.

E. CENTRIFUGE TESTS

1. Test Parameters

A total of 85 centrifuge tests were conducted over the course of this research. Seventy-eight of these tests were conducted on dry samples of the test sands. Projectile test sequences were designed for both loose and dense samples prepared with Ottawa Flintshot sand, for dense samples of Ottawa F-58 and Florida Beach sands, and for dense samples of the soil blend. Centrifuge tests involving moist and nearly saturated sand were conducted in samples prepared from Ottawa F58 sand.

Projectiles were fired at an average velocity of 305 meters/second at an impact angle normal to the sample surface. The majority of the tests were performed using 22-, 30-, 35- and 44-caliber brass projectiles because of the higher prototype masses modeled by these heaviest projectiles. A small number of tests were conducted using aluminum, nylon, and PVC projectiles.

2. Test Procedures

Because of the number of critical variables involved in a complete projectile penetration centrifuge test sequence, a test procedure was devised and carefully followed for all centrifuge tests. Before assembling equipment and mounting the test sample on the centrifuge, the balance motor was turned off to prevent damage to the self-leveling mechanism and the payload platform was locked in the horizontal position to prevent movement. A soil sample was then prepared with the pluviator, as previously described. The completed sample was carefully lifted by hand crane onto a balance and weighed, then raised over the

top of the centrifuge housing and lowered onto the centrifuge payload platform. The bucket was positioned and bolted in place on the platform. Moist samples were prepared with the bucket in place on the platform, using the techniques described in Section IV. The number and location of eccentric weights required to balance the sample bucket were calculated and the weights were assembled and bolted onto the payload platform. The total weight of the sample bucket plus eccentric weights was determined, and the appropriate number of counterweights was placed on the opposing payload platform.

The next step was to determine the eccentric mounting and gun angle requirements for the planned test velocity, g-level and radial mounting location of the gun assembly. The gun was then positioned by rotating the upper swivel plate of the gun mount to the required angle, loosening the tie bar screws, and sliding the rack gears to position the gun at the proper eccentric distance from the center line. The rack gear clamps were bolted in place and all assembly screws were tightened. A check was made to ensure that all equipment and counterweights were properly bolted and that no bolts or screws were loose. The payload platform was then freed from the locked position and the balance motor was activated. The rotor arms were moved up or down with respect to each other until static balance was achieved; adjustments to the counterweights were made as necessary.

The test projectile was loaded using procedures previously outlined. Because the quantity of powder required varied slightly with humidity and temperature, calibration tests were performed between different series of centrifuge tests.

A sandbag was temporarily placed on the centrifuge payload platform in front of the aluminum sample bucket wall for added safety during the loading and cocking process. Also, the connection between the control room D.C. power unit and the slip ring used for the triggering system was disconnected, and all unnecessary personnel were removed from the centrifuge housing. The loaded cartridge was then placed inside the gun chamber and the chamber was closed. Next, the triggering system was arranged. For the solenoid triggering systems, the mechanical arm was carefully positioned in front of the trigger and the solenoid terminals were connected to wires which routed current from the slip rings. For the servomotor triggering system, the cupped rod attached to the servomotors was placed in front of the trigger and the motor

pistons were aligned in the appropriate position. A final check of the centrifuge housing was made to ensure that there were no loose tools or other extraneous equipment. The gun was then cocked and the sandbag was carefully removed. All personnel exited the centrifuge housing, the access ladder was pulled out, and the access hatches were closed.

System and pretest checks were performed in the control room and the safety switches were activated. The centrifuge was then started and brought up to the appropriate rpm for the planned g-level, and the slip ring connection to the triggering system was attached to the D.C. power unit. After rotating at the desired rpm, the gun was triggered and projectile impact was observed on the video monitor. The centrifuge was then decelerated and brought to a complete stop.

Once the centrifuge was stopped, the centrifuge housing access doors were reopened and the access ladder was lowered. The gun was removed from the gun mount and the spent cartridge was extracted from the chamber. The payload platform was then locked in the horizontal position and the balance motor was turned off. The depth of penetration into the sample was measured by techniques identical to those employed in the 1-g tests. In addition to determining the penetration depth, the x-y coordinates of the center of the impact crater and the projectile were measured.

Finally, the sample bucket was unbolted and the sample was raised by crane out of the centrifuge housing. The counterweights were unbolted and removed, and preparations were made for the next centrifuge test.

SECTION VI

RESULTS, CONCLUSIONS AND RECOMMENDATIONS

A. TEST RESULTS FOR DRY SAND

The actual penetration depths measured for 1-g tests in dense Ottawa Flintshot sand are shown in Figure 20. The penetration depths are plotted with respect to the actual projectile mass, for an impact velocity of approximately 305 meters/second. A comparable plot for 1-g tests in loose Ottawa Flintshot sand is presented as Figure 21.

As previously discussed, the major purpose of conducting the 1-g penetration tests was to allow a comparison to be made between the 1-g and the accelerated g penetration test results which will be presented in subsequent figures. Figures 20 and 21 show that the heavier brass projectiles consistently reached greater penetration depths than the lighter aluminum projectiles, which in turn penetrated to greater depths than did the PVC and nylon projectiles. In Figure 20, duplicate tests performed with brass 22 projectiles and brass 44 projectiles indicate the reproducibility of the penetration test results at 1-g. Penetration depths were also measured in a number of 1-g tests conducted at different velocities as part of the velocity determination tests discussed in Section V.

The initial series of centrifuge tests conducted in this research was performed at g levels up to 60 g and at approximate velocities of 305 meters/second. These tests utilized four different projectile material types (brass, aluminum, nylon and PVC) and targets of dense Ottawa Flintshot sand. The results from these tests are presented in the prototype mass versus prototype penetration depth plot of Figure 22. As in the 1-g test results, it is clear that a difference in penetration depth magnitude exists among the different projectile material types, with brass projectiles exhibiting the greatest penetration depths, aluminum exhibiting intermediate penetration depths, and nylon and PVC exhibiting fairly comparable small penetration depths. That projectile material type significantly affects the magnitude of penetration is clearly expected from the discussion of Section III; π_{11} and π_{12} are essentially statements of this fact. From an experimental standpoint, the effects of material type on penetration depth

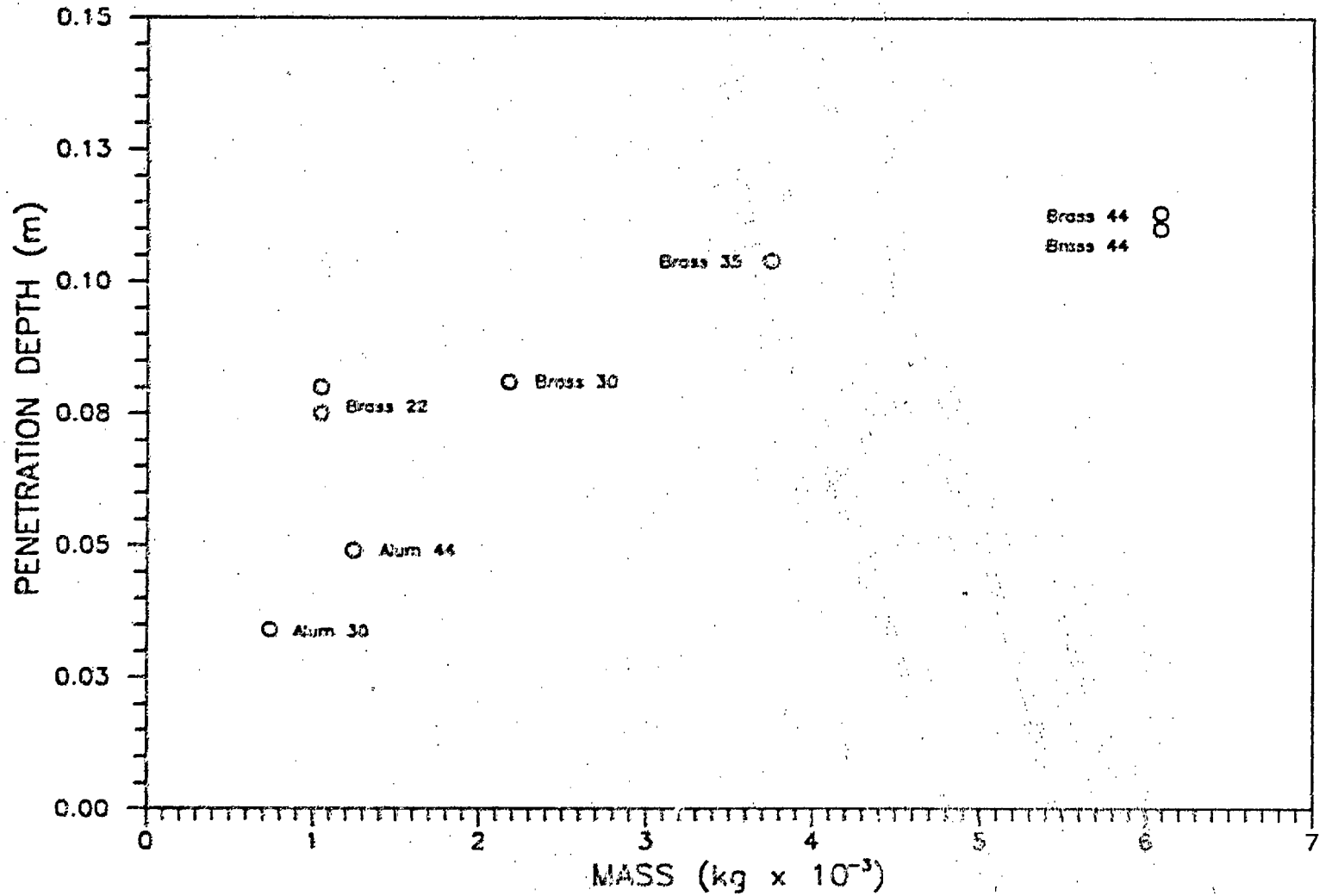

Figure 20. Projectile Mass vs. Penetration Depth for 1-g Tests in Ottawa Flintshot Sand (Dense), Velocity = 305 m/s

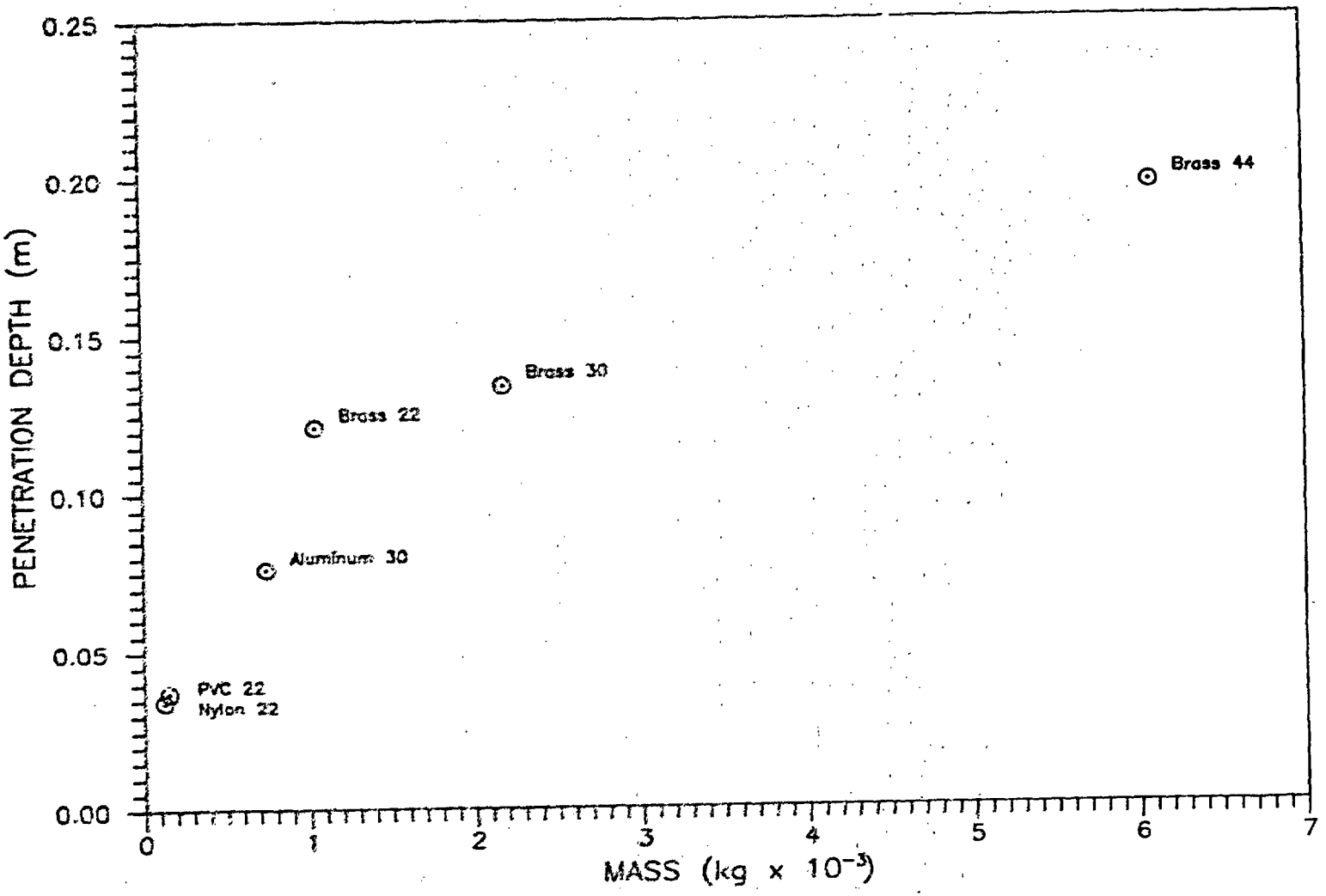

Figure 21. Projectile Mass vs. Penetration Depth for 1-g Tests in Ottawa Flintshot Sand (Loose), Velocity = 305 m/s

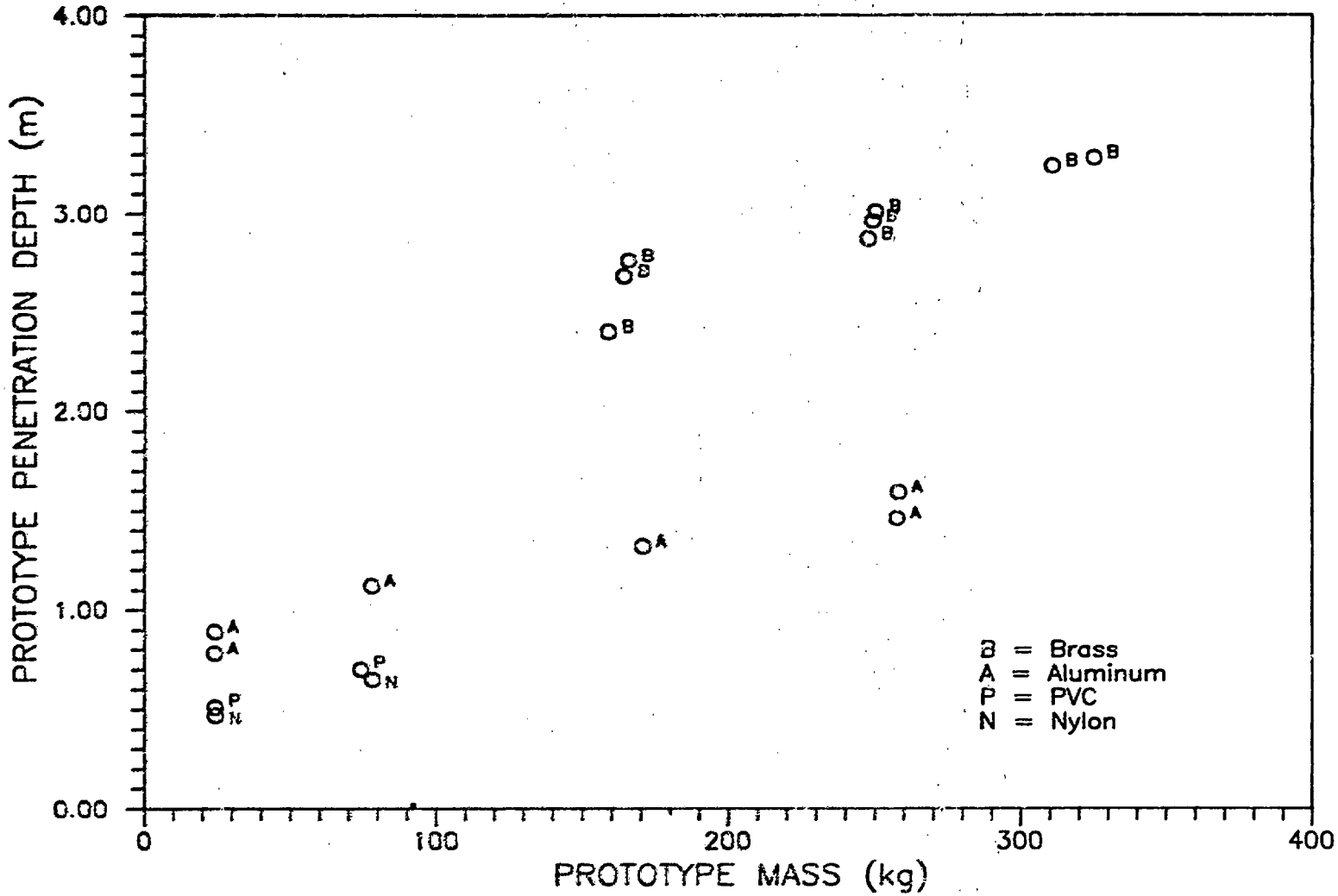

Figure 22. Prototype Mass vs. Prototype Penetration Depth for Initial Series of Centrifuge Tests, Illustrating Projectile Material Differences

have been documented by a number of investigators (References 17, 19, 10, 82 and 2).

As discussed in Section V, the X-Y coordinates of the center of the crater were determined. Because the orientation of the gun is based on the intended impact point and the velocity of the projectile, the comparison between actual and intended crater center was used to verify projectile velocity. As expected based on the reproducibility of projectile velocity in the velocity determination tests, no significant deviations were noted.

A comprehensive plot of all centrifuge tests conducted in Ottawa Flintshot sand using brass projectiles is presented in Figure 23 in the form of prototype penetration depth versus prototype mass. All tests shown in this figure were conducted at approximate velocities of 305 meters/second using brass projectiles of all four calibers; no distinction, between calibers is shown in this figure. A similar plot for the other test sands used in this research is presented in Figure 24.

Different projectile calibers are distinguished between in Figure 25 to illustrate the modeling-of-models testing technique for centrifuge tests in dense and loose Ottawa Flintshot sand. This figure shows that different projectile calibers were successfully used to simulate the same prototype masses over a wide prototype mass range, from approximately 20 to 950 kilograms. Very similar prototype penetration depths were obtained for the different calibers used in each of the five tests. The higher magnitude of penetration observed in loose Ottawa Flintshot sand is readily apparent in the modeling-of-models tests conducted to simulate a prototype mass of approximately 340 kilograms. Comparison of the test results from brass projectiles used to model prototype masses of approximately 90, 240 and 950 kilograms, to the penetration depth magnitudes associated with the aluminum projectiles used to model a prototype mass of approximately 25 kilograms, clearly illustrate again the difference in penetration depth magnitudes with projectile material type.

B. ANALYSIS OF TEST RESULTS FOR DRY SAND

In the initial analysis of the centrifuge data, an attempt was made to correlate the prototype penetration depths to the prototype projectile mass to area ratio. A strong linear correlation was observed (correlation coefficient,

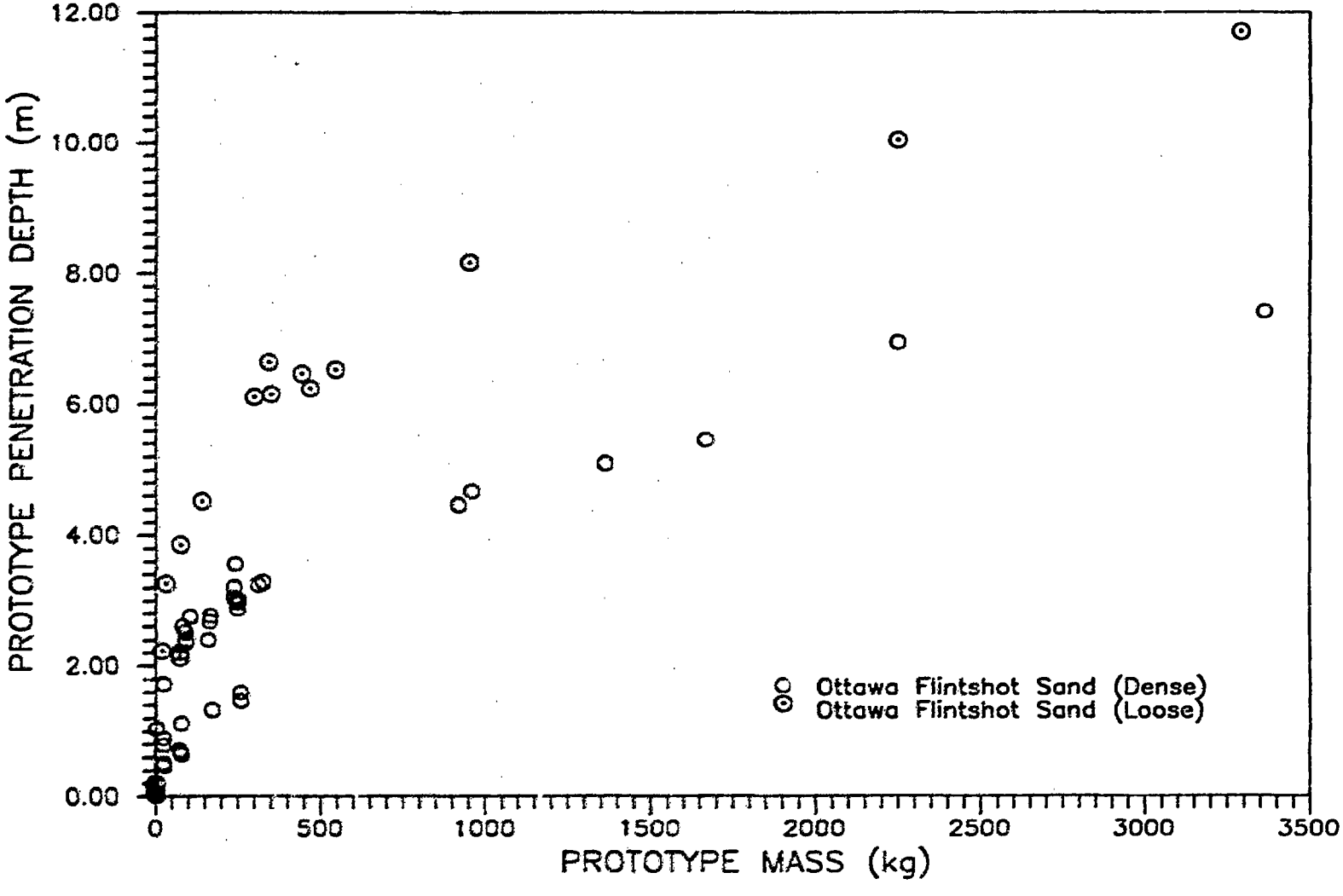

Figure 23. Prototype Mass vs. Prototype Penetration Depth for Centrifuge Tests in Ottawa Flintshop Sand

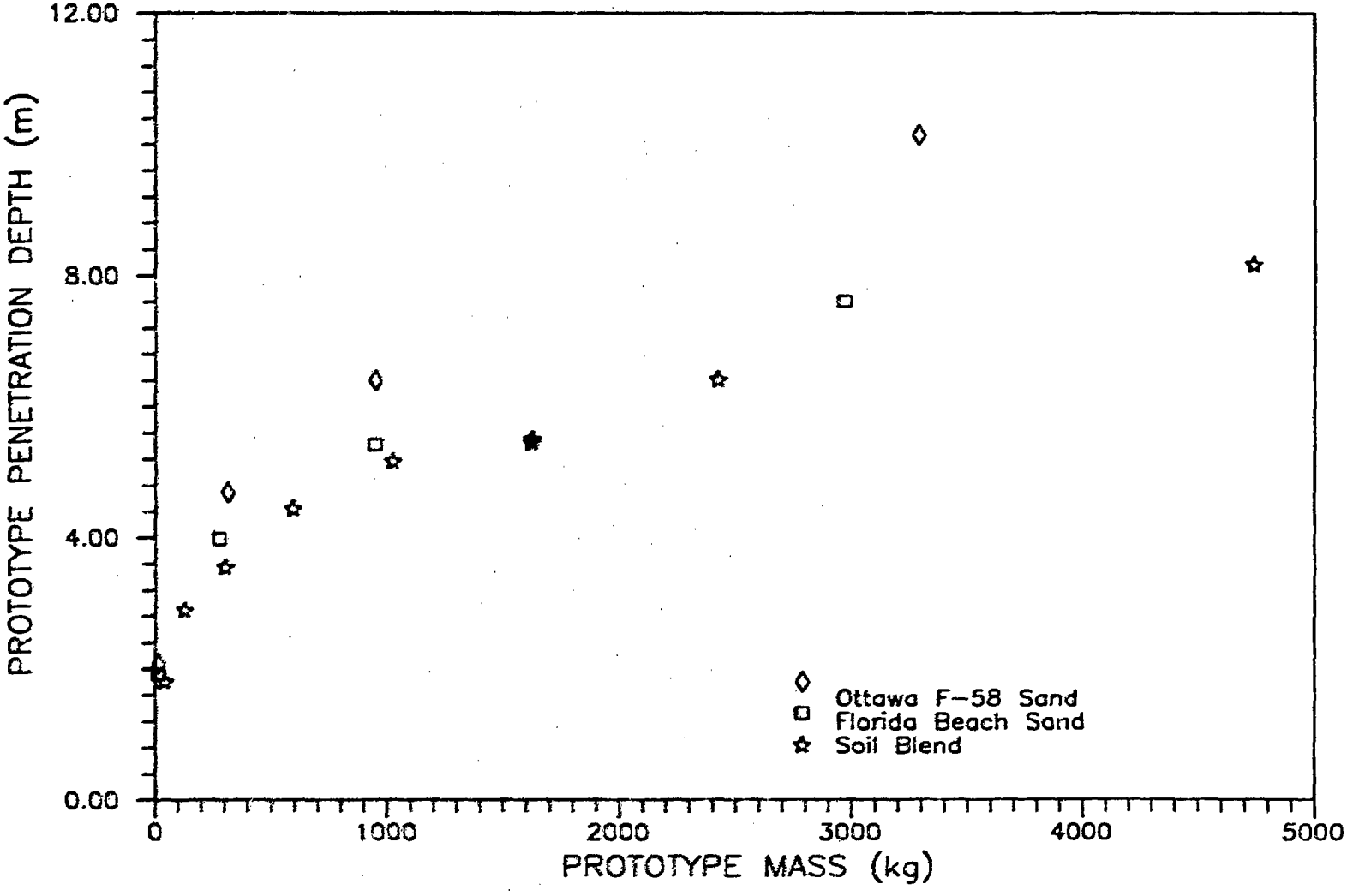

Figure 24. Prototype Mass vs. Prototype Penetration Depth for Centrifuge Tests in Different Test Sands

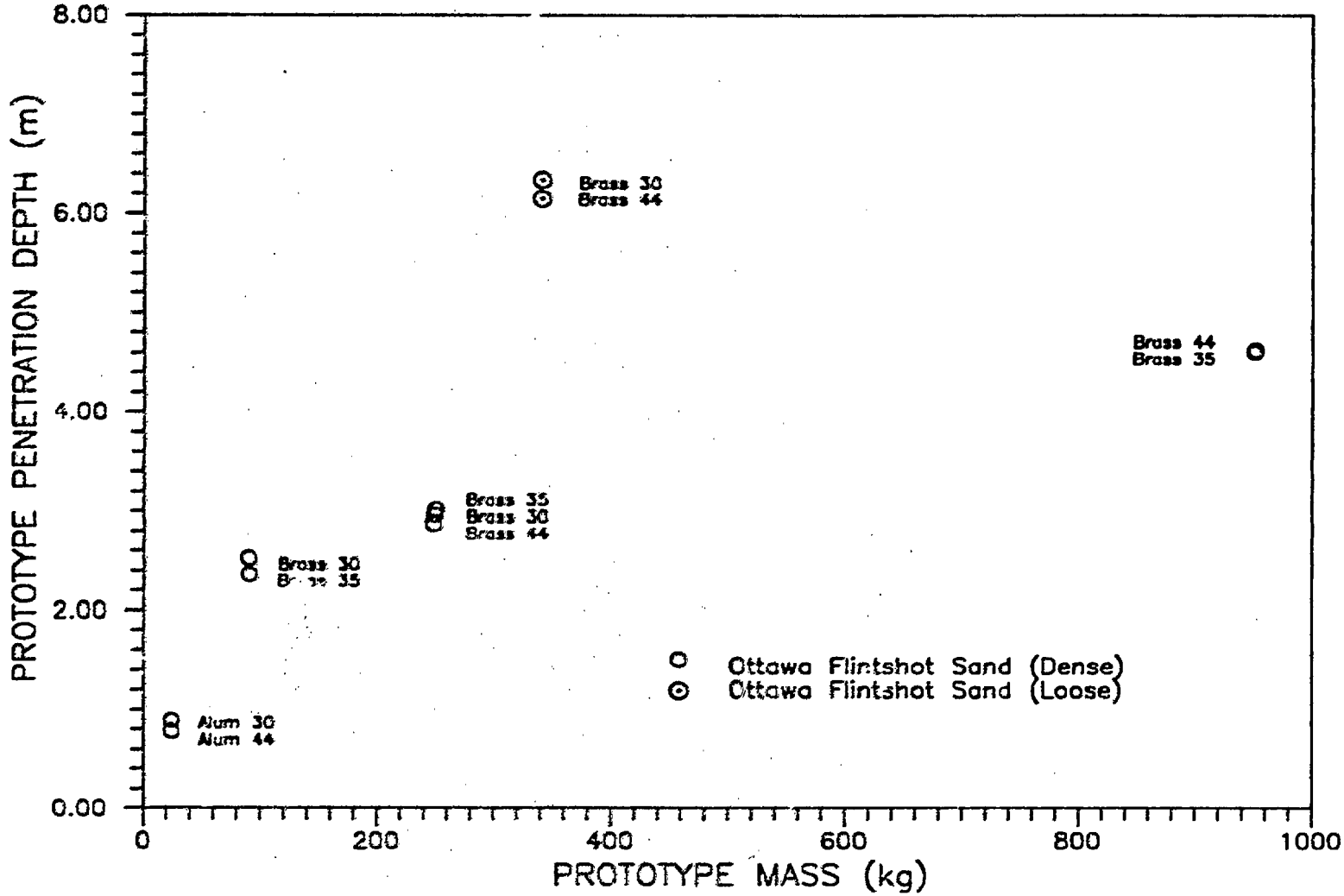

Figure 25. Prototype Penetration Depths in Ottawa Flintshot Sand for Similar Prototype Masses, Illustrating Modeling-of-Models

r = 0.994 for centrifuge and 1-g tests in dense Ottawa Flintshot sand); however, extrapolation to 1-g test data resulted in overprediction of penetration depths at low g-levels, with significant penetration depths predicted at a prototype mass to prototype area ratio of zero. Better statistical correlation is obtained using best-fit power curves, which has the additional advantage of including the 1-g test data. Figure 26 is a plot of these curves for Ottawa Flintshot sand, with the 1-g data points omitted for clarity but included in determination of the illustrated best-fit curves. The correlation coefficients for the dense and loose Ottawa Flintshot sand 0.998 and 0.994, respectively. For dense Ottawa Flintshot sand the equation of the curve is:

$$P = 0.00277(M/A)^{0.917} \quad (41)$$

For loose Ottawa Flintshot sand the equation is:

$$P = 0.0084(M/A)^{0.845} \quad (42)$$

where P is the prototype penetration depth, M is the prototype projectile mass and A is the prototype projectile area.

Figure 27 includes the 1-g data points on the best-fit power curve for dense Ottawa Flintshot sand. Figure 28 provides an exploded view of 1-g and low-g data points to better illustrate the goodness of fit to the curve for both 1-g and centrifuge test data. Similar comparisons for loose Ottawa Flintshot sand are made in Figures 29 and 30. The best-fit power curves established for the other test soils are shown in Figure 31. Statistical calculations were not performed for the soils in this figure because of the limited number of data points. The equation for the best-fit power curve for Ottawa F58 sand is:

$$P = 0.0061(M/A)^{0.66} \quad (43)$$

For the Florida Beach sand, the equation is:

$$P = 0.011(M/A)^{0.765} \quad (44)$$

while for the soil blend

$$P = 0.0037(M/A)^{0.682} \quad (45)$$

Penetration tests performed using these three soils were limited to centrifuge tests; thus, determination of equations 43 through 45 was made without inclusion of 1-g data.

In analyzing the penetration tests conducted in this research, it must be emphasized that the penetration variables of velocity and projectile geometry were essentially treated as constants throughout the test program. Thus, the utility of expressing the test results in terms of dimensionless parameters prior to

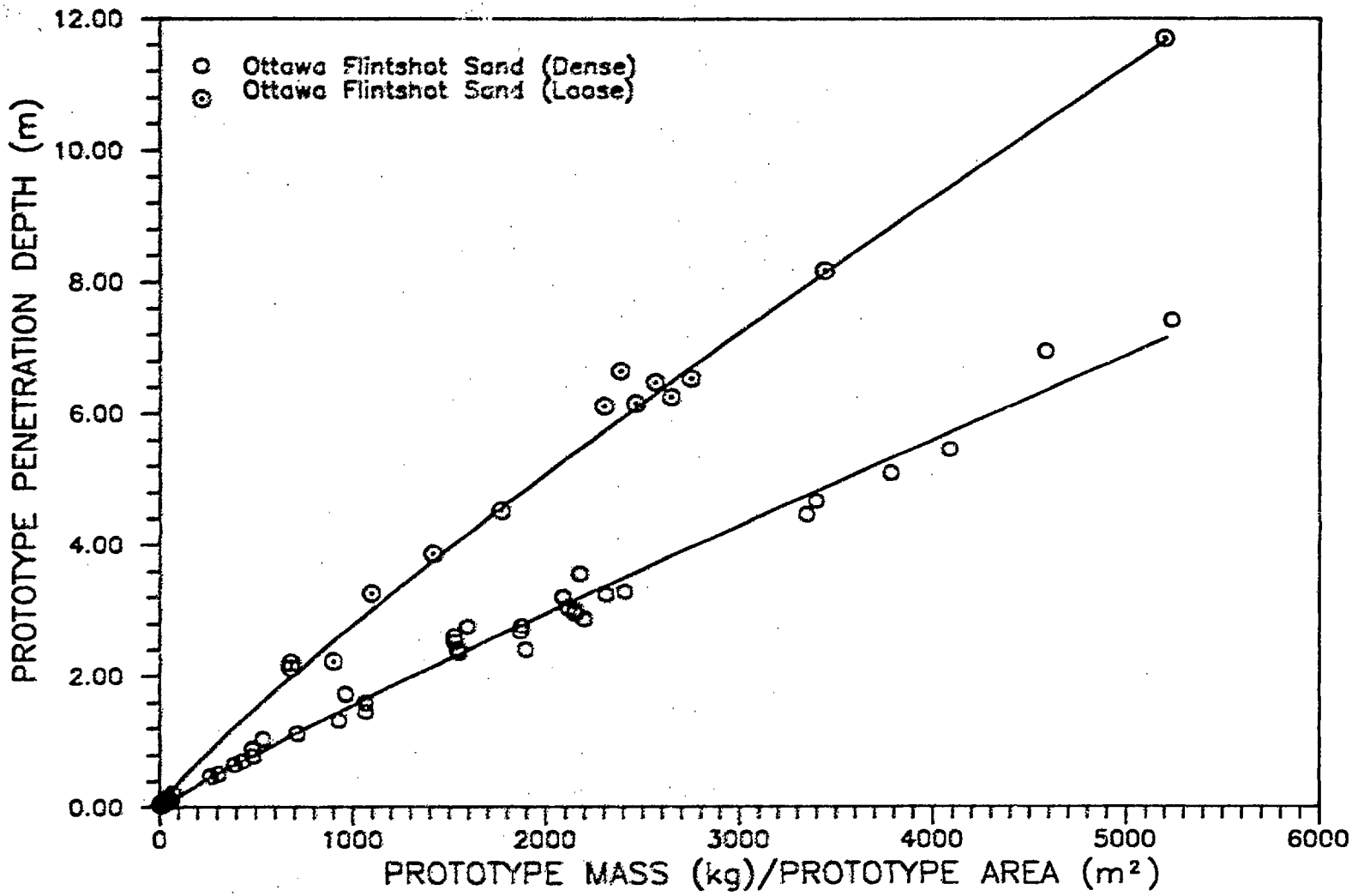

Figure 26. Prototype Mass/Prototype Area vs. Penetration Depth for Ottawa Flintshot Sand

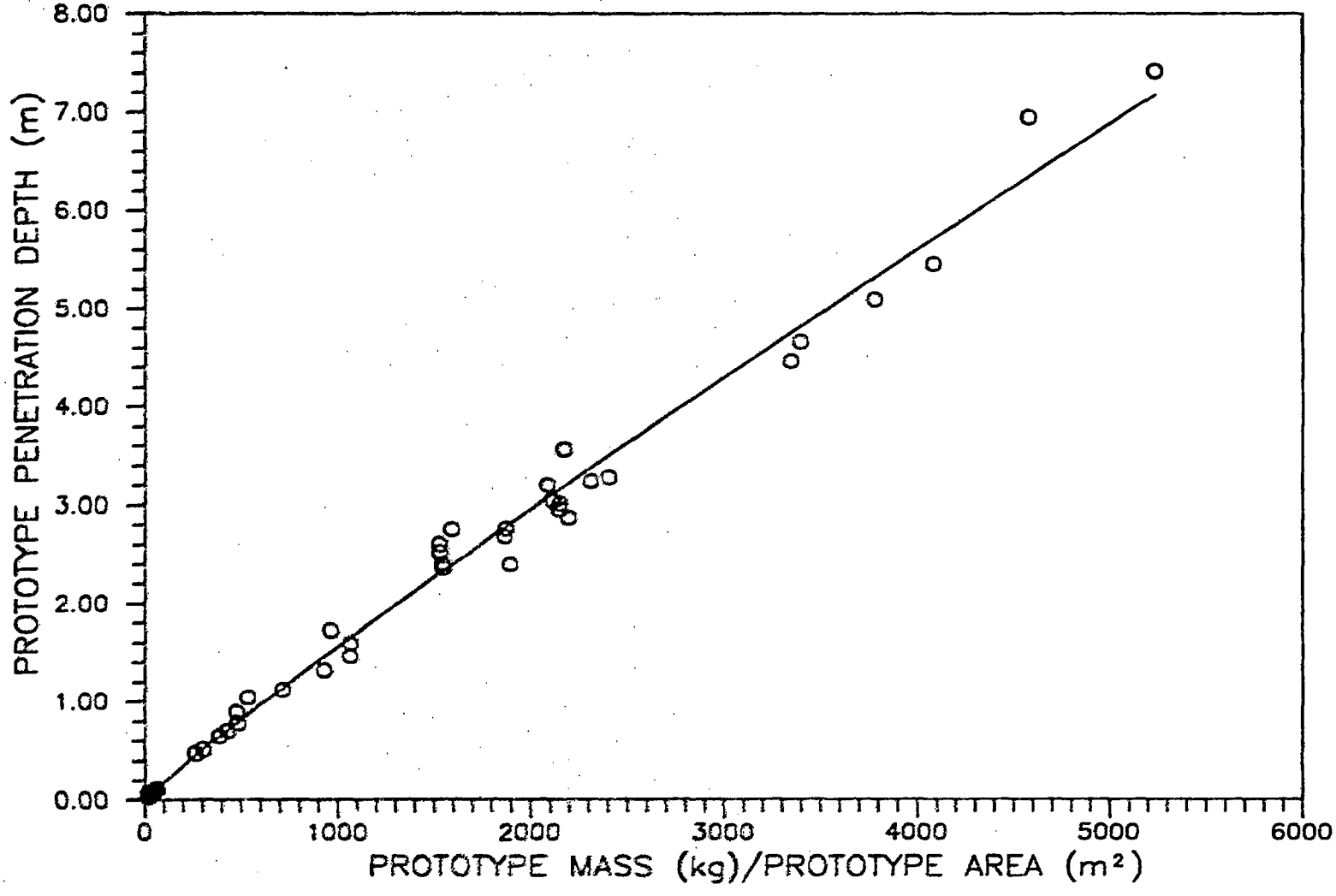

Figure 27. 1-g and ng Test Results for Prototype Mass/Prototype Area vs. Prototype Penetration Depth, Ottawa Flintshot Sand (Dense)

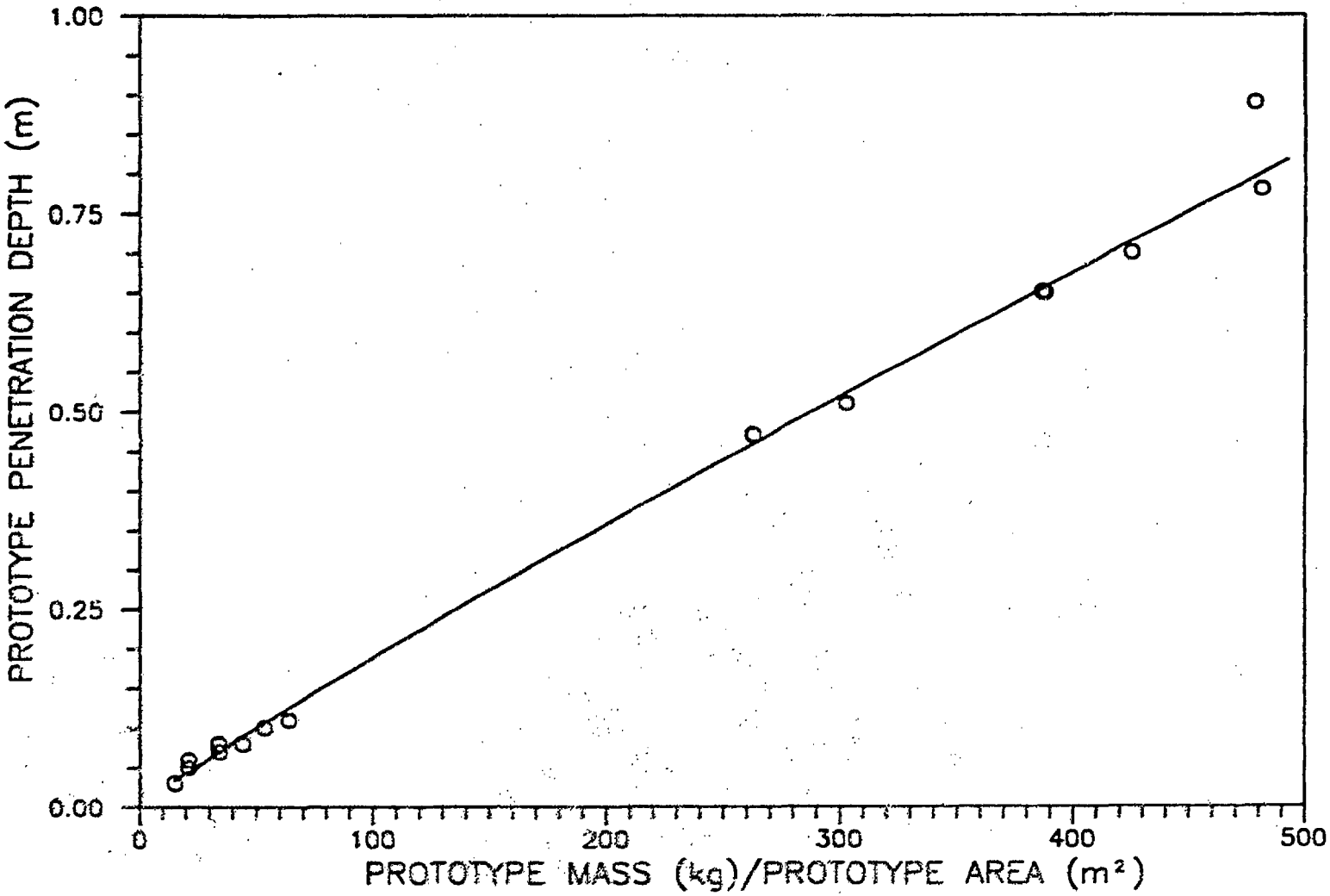

Figure 28. Exploded View, Low g Test Results for Prototype Mass/Area vs. Prototype Penetration Depth, Ottawa Flintshot Sand (Dense)

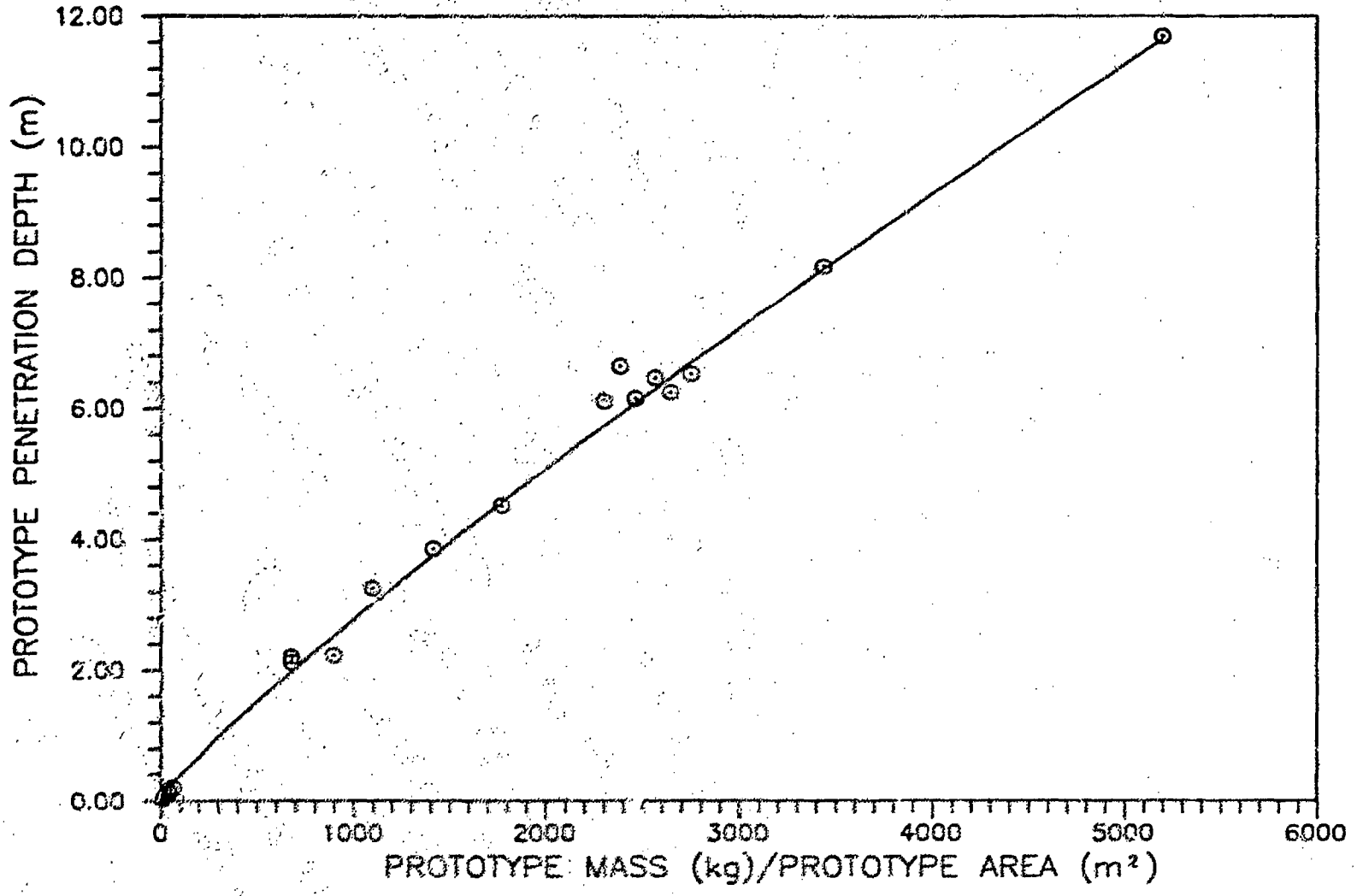

Figure 29. 1-g and ng Test Results for Prototype Mass/Prototype Area vs. Prototype Penetration Depth, Ottawa Flintshot Sand (Loose)

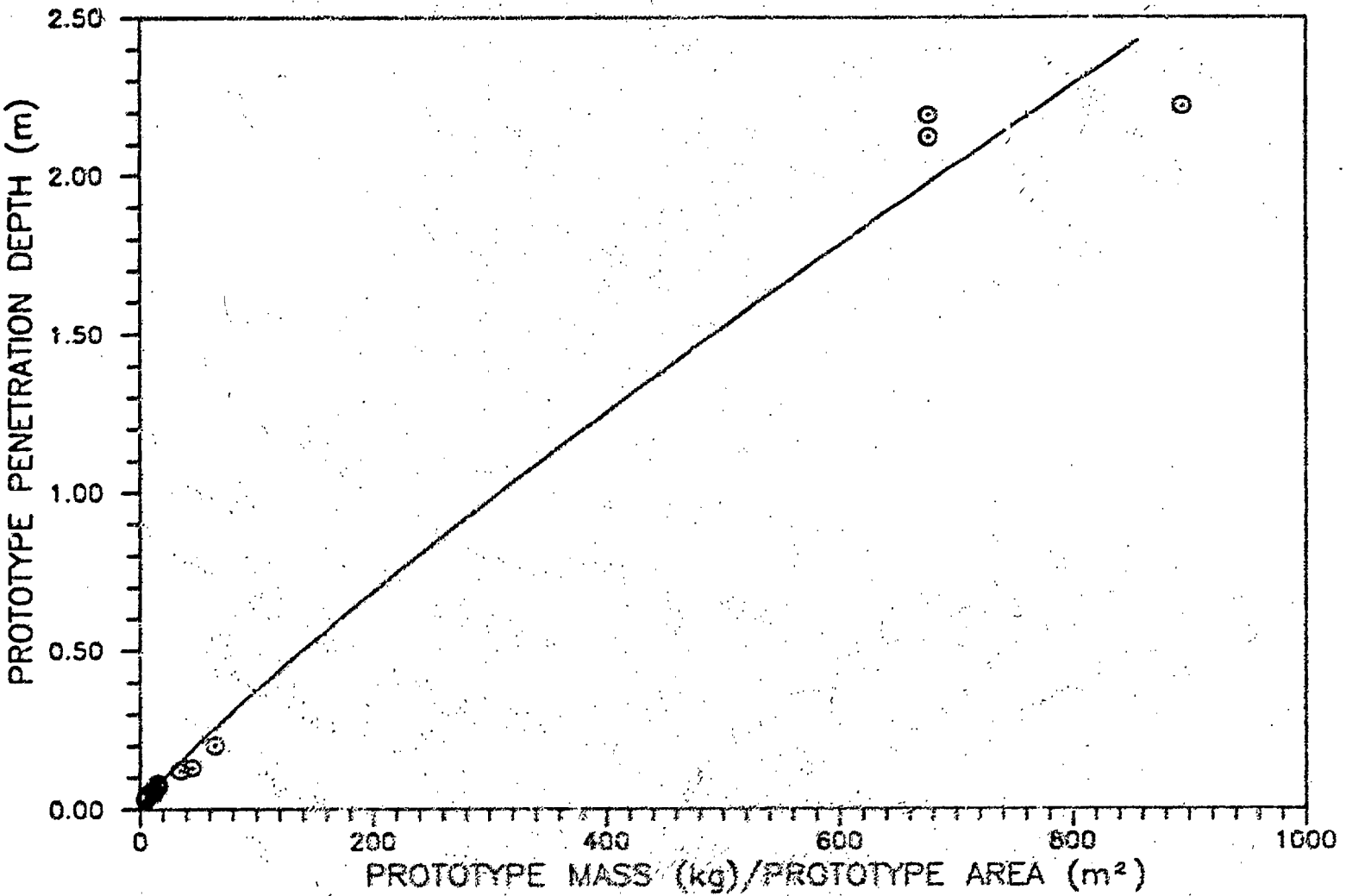

Figure 30. Exploded View, Low g Test Results for Prototype Mass/Area vs. Prototype Penetration Depth, Ottawa Flintshot Sand (Loose)

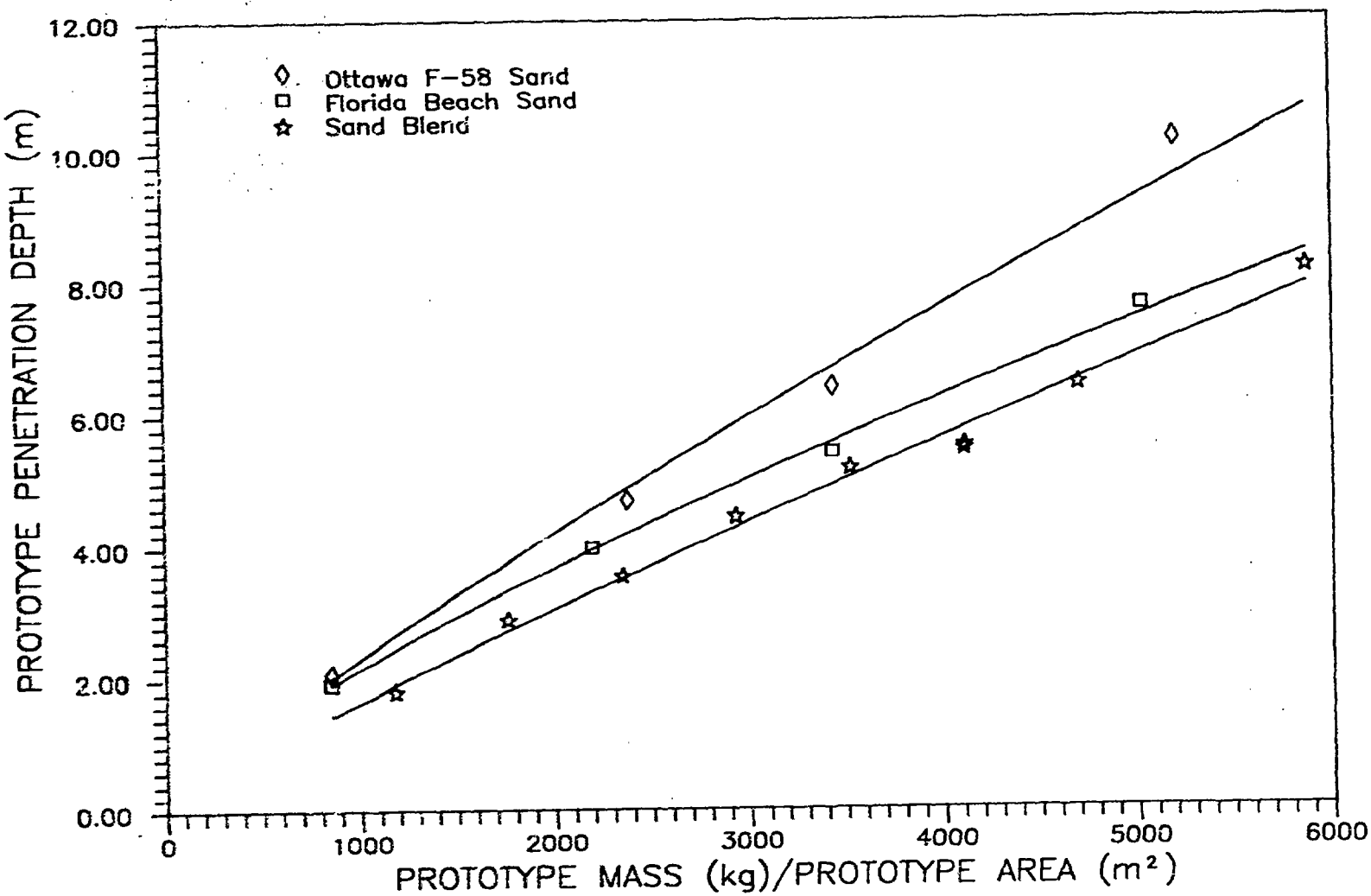

Figure 31. Prototype Mass/Prototype Area vs. Penetration Depth for Different Test Sands

investigation of these variables is somewhat limited in terms of a complete description of the penetration phenomenon, but is a useful method of providing insight into the specific concerns of this research.

The preceding figures show a strong correlation between prototype penetration depth and prototype projectile mass to area ratio exists. Therefore, a dimensionless parameter involving the ratio of projectile mass to projectile area is suggested. Recall that the definition of π_{13} developed from the dimensional analysis of Section III is:

$$\pi_{13} = \delta_t v^2/\sigma \tag{46}$$

where

$$\sigma = \delta_t g z \tag{47}$$

Using

$$\pi_{11} = \delta_p/\delta_t \tag{48}$$

and

$$\pi_7 = d/s \tag{49}$$

it follows that a new pi term, π_{11}', can be defined as

$$\pi_{11}' = (M/A)_p/(M/A)_t = (M_p/A_p)/(M_t/A_t) \tag{50}$$

where A_p and A_t are the areas of the projectile and target, respectively, and M_p and M_t are the masses of the projectile and target, respectively. If the target mass is defined by

$$M_t = \delta_t z A_t \tag{51}$$

where z is the "length" of the target (i.e. the depth below the ground surface), then

$$M_t/A_t = \delta_t z A_t/A_t = \delta_t z \tag{52}$$

and

$$\pi_{11}' = M_p/A_p\delta_t z \tag{53}$$

π_{13} may be expressed:

$$\pi_{13} = \delta_t v^2/\sigma = \delta_t v^2/\delta_t g z = v^2/gz \tag{54}$$

Dividing π_{11}' by π_{13} results in development of a new pi term, π_{14}, which includes the mass to area ratio of the projectile:

$$\pi_{14} = M_p g/A_p\delta_t v^2 \tag{55}$$

Use of π_{14} in analysis of the test results has the advantage of including the target density and the projectile impact velocity; consequently, although these variables were kept as constant as possible for each test series, actual values (where known) can be employed to calculate π_{14} for data analysis. Figure 32 is a

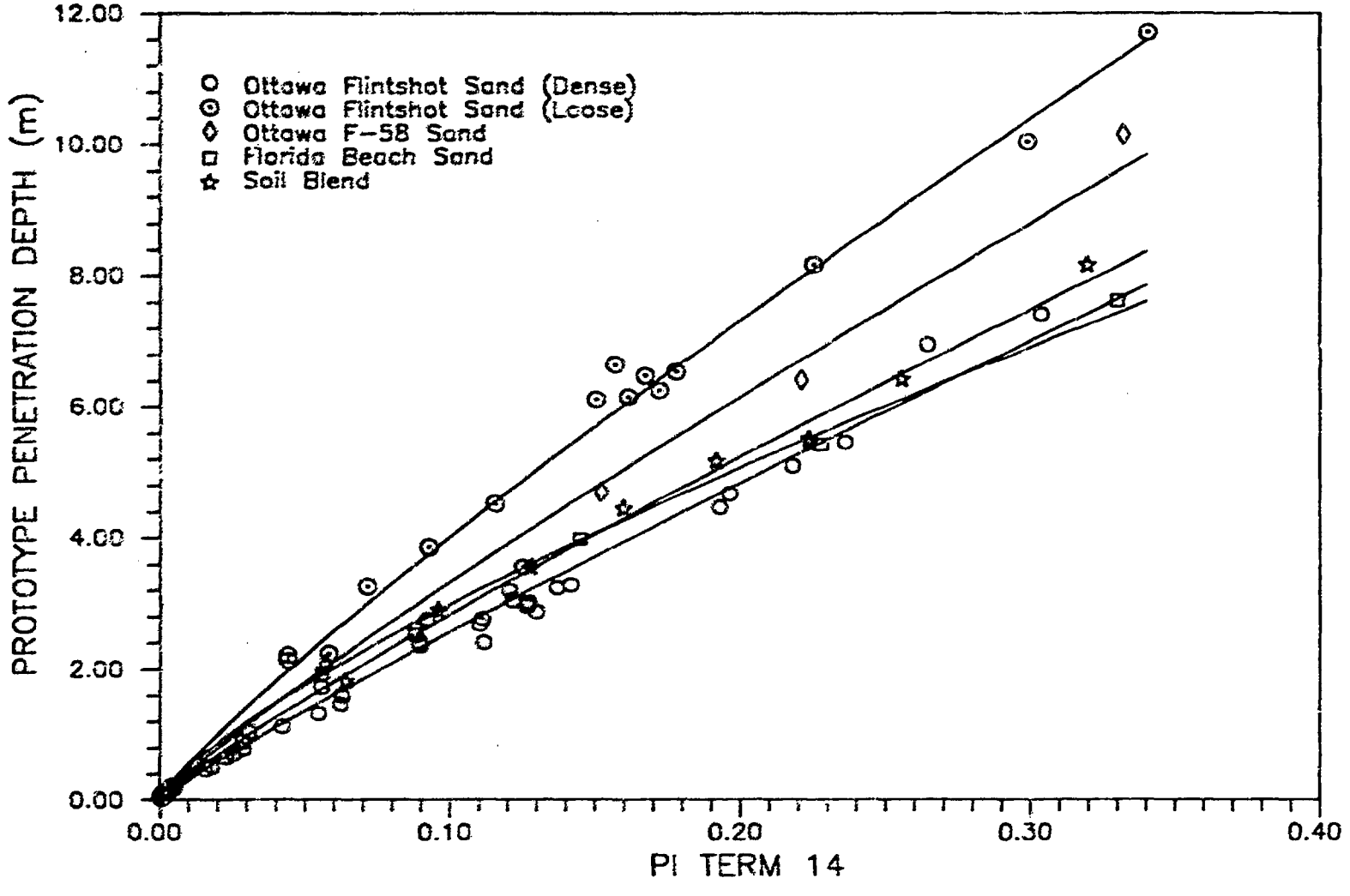

Figure 32. Pi Term 14 vs. Prototype Penetration Depth for All Test Sands

plot of prototype penetration depth versus π_{14} for all of the test soils, with best-fit power curves superimposed. The actual values of soil density and actual velocity values measured in 1-g tests were used in the plot; velocity values for the centrifuge tests were again estimated. It is apparent from consideration of Figure 32 that inclusion of the absolute density of the target material does not provide sufficient description of target properties to allow convergence of the separate curves for the different soils. To consider the effect of relative density, Dimensionless Parameter One (DP1) was created by dividing π_{14} by π_5:

$$DP1 = M_p g/A_p \delta_t v^2 (D_r)^{x_1} \quad (56)$$

where x_1 represents some exponent providing best data correlation. To assess the value of x_1 that would produce the best convergence of the different soil densities, a statistical analysis of the data fit for all of the penetration tests in Ottawa sands was made for a range of x values between 0.2 and 1.0. Based on the results of this analysis, an x_1 value of 0.5 was determined to provide the best correlation. Figure 33 is a plot of the resulting best-fit power curve for all penetration tests conducted in Ottawa sands, in terms of Dimensionless Parameter One versus prototype penetration depth. Figure 34 is an exploded view better illustrating the correlation at 1-g and low g-levels. It is clear from these figures that inclusion of the relative density in the data analysis for Ottawa Flintshot sand allows the curves for different densities to converge and be well-defined by a single best-fit power curve with the equation:

$$P = 21.427(DP1)^{0.694} \quad (57)$$

Use of the relative density in the denominator of Dimensionless Parameter One, however, causes potential difficulties for soils with relative densities of zero. Thus, a similar parameter, Dimensionless Parameter Two (DP2), was developed to incorporate the void ratio (e) instead of relative density in a dimensionless term. This was accomplished by multiplying π_{14} by π_6:

$$DP2 = Mge^{x_2}/A_p \delta_t v^2 \quad (58)$$

where x_2 is defined like x_1 as some exponent providing the best data correlation. The value of x_2 was determined statistically; Figure 35 illustrates the sensitivity of best-fit power curves for Dimensionless Parameter Two versus prototype penetration depth to variation in void ratio. The resulting best-fit curve defined for $x_2 = 1.5$ is shown in Figure 36 with centrifuge and 1-g test data from tests in both Ottawa Flintshot and Ottawa F58 sands superimposed. Not surprisingly, it is clear from this figure that the Ottawa F58 sand penetration data does not

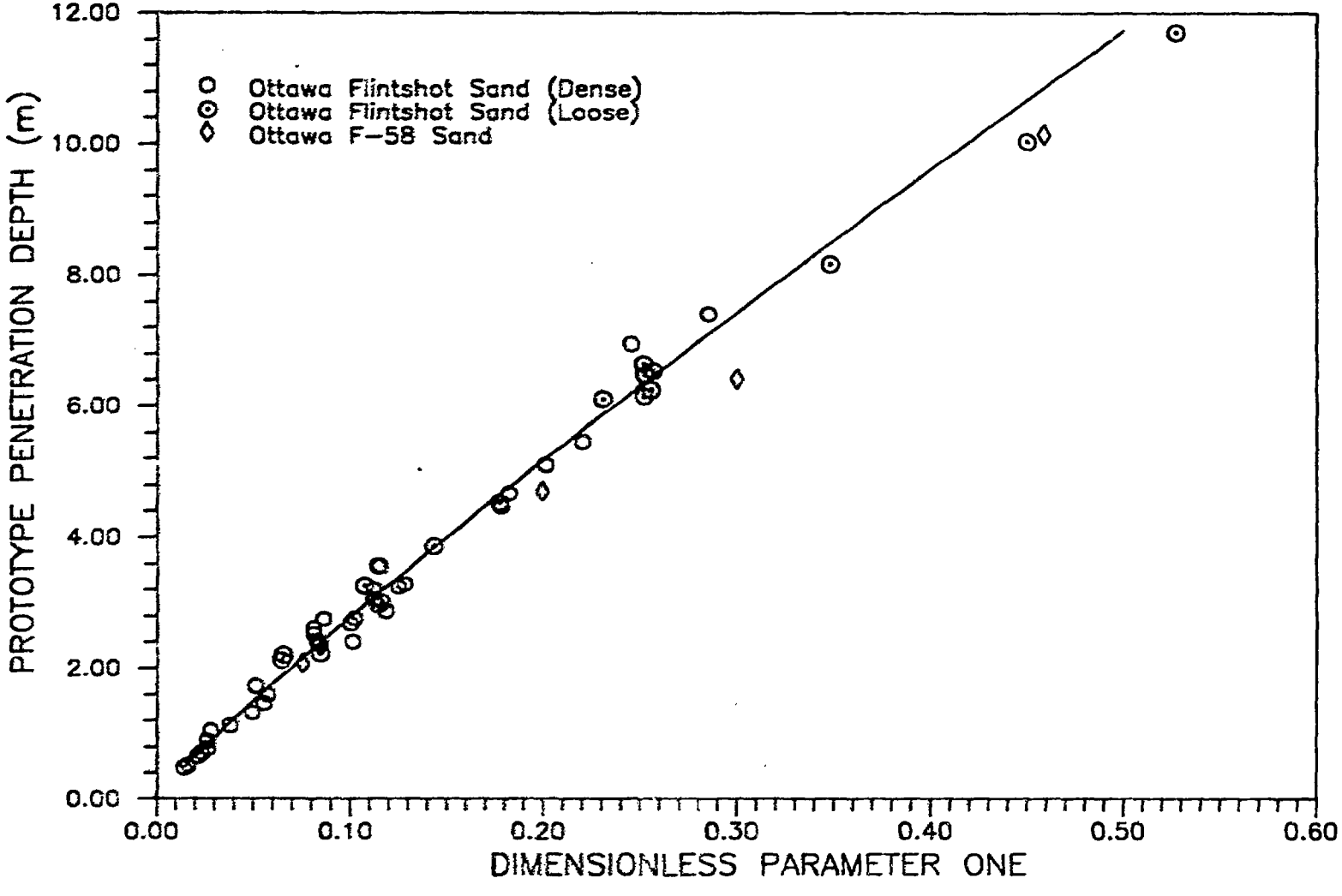

Figure 33. Dimensionless Parameter One vs. Prototype Penetration Depth for Ottawa Sands

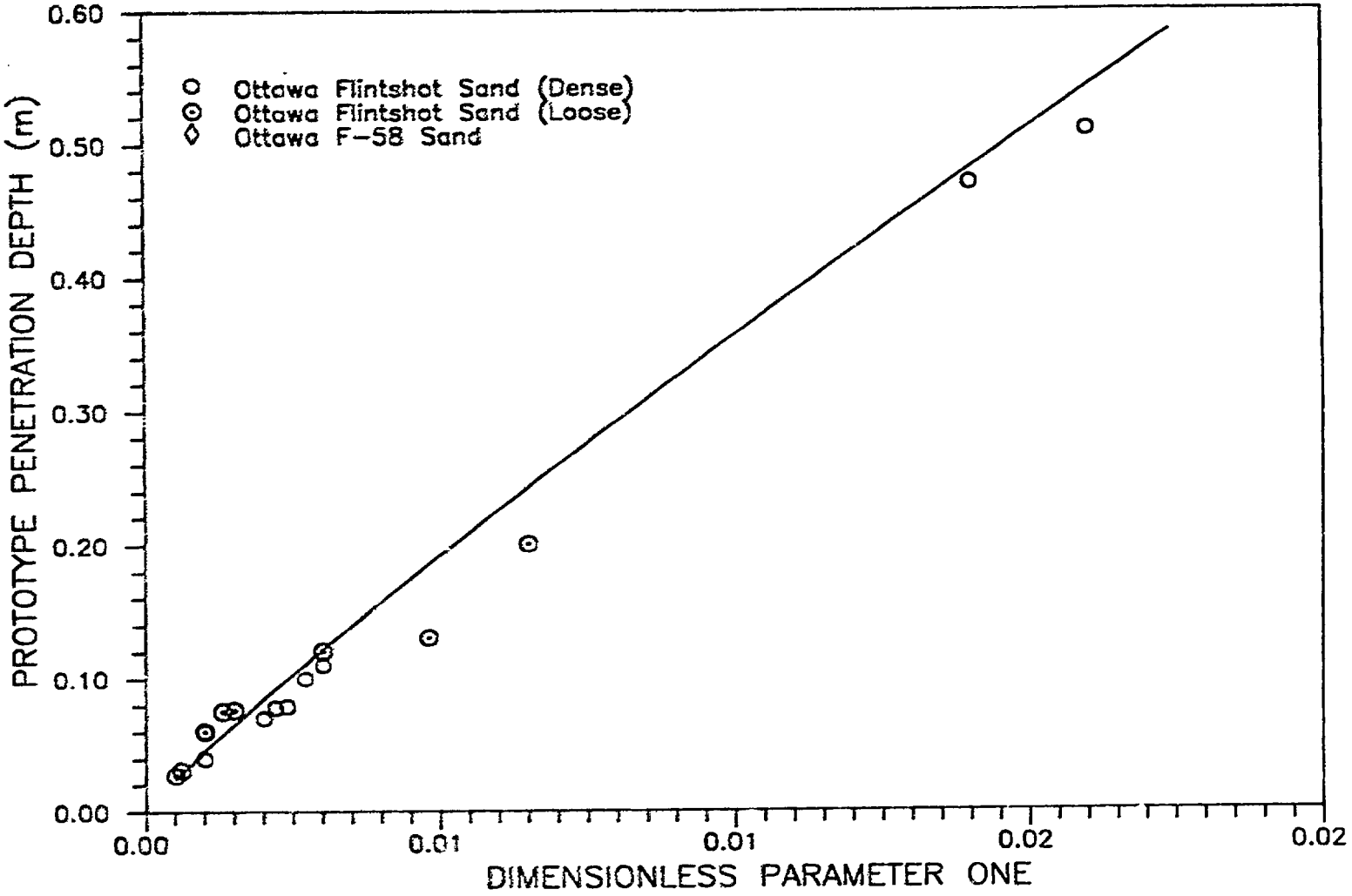

Figure 34. Exploded View, Low g Test Results for Dimensionless Parameter One vs. Prototype Penetration Depth, Ottawa Flintshot Sand

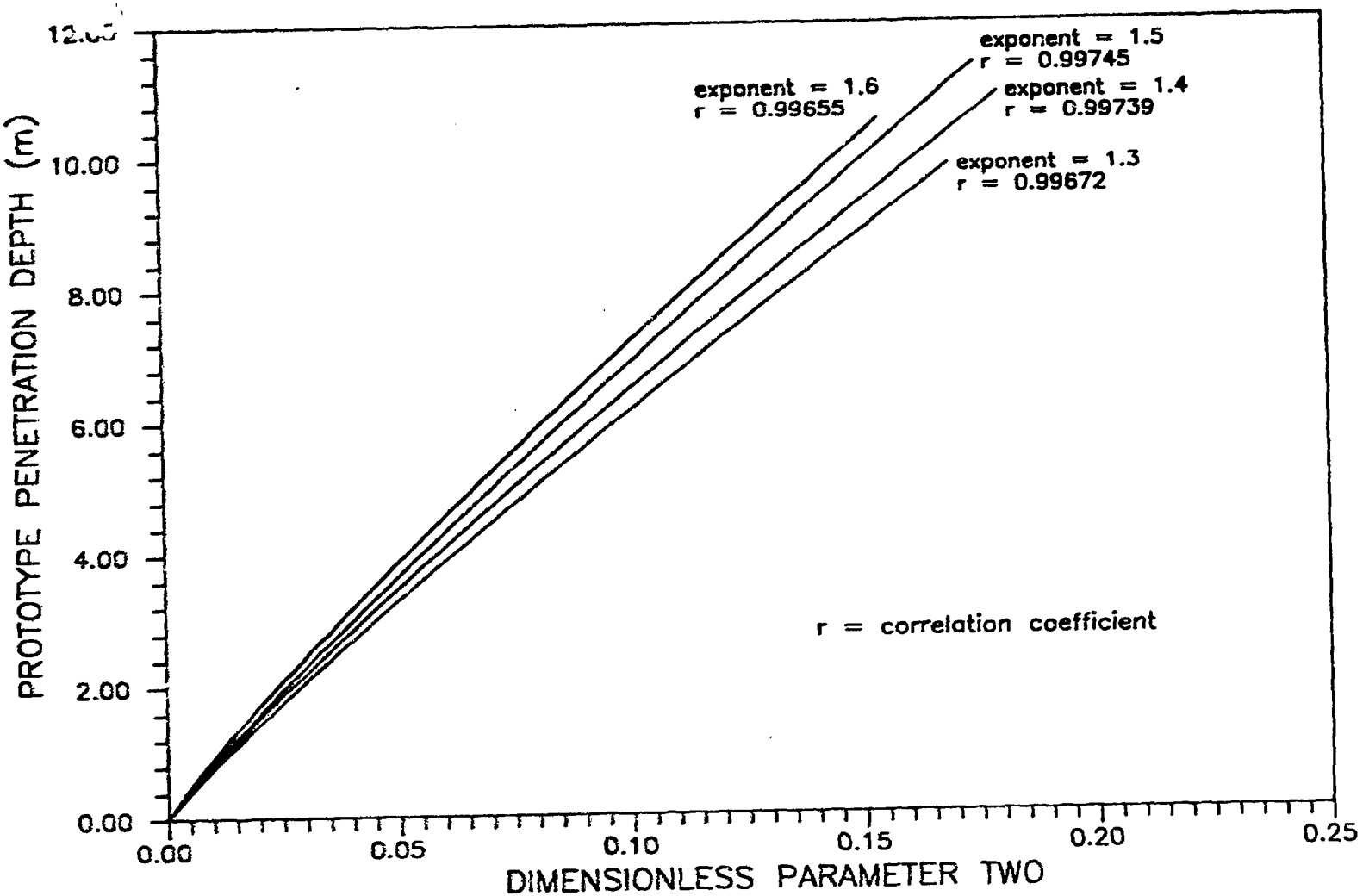

Figure 35. Best Power Fit Analysis for Pi Term 6 (Void Ratio) in Dimensionless Parameter Two

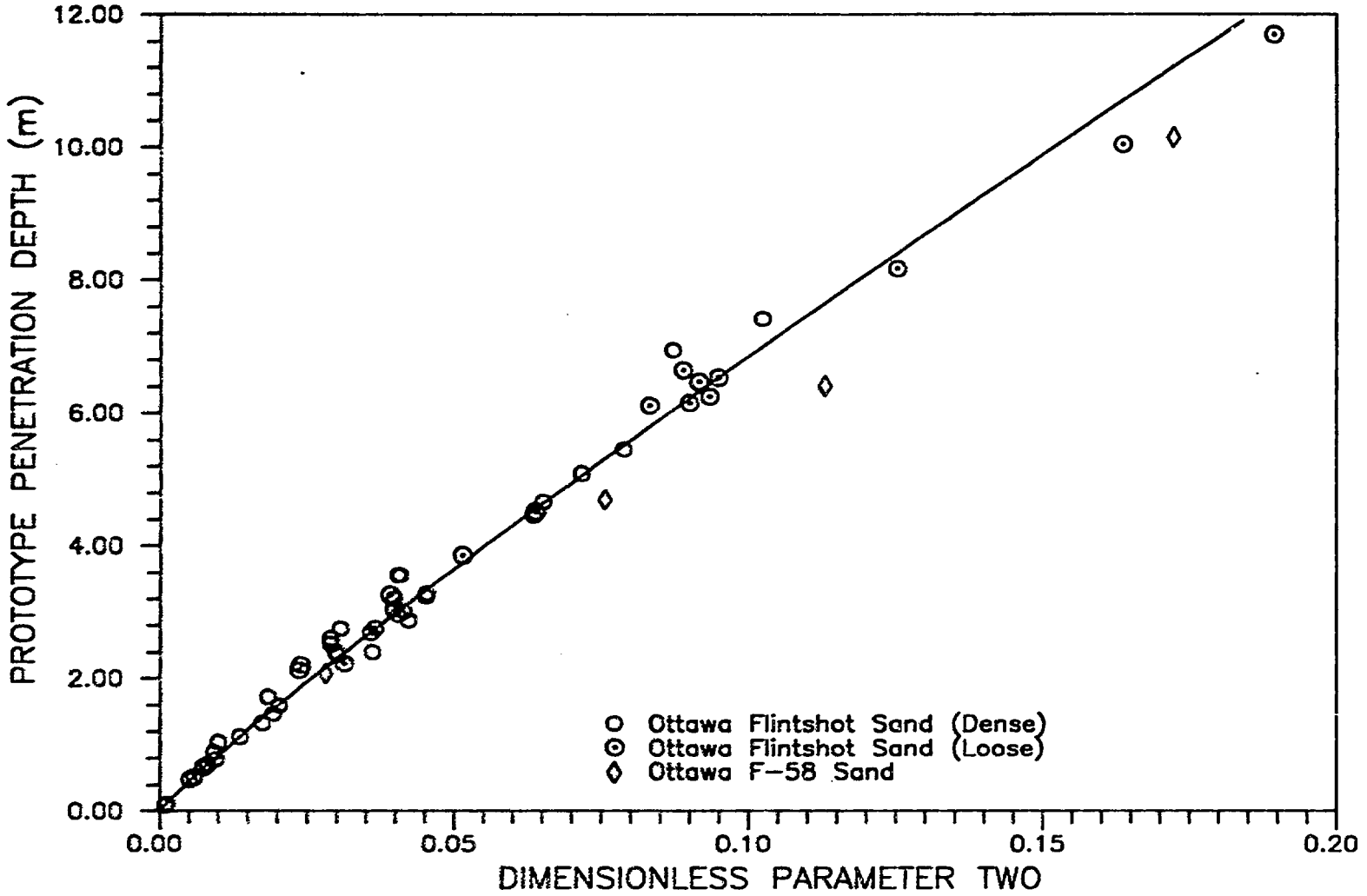

Figure 36. Dimensionless Parameter Two vs. Prototype Penetration Depth for Ottawa Sands

correlate as well as does the data for the two densities of Ottawa Flintshot sand. Further evidence that adjusting for void ratio alone does not allow convergence of curves for separate soil types is provided in Figure 37, which superimposes the test data for all test soils on the curve expressed by Equation (58).

To further assess the soil parameters resulting in the separate curves of Figure 37, attempts were made to develop correlations for other pi terms representing different soil properties. Analysis of various friction angles for the test soils (π_4) met with no real success; similarly, no coherent pattern emerged for particle shape or particle size. These latter analyses were, however,based largely on assumed values and relationships; consequently, their potential significance cannot be ignored in future work dedicated to determining the sensitivity of the penetration depth to different quantifiable soil properties. At this point, however, it is clear that the void ratio (or relative density) of a soil target is a significant factor in the magnitude of penetration depth.

C. COMPARISON TO YOUNG'S EQUATION

The largest and best quantified group of full-scale penetration tests that have been conducted are the previously described penetrator tests conducted by the Sandia Corporation and expressed by Young's empirical equation. Thus, comparison of Young's Equation to centrifuge penetration test data is an appropriate method of assessing comparative magnitudes of centrifuge versus full-scale penetration test results.

Figure 38 is a plot of the centrifuge test results with Young's Equation superimposed for the range of S values applicable to most sands (Appendix A). Excellent agreement in the magnitudes of predicted penetration depths is seen. In addition, the increase in penetration depth with the decrease in soil density described by Young's S values is seen in the centrifuge test results. The narrower range of penetration depths defined by the centrifuge test data is likely the result of the more carefully controlled, well-defined targets used in this research. Based on the large variation in penetration depths observed between the dense and loose samples of Ottawa Flintshot sand, it is expected that significant differences would also be observed for very different soil types.

A consideration of the wide range of geologic material types included in the description of individual S values strongly suggests the potential for refined depth estimates given more specific selection and/or definition of S values.

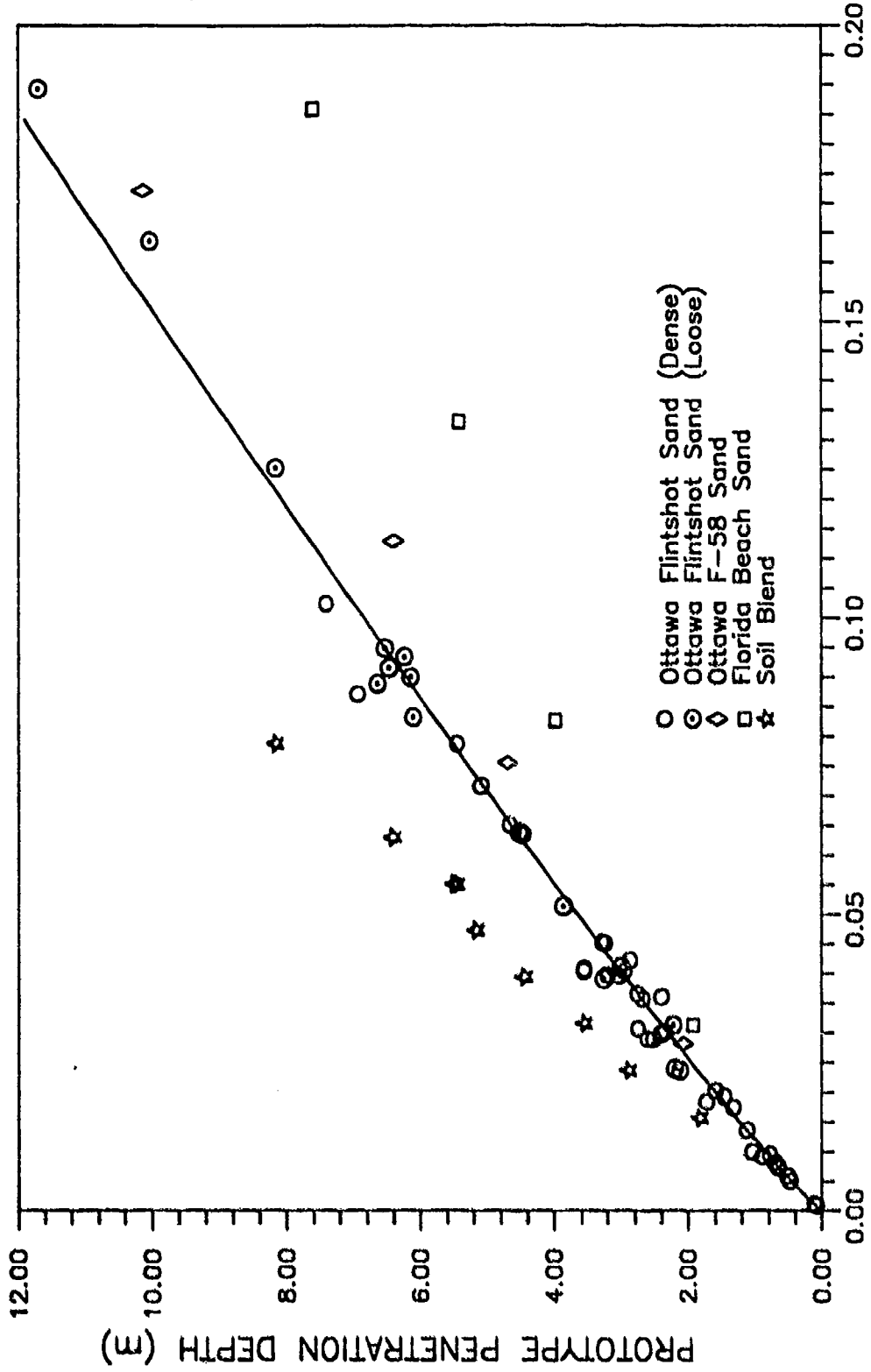

Figure 37. Dimensionless Parameter Two vs. Prototype Penetration Depth for All Test Sands

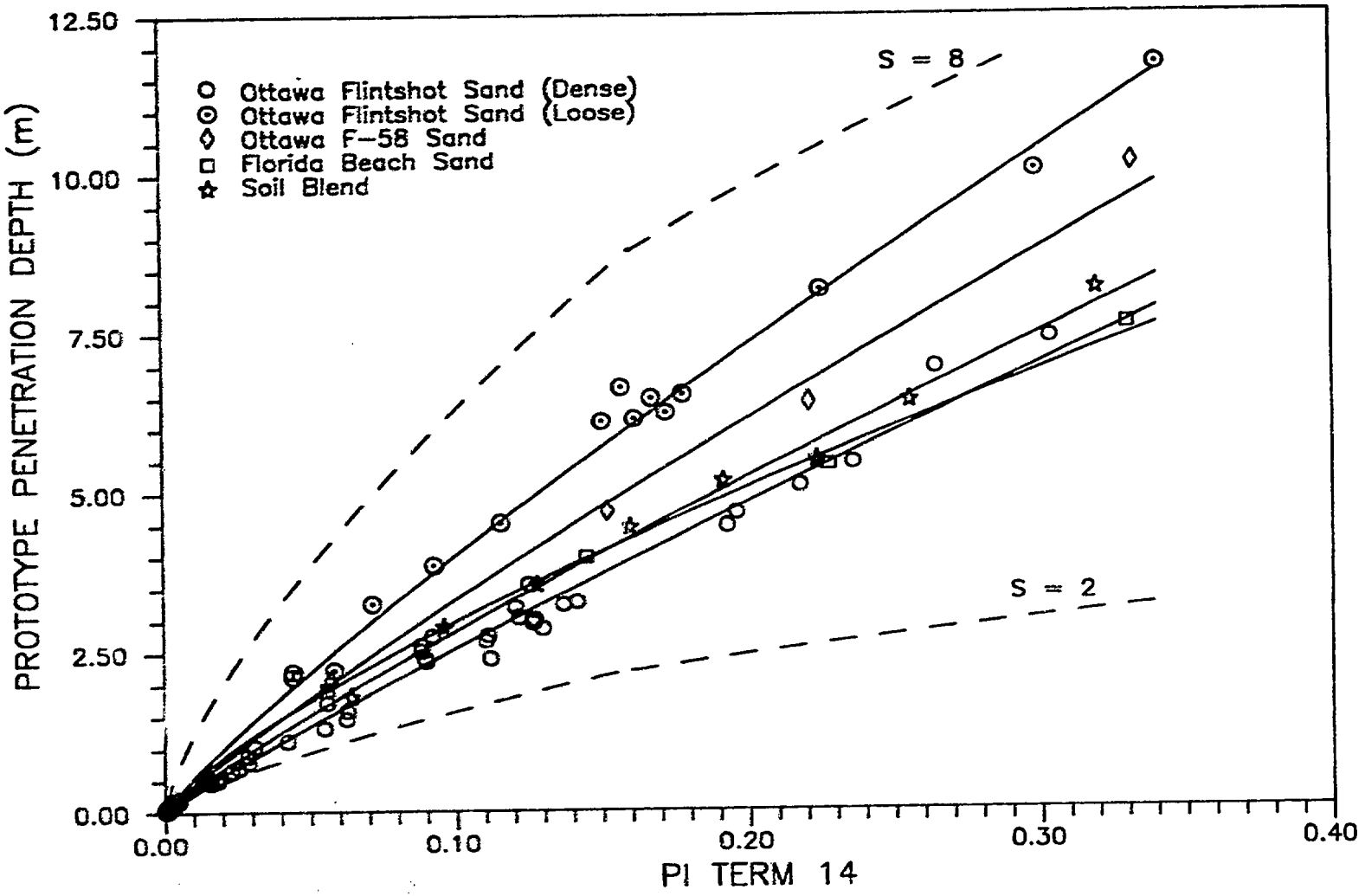

Figure 38. Pi Term 14 vs. Prototype Penetration Depth for all Test Sands with Young's Equation Results Superimposed

Figure 39 is a plot of the S values back-calculated from the centrifuge test data using Young's equation. It is clear from this figure that the S values obtained in this manner are not constants for any given soil type. In contrast, Figure 40 presents the results of back-calculated S values using the best-fit power curves for dense and loose Ottawa Flintshot sand (equations 41 and 42). In this plot, the backcalculated S values are nearly constant. Thus, use of a soil-dependent exponent for the mass to area ratio of the projectile, as opposed to a single constant soil descriptor term, appears to be essential to defining differences in soil target penetrability. It would be desirable to verify this conclusion with penetration data from full-scale tests performed in controlled soil samples; unfortunately, for the many reasons discussed earlier, such data are not available in the published literature.

The breaks in the S = 2 and S = 8 curves shown in Figure 38 that occur at a π_{14} value of approximately 0.16 are a consequence of Young's mass scaling factor, K (Appendix A), used for prototype masses less than approximately 27 kilograms. Inclusion of this factor in Young's equation depresses the lower portion of the curves, and results in better bracketing of the centrifuge test data. As discussed in Section II, although the need for this scaling factor is not fully understood, it was introduced into Young's Equation to compensate for the reduced penetration depths observed for small projectile masses. A similar difficulty in scaling low mass projectile data was encountered in early analysis attempts to linearly correlate the centrifuge and 1-g penetration test data of this research. As previously noted, although good linear correlation existed between the centrifuge data, the correlation could not be extended to the 1-g penetration data, unless some scale factor was introduced. Young initially used a linear correlation to describe the relationship between projectile mass to area ratio and penetration depth (Reference 11). To provide better correlation with additional large-scale test data that became available, this linear relationship was subsequently revised to a power curve, with a mass to area ratio exponent of 0.5. From the analysis of this research, it appears that selection of an appropriate soil-specific exponent may effectively eliminate the need to use an arbitrary mass-scaling factor to describe penetration depths for low projectile masses.

The preceeding information seems to show significant potential for

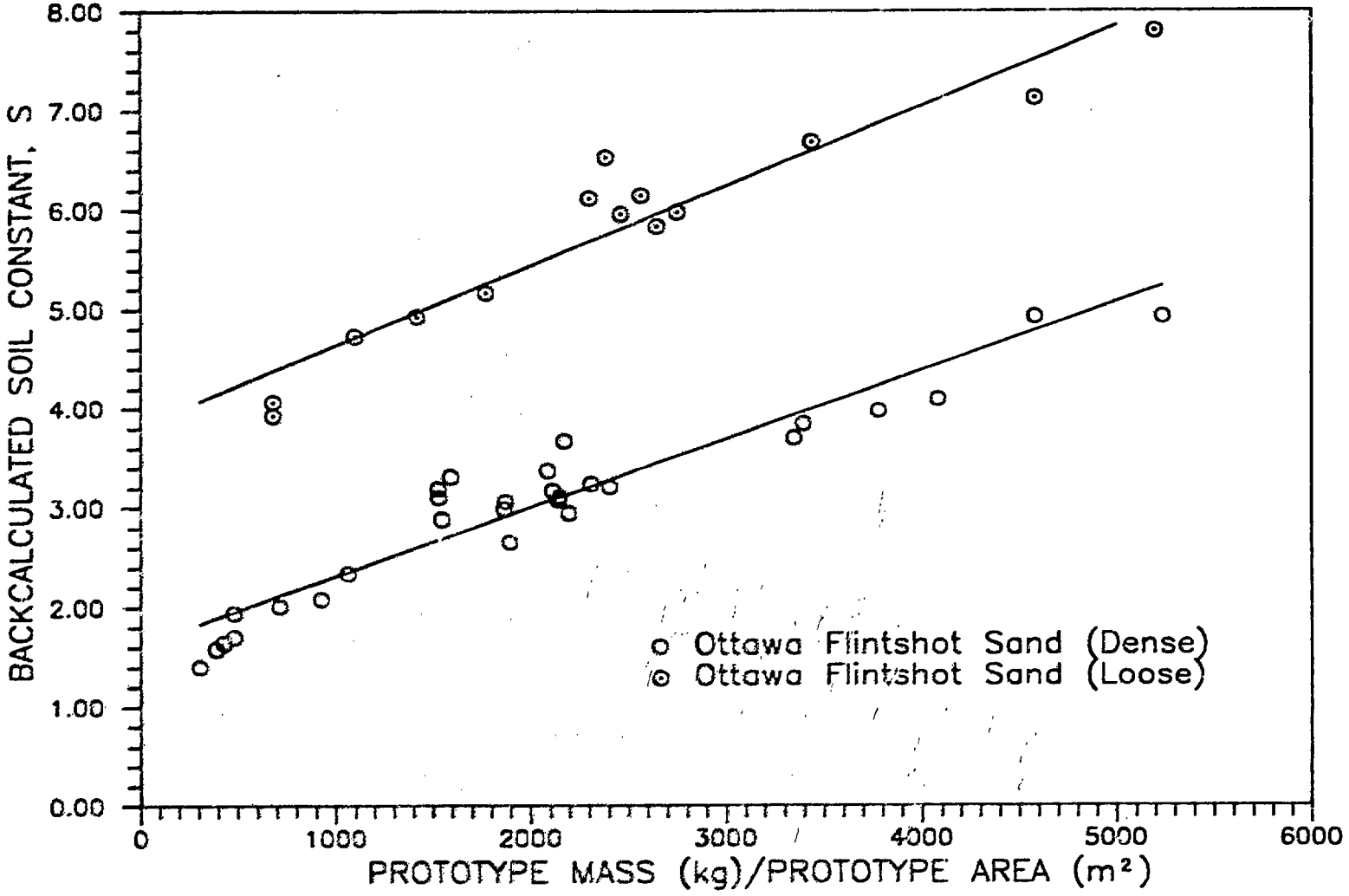

Figure 39. Prototype Mass/Prototype Area vs. Backcalculated S Values from Young's Equation, for Ottawa Flintshot Sand

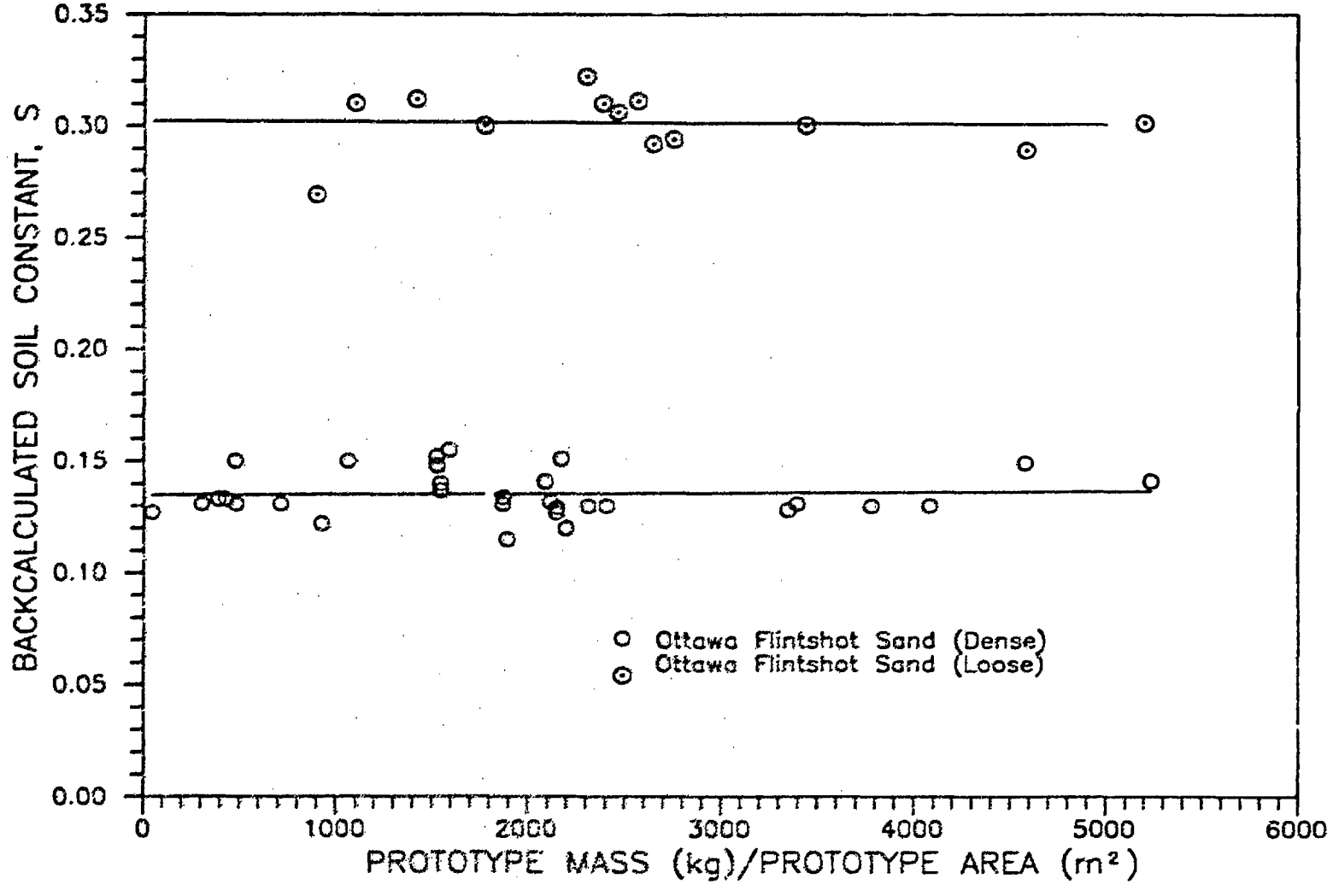

Figure 40. Prototype Mass/Prototype Area vs. Backcalculated S Values from Power Fit Equations, for Ottawa Flintshot Sand

improvements to Young's Equation. The potential modifications include:

1. Refinement of soil descriptions based on controlled sample preparation and testing at elevated g-levels;

2. Definition of soil-specific exponents for the weight to area ratio of the projectile;

3. Elimination of the arbitrary mass scaling factor.

The preceding potential modifications are limited to the parameters investigated in this research. The validity of equation components such as the nose shape factor, the omission of projectile length to diameter ratio, and the exact relationship of velocity to penetration depth are beyond the scope of this investigation. It appears, however, that very significant refinements to Young's Equation can be made for the most arbitrary components of the equation--mass scaling factor and soil description--with the performance of additional centrifuge tests on different soil types.

D. ANGLED IMPACT TESTS

A series of centrifuge tests, using 44 caliber brass projectiles, was performed at 60 g to demonstrate the flexibility of the gun mount system. To better illustrate the differences in impact angle and location that can be obtained by varying the gun angle and eccentricity, the same soil sample was used for each of several series of three shots; each shot within a series had a different planned impact angle and location. Figure 41 shows the results of one such series of shots, for the gun positioned approximately 0.76 meters from the center of rotation. Impact angles approximately 20 degrees from vertical could be obtained with the gun mounted at this location. Larger deviation from vertical could be obtained with the gun mounted at greater distances from the center of rotation.

E. TEST RESULTS AND ANALYSIS FOR MOIST SAND

As discussed in Section IV, the sample preparation techniques used in this research could not produce 100 percent saturation. Thus, the term "saturated" is used herein to refer to samples as nearly saturated as possible using the available saturation techniques. Test results are reported in Appendix F.

Ottawa F58 sand was used for most of the tests involving saturated and partially saturated soil. A series of tests was conducted on dry samples to

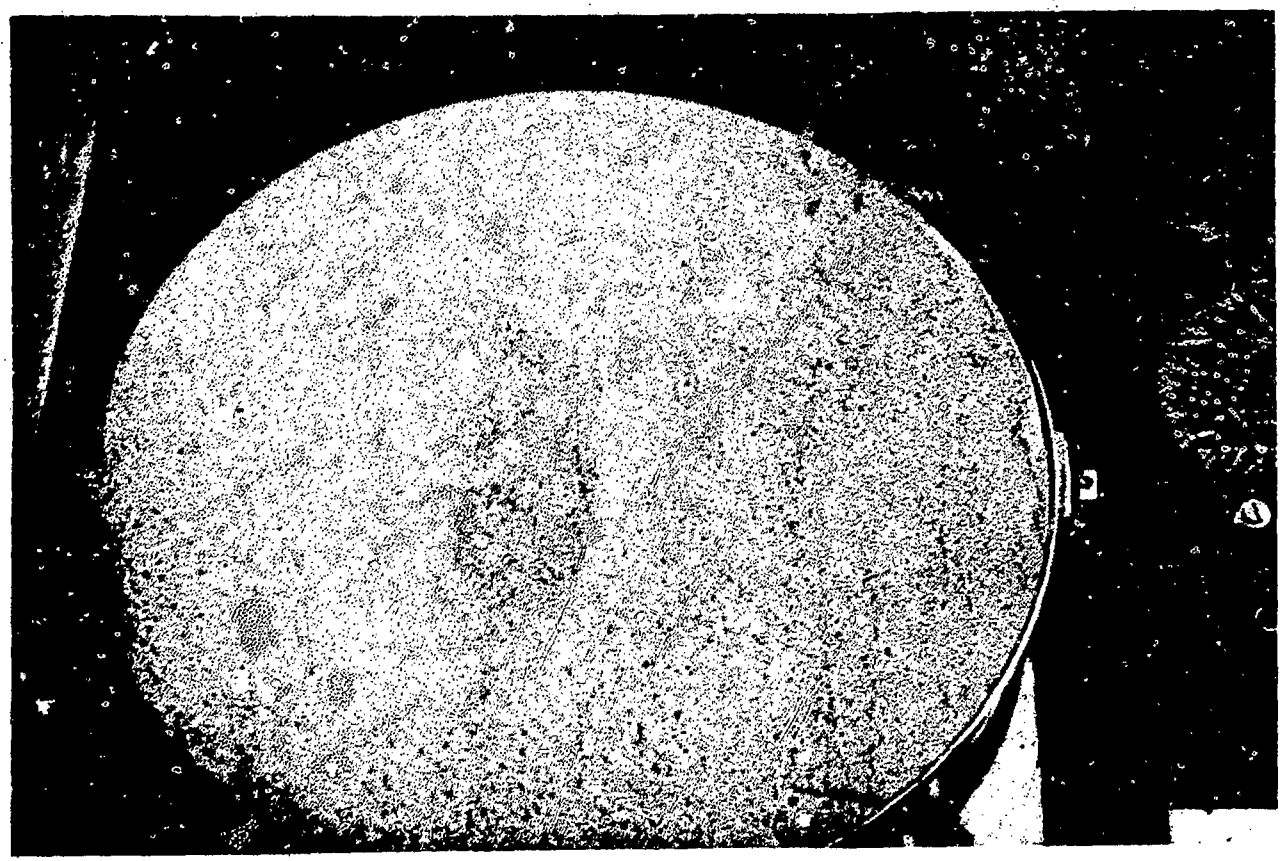

Figure 41. Angled Impact Tests

correspond to the tests conducted on samples prepared with water. Two different densities of Ottawa F58 sand were tested.

Although the number of tests conducted on samples prepared with water was too small to establish penetration depth curves comparable to those developed for the dry samples, the results of the tests on saturated and partially saturated soil provide significant insight into the response of such samples to a penetrating projectile. Further, the differences observed between 1-g and higher g conditions indicate a definite need to experimentally address the penetration problem using a technique such as centrifuge testing.

In all test sequences performed, the actual penetration depths for saturated samples under 1-g conditions were less than the actual penetration depths for comparable dry samples. However, at higher g-levels, the reverse was observed--actual penetration depths in saturated samples were greater than those in dry samples. This phenomenon is a function of the differences in effective confining pressures in the soil samples between 1-g and higher g conditions. The response of a granular soil to an applied external load, such as that imposed by the action of the penetrating projectile, depends not only on the applied load, but also on the initial void ratio (or relative density) of the soil sample and on the magnitude of the effective confining pressure imposed by the surrounding soil. At the extremely low confining pressures existing under 1-g test conditions the soil dilates, or increases in volume. In dry samples, this results in greater actual penetration depths than are observed for the dry centrifuge tests where the higher confining pressures induced by the accelerated g levels lead to a reduction in sample volume and decreased actual penetration depths.

For the saturated samples, however, dilation at the very low confining pressures results in a decrease in pore pressure and accompanying increase in effective confining pressure. The increased soil strength associated with the increased effective stress consistently resulted in smaller observed actual penetration depths in the saturated samples under 1-g conditions, compared to the actual penetration depths in the dry samples.

At higher g levels, the increased confining pressures and corresponding volume reduction on loading leads to an increase in pore pressure and consequent reduction in effective confining pressure. Thus, greater actual penetration depths are observed for the saturated compared to the dry centrifuge tests.

The actual penetration depths obtained for the partially saturated soil samples under the same test conditions were significantly less than the actual penetration depths observed for both dry and saturated samples. This is a function of the high negative pore pressures associated with capillary rise in the partially saturated soil. These high negative pore pressures create a significant increase in the soil strength, thus resulting in decreased actual penetration depths in both the 1-g and higher g environments.

F. CONCLUSIONS AND RECOMMENDATIONS

A method for preparing soil samples using pluviation was developed that allowed uniform, level, and reproducible soil samples to be formed over a wide range of densities. Samples were prepared using uniform Ottawa Flintshot and F58 sands, a uniform Florida Beach sand, and a nearly well-graded sand blend. These samples were used in a series of projectile penetration tests performed under 1-g conditions and at elevated g levels developed by rotating the soil samples in a centrifuge during testing.

The projectile penetration tests were undertaken in an attempt to better understand soil parameters affecting penetration depth of projectiles, in particular the effect of confining pressure. Use of a centrifuge allowed duplication of the stress levels between large-scale in situ target soils and the small-scale test targets. By careful preparation of the soil samples, many of the variables inherent to in situ soil targets could be eliminated, and the penetration event could be studied for specific soil types and densities.

A Thompson Contender® pistol with interchangeable barrels in four calibers was used to fire spherical projectiles of brass, aluminum, nylon and PVC. The four material types were used to assess whether differences in penetration depth were observed as a function of material type. Most of the penetration tests were conducted with the brass projectiles to most closely simulate material properties of manufactured projectiles. Vertical impact angle tests were conducted at average velocities of approximately 305 meters/second. To allow the tests to be conducted in the centrifuge environment, a remote triggering system and a variable mechanical mount accommodating the different angular velocities of the gun and the soil target were developed.

The results of the test program indicate that the centrifuge technique is a useful and effective method of studying the projectile penetration phenomenon.

The delivery system resulted in very reproducible actual penetration depths in both the 1-g and the elevated g environments. Comparison of the results of the 1-g penetration tests to the centrifuge penetration tests indicates a distinct difference in actual penetration depths. This observed difference is in accord with difficulties that have been experienced by other researchers in scaling results of 1-g penetration tests to prototype dimensions, and provides strong evidence of the need to include g-level in design of penetration experiments in granular soils. Such a need is also suggested by the results of a dimensional analysis that was performed in conjunction with the test program. Further evidence of the effectiveness of the centrifuge testing technique is provided by the excellent agreement between prototype penetration depths predicted by the centrifuge tests and actual penetration depth values that have been obtained in full-scale penetration tests.

Analysis of the test results suggests that, within the subordnance velocity regime of the test program, penetration depth is best described by a power curve involving the ratio of the projectile mass to area raised to some exponent less than one. The exact value of this exponent is very much a function of the soil type and properties. The relative density or void ratio of the soil is a significant factor in determining the magnitude of this exponent for a particular soil type.

A comparison of the test results was made to Young's equation, an empirically-derived penetration depth prediction equation based on a large number of in situ full-scale penetration tests. Penetration depth magnitudes very comparable to observed depths from full-scale tests were predicted by the centrifuge test results. With additional centrifuge testing, modification of Young's equation to allow better selection of a soil descriptor (involving a soil-specific exponent for the projectile mass to area ratio) and to eliminate the need for an arbitrary mass scaling factor for small projectiles appears very promising.

There is significant potential for improvement in the state-of-the-art of penetration depth prediction with continuation of this research. Of most immediate importance is the performance of centrifuge tests on controlled soil samples of different types with different engineering characteristics. Such tests would include additional sands, silts, clays and manufactured mixtures designed to simulate natural soils. Performance of these tests will provide better definition of the appropriate soil-specific exponent values, and allow realistic groupings by soil type and properties to be made. Such tests will also promote a better

understanding of the engineering characteristics of soils that most significantly affect penetration depth. Tests should be conducted on soils in dry, saturated and partly saturated states. Although the pilot tests involving moist samples that were conducted for this research provided useful information on saturation techniques, and clear evidence of the need for testing at elevated g levels; insufficient tests were conducted to establish the prototype penetration depth relationships comparable to those developed for the dry samples.

Although determination of specific exponential values should be made using specific soil types, some tests using layered targets would be desirable to assess the variability of the exponents obtained with targets more representative of in situ soils. This would also allow comparison of results to full-scale field tests on layered soils, as well as evaluation of the various empirical methods that have been developed to weigh individual layers within a layered target material.

A velocity measurement system for use on the centrifuge was actually designed and constructed for this test program; however, time constraints prevented the equipment modifications and shakedown tests necessary for its use. Future tests should incorporate actual velocity measurements in the centrifuge environment to allow more precise control of the test variables. In addition, different velocities should be investigated to expand the range of applicability of the penetration depth data, particularly into the higher velocity regimes of interest for numerous penetration applications.

Once the variability of penetration depth with soil target properties has been more fully investigated, tests involving different projectile geometries could be conducted. There is potential for the different mechanisms involved with the penetration process as a function of nose shape and projectile geometry to be significantly affected by the soil type and properties. Similarly, the blunt versus piercing penetration that may be obtained depending on the angle of attack of a projectile could be investigated by utilizing the variable impact angle capabilities of the firing system. These latter tests, in particular, would be complemented by numerical parametric studies.

LIST OF REFERENCES

1. McNeill, R. L., "Rapid Penetration of Terrestrial Materials--The State of the Art," Proceedings, Conference on Rapid Penetration of Terrestrial Materials, Texas A & M University, College Station, Texas, February, 1972, pp. 11-126.

2. Backman, M. E. and Goldsmith, W., "The Mechanics of Penetration of Projectiles into Targets," International Journal of Engineering Science, Vol. 16, No. 1, 1978, pp. 1-99.

3. Logan, D. L., "Evaluation of Projectile Impact on Earth-Covered Structures," Final Report, Air Force Engineering and Services Center, Tyndall Air Force Base, Florida, 1984, 18 pp.

4. Byers, R. K., Yarrington, P. and Chabai, A. J., "Dynamic Penetration of Soil Media by Slender Projectiles," International Journal of Engineering Science, Vol. 16, No. 11, 1978, pp. 835-844.

5. Melzer, I. K. J., "Soil Exploration from the Air," Journal of the Indian National Society of Soil Mechanics and Foundation Engineering, Vol. 9, No. 4, October, 1970, pp. 363-369.

6. True, Daniel, G., "Rapid Penetration into Seafloor Soils," Offshore Technology Conference, 1974, pp. 607-618.

7. Setchell, R.E. and Guzman, J.A., "Laboratory Techniques for Simulation of Projectile Penetration into Geological Targets," Sandia Laboratory, Albuquerque, New Mexico, January, 1983, 22 pp.

8. Chabai, A. J., Young, C. W., Yarrington, P., Patterson, W.J., Byers, R. K., "Terradynamic Technology: Theory and Experiment," Report No. SAND-77-0523C, Sandia Laboratory, Albuquerque, New Mexico, 1977, 27 pp.

9. Thigpen, L., "Penetration of Projectiles into Continuous Earth Media," Report No. SC-RR-720204, Sandia Laboratory, Albuquerque, New Mexico, May, 1972, 58 pp.

10. True, D. G., "Penetration of Projectiles into Seafloor Soils," Final Report No. CEL-TR-822, Navy Civil Engineering Lab, Port Hueneme, California, May, 1975, 63 pp.

11. Young, C. W., "The Development of Empirical Equations for Predicting Depth of an Earth-Penetrating Projectile," Report No. SC-DR-67-60, Sandia Laboratory, Albuquerque, New Mexico, May, 1967, 41 pp.

12. Bernard, R. S., "Depth and Motion Prediction for Earth Penetrators," Final Report No. WES-TR-S-78-4, U. S. Army Engineering Waterways Experiment Station, Vicksburg, Mississippi, June, 1978, 31 pp.

13. Al-Hussaini, M. M., "Centrifuge Model Testing of Soils: A Literature Review," Miscellaneous Paper S-76-9, U. S. Army Engineering Waterways Experiment Station, Vicksburg, Mississippi, June, 1976.

14. Cheney, J. A. and Fragaszy, R. J., "The Centrifuge as a Research Tool," Geotechnical Testing Journal, ASTM, Vol. 7, No. 4, December, 1984, pp. 182-187.

15. Anandarajah, A., Kim, Y. S., Thompson, P. Y., and Rosengren, P., "Progress in Geotechnical Dynamic Centrifuge Modeling," Final Report, Air Force Engineering Services Center, Tyndall Air Force Base, Florida, June, 1985, 25 pp.

16. Wang, W. L., "Experimental Study of Projectile Penetration into Ottawa Sand at Low Velocities," Journal of Spacecraft and Rockets, Vol. 6, No. 4, April, 1969, pp. 497-498.

17. Rohani, B., "High Velocity Fragment Penetration of Soil Targets," Proceedings, Conference on Rapid Penetration of Terrestrial Materials, Texas A & M University, College Station, Texas, February, 1972, pp. 251-280.

18. Mumma, D. and Randall, D., "Test Results of Earth Penetrators," Final Report No. DNA-4180F, Defense Nuclear Agency, November, 1977, 47 pp.

19. Butler, D. K., "Development of a High-Velocity Powder Gun and Analysis of Fragment Penetration Tests into Sand," Misc. Paper No. S-75-27, U. S. Army Engineering Waterways Experiment Station, Vicksburg, Mississippi, October, 1975, 59 pp.

20. Henderson, D., "Impact and Penetration Technology Program Parametric Study," Final Report No. AVSD-0055-76-RR, AVCO Systems Division, Wilmington, Maryland, May, 1976, 129 pp.

21. Yankelevsky, D. Z. and Gluck, J., "Nose Shape Effect on High Velocity Soil Penetration," International Journal of Mechanical Science, Vol. 22, No. 5, 1980, pp. 297-311.

22. Yankelevsky, D. Z., "The Optimal Shape of an Earth Penetrating Projectile," International Journal of Solids and Structures, Vol. 19, No. 1, 1983, pp. 25-31.

23. Wagner, M. H., Fulton, C. C., and Kreyenhagen, K. N., "Parametric Study of the Effects of Target Properties, Projectile Design, and Impact Conditions on Earth Penetrator Processes," Topical Report No. DNA-4160T, Defense Nuclear Agency, November, 1976, 85 pp.

24. Robins, B., New Principles in Gunnery, Nourse, London, England, 1742.

25. Euler, L., Neue Grundsatze der Artillerie, Berline, Germany, 1745.

26. Poncelet, J. V., Cours de Mecanique Industrielle, Bruxelles, France, 1829.

27. Resal. M. H., Compt. rend., Vol. 120, 1895.

28. Petry, Monographies de Systems d'Artillerie, Brussels, 1910.

29. Allen, W. A., Mayfield, E. B. and Morrison, H. L., "Dynamics of a Projectile Penetrating Sand," Journal of Applied Physics, Vol. 28, No. 3, March, 1957, pp. 370-376.

30. Allen, W. A., Mayfield, E. B. and Morrison, H. L., "Dynamics of a Projectile Penetrating Sand. Part II," Journal of Applied Physics, Vol. 28, No. 11, Nov., 1957, pp. 1331-1335.

31. Hakala, W. W., "Resistance of a Granular Medium to Normal Impact of a Rigid Projectile," Ph.D. Thesis, Virginia Polytechnic Institute, Blacksburg, Virginia, June, 1965, 231 pp.

32. Wang, W. L., "A Study of the Penetration of Projectiles Impacting Upon Soil at Low Velocities," Ph.D. Dissertation, University of New Mexico, Albuquerque, New Mexico, January, 1968, 112 pp.

33. Young, C. W., "Depth Prediction for Earth-Penetrating Projectiles," Journal of the Soil Mechanics and Foundations Division, ASCE,, Vol. 95, No. SM3, May, 1969, pp. 803-817.

34. Young, C. W., "The Terradynamic Development of a Low-Velocity Earth Penetrating Projectile," Report No. SC-DR-70-302, Sandia Laboratory, Albuquerque, New Mexico, July, 1970, 102 pp.

35. Young, C. W., "Empirical Equations for Predicting Penetration Performance in Layered Earth Materials for Complex Penetrator Configurations," Report No. SC-DR-720523, Sandia Laboratory, Albuquerque, New Mexico, December, 1972, 65 pp.

36. Young, C. W., "A Review of Full Scale Terradynamic Testing," Report No. SAND78-1767c, Sandia Laboratory, Albuquerque, New Mexico, 1978, 6 pp.

37. Colp, J. L., "Terradynamics: A Study of Projectile Penetration of Natural Earth Materials," Report No. SC-DR-68-215, Sandia Laboratory, Albuquerque, New Mexico, June 1968, 61 pp.

38. Aitken, G. W., Swinzow, G. K., and Farrell, D. R., "Projectile and Fragment Penetration in Soil and Frozen Soil," Cold Regions Research and Engineering Lab, Hanover, New Hampshire, 1976, 14 pp.

39. Hadala, P. F., "Evaluation of Empirical and Analytical Procedures Used for Predicting the Rigid Body Motion of an Earth Penetrator," Report No. AEWES-MISC-PAPER-S-75-15, U.S. Army Engineering Waterways Experiment Station, Vicksburg, Mississippi, June, 1975, 81 pp.

40. Bishop, R. F., Hill, R. and Mott, N. F., "The Theory of Indentation and Hardness Tests," Proceedings, London Physical Society, Vol. 57, 1945, pp. 142-159.

41. Goodier, J. N., "On the Mechanics of Indentations and Cratering in Solid Targets of Strain-Hardening Metal by Impact of Hard and Soft Spheres," Technical Report No. 002-64, Stanford Research Institute, Poulter Laboratories, Menlo Park, California, July, 1964.

42. Hanagud, S. V., and Ross, B., "Large Deformation, Deep Penetration Theory for a Compressible Strain-Hardening Target Material," AIAA Journal, American Institute of Aeronautics and Astronautics, Vol. 9, No. 5, May, 1971, pp. 905-911.

43. Bernard, R. S. and Hanagud, S. V., "Development of a Projectile Penetration Theory: Penetration Theory for Shallow to Moderate Depths," Report No. S-75-9, U. S. Army Engineering Waterways Experiment Station, Vicksburg, Mississippi, 1975.

44. Ross, B. and Hanagud, S., "Penetration Studies of Ice with Application to Arctic and Subarctic Warfare," Final Report, Project 7000-452, Stanford Research Institute, Poulter Laboratories, Menlo Park, California, September, 1969.

45. Norwood, F. R., "Cylindrical Cavity Expansion in a Locking Soil," Report No. SLA-74-0201, Sandia Laboratory, Albuquerque, New Mexico, July, 1974, 35 pp.

46. Yew, C. H. and Stirbis, P. P., "Penetration of Projectile into Terrestial Target," Journal of the Engineering Mechancis Division, ASCE, Vol. 104, No. EM2, April, 1978, pp. 273-286.

47. Allen, R. T., "Prediction of the Deceleration of an Earth Penetrating Vehicle," Report No. SSS-IR-74-2192, Systems, Science and Software, La Jolla, California, April, 1974.

48. Karnes, C. H., Dawson, P. R., Silva, A. J. and Brown, W. T., "Sediment Mechanical Response Due to Emplacement of a Waste Canister," Marine Geotechnology, Vol. 5, No. 3-4, 1984, pp. 379-401.

49. Yankelevsky, D. Z. and Adin, M. A., "A Simplified Analytical Method for Soil Penetration Analysis," International Journal for Numerical and Analytical Methods in Geomechanics, Vol. 4, 1980, pp. 233-254.

50. Byers, R. K., Chabai, A. J., Walsh, R. T., "Predictions of Projectile Penetration Phenomena and Comparison with Experiments in a Soil Medium," Report No. SAND-75-0174, Sandia Laboratory, Albuquerque, New Mexico, May 1975, 356 pp.

51. Wagner, M. H., Kreyenhagen, K. N., and Goerke, W. S., "Numerical Analysis of DNA Earth Penetrator Experiment at DRES," Final Report No. CRT-2050-2, California Research and Technology Institute, Woodland Hills, California, June, 1975, 161 pp.

52. Werne, R. W., "Structural Response of an Earth Penetrator," Report No. UCID-17327, Sandia Laboratory, Albuquerque, New Mexico, November, 1976, 51 pp.

53. Stirbis, P. P., "Analytical Response of an Earth Penetrator," Report No. 76-0351, Sandia Laboratory, Albuquerque, New Mexico, 1977, 87 pp.

54. Wagner, M. H. and Fulton, C. C., "Numerical Analyses of Penetration Dynamics in Support of Investigations of Scaling Relationships for Earth Penetrators," Final Report No. WES-MP-S-77-23, California Research and Technology Institute, Woodland Hills, California, November, 1977, 37 pp.

55. Yarrington, P. and Ruiz, N. K., "PENAP: An Interactive Computer Program for Calculating Surface Loads on Conical- and Ogival- Nosed Earth Penetrators," Report No. 77-1359, Sandia Laboratory, Albuquerque, New Mexico, 1978, 72 pp.

56. Yarrington, P., Norwood, F. R. and Ruiz, N. K., "PENOB: A Modification of the PENAP Code to Treat Oblique Impact of Earth Penetrators," Report No. 78-1154, Sandia Laboratory, Albuquerque, New Mexico, 1980, 47 pp.

57. Montgomery, S. T., "Computer Simulations of 75-mm Projectiles Impacting Sand Targets," Report No. SAND-82-0831, Sandia Laboratory, Albuquerque, New Mexico, 1982, 53 pp.

58. Norwood, F. R., "RUNNOS and RUNDEP: Computer Programs for Calculating Loads on Earth Penetrators," Sandia Laboratory, Albuquerque, New Mexico, May, 1982, 22 pp.

59. Davie, N. T. and Richgels, M. A., "GNOME: An Earth-Penetrator Code," Report No. SAND-82-2358, Sandia Laboratory, Albuquerque, New Mexico, 1983, 66 pp.

60. Caudle, W. N., Pope, A. Y., McNeill, R. L. and Margason, B. E., "The Feasibility of Rapid Soil Investigations Using High-Speed, Earth-Penetrating Projectiles," Proceedings, International Symposium on Wave Propagation and Dynamic Properties of Earth Material, ASCE, 1967, pp. 945-955.

61. Patterson, W. J., "Terradynamic Results and Structural Performance of a 650-Pound Penetrator Impacting at 2570 Feet Per Second," Report No. SC-DR-69-782, Sandia Laboratory, Albuquerque, New Mexico, December, 1969, 27 pp.

62. Seamons, L. O., "A Davis Gun Penetrator Launch System," Report No. SAND-74-5048, Sandia Laboratory, Albuquerque, New Mexico, August, 1974, 9 pp.

63. Sierakowski, R. L., Malvern, L. E., Milton, J. E., Ross, C. A. and Collins, J. A., "Penetrator Impact Studies of Soil/Concrete," Final Report No. AFOSR-TR-78-0164, University of Florida, Gainesville, Florida, November, 1977, 257 pp.

64. Malvern, L. E., Sierakowski, R. L., Ross, C. A., Milton, J. E., Ting, C. S., and Collins, J. A., "Study of Penetration Technology," Report No. AFATL-TR-76-129, Air Force Armament Laboratory, Eglin Air Force Base, Florida, November, 1976.

65. Butler, S. K., "High-Velocity Fragment Penetration into Sand: A Comparison of Experimental Results with Theoretical Predictions," Report No. AD-A025983, U. S. Army Engineering Waterways Experiment Station, Vicksburg, Mississippi, 1976, 15 pp.

66. Forrestal, M. J. and Grady, D. E., "Penetration Experiments for Normal Impact into Geological Targets," International Journal of Solids and Structures, Vol. 18, No. 3, 1982, pp. 229-234.

67. Forrestal, M. J., Lee, L. M., Jenrette, B. D. and Setchell, R. E., "Gas-Gun Experiments Determine Forces on Penetrators into Geological Targets," Journal of Applied Mechanics, ASME, Vol. 51, September, 1984, pp. 602-607.

68. Braslau, D., "Partitioning of Energy in Hypervelocity Impact Against Loose Sand Targets," Journal of Geophysical Research, Vol. 75, No. 20, July, 1970, pp. 3987-3999.

69. Schmidt, R. M., "Meteor Crater: Energy of Formation--Implications of Centrifuge Scaling," Proceedings, Eleventh Lunar and Planetary Science Conference, 1980, pp. 2099-2128.

70. Holsapple, K. A. and Schmidt, R. M., "On the Scaling of Crater Dimensions, 1. Explosive Processes," Journal of Geophysical Research, Vol. 85, No. B12, 1980.

71. Pokrovsky, G. I. and Fyodorov, I. S., Centrifuge Model Testing in the Construction Industry, Vol. I, Niedra Publishing House, Moscow, USSR, 1969.

72. Thigpen, L., "Projectile Penetration of Elastic-Plastic Earth Media," Journal of the Geotechnical Engineering Division, ASCE, Vol. 100, No. GT3, March, 1974, pp. 279-294.

73. Murff, J. D. and Coyle, H. M., "A Laboratory Investigation of Low Velocity Penetration," Proceedings, Conference on Rapid Penetration of Terrestrial Materials, Texas A & M University, College Station, Texas, February, 1972, pp. 319-360.

74. Murff, J. D. and Coyle, H. M., "Low Velocity Penetration of Kaolin Clay," Journal of the Soil Mechanics and Foundations Division, ASCE, Vol. 99, No. SM5, May 1973, pp. 375-389.

75. Buckingham, E., "Model Experiments and the Forms of Empirical Equations," Transactions, ASME, Vol. 37, 1915, pp. 263.

76. Baker, W. E., Westine, P. S., and Dodge, F. T., Similarity Methods in Engineering Dynamics, Theory and Practice of Scale Modeling, Hayden Book Company, Inc., Rochelle Park, New Jersey, 1973, pp. 171-199.

77. Schmidt, R. M. and Holsapple. K. A., "Theory and Experiments on Centrifuge Cratering," Journal of Geophysical Research, Vol. 85, No. B1, 1980.

78. Bolton, M. D., and Lau, C. K., "Scale Effects Arising from Particle Size," Proceedings, Centrifuge '88 International Conference on Geotechnical Centrifuge Modelling, Paris, France, 1988, pp. 127-131.

79. Rad, N. S. and Tumay, M. T., "Factors Affecting Sand Specimen Preparation by Raining," Geotechnical Testing Journal, Vol. 10, No. 1, March, 1987, pp. 31-37.

80. Kildalen, S. and Stenhamar, P., "Internal Report NGI Laboratory Sand Rainer," Internal Report 51505-15, Norwegian Geotechnical Institute, Oslo, Norway, February, 1977, 20 pp.

81. Eid, W. K., "Scaling Effect in Cone Penetration Testing in Sand," Ph.D. Dissertation, Virginia Polytechnic Institute, Blacksburg, Virginia, March, 1987.

82. Kar, A. K., "Projectile Penetration into Buried Structures," Journal of the Structural Division, ASCE, Vol. 104, No. ST1, January 1978, pp. 125-139.

(The reverse of this page is blank)

APPENDIX A

INPUT PARAMETERS FOR YOUNG'S EQUATION
(after Young, 1972)

Typical Soil Constants for Natural Earth Materials:

S	Material
0.2 - 1	Massive medium to high strength rock, with few fractures. Concrete, 14 MPa to 35 MPa, reinforced.
1 - 2	Frozen clay or silt, saturated, very hard. Rock, weathered, low strength, fractured. Sea or fresh water ice more than 3 m thick.
2 - 3	Massive gypsite deposits. Well-cemented coarse sand and gravel. Caliche, dry. Frozen moist silt or clay.
4 - 6	Sea or fresh water ice from 0.3 to 0.9 m thick. Medium dense, medium to coarse sand, no cementation, wet or dry. Hard, dry dense silt or clay. Desert alluvium.
8 - 12	Very loose, fine sand, excluding topsoil. Moist, stiff clay or silt, medium dense, with less than about 50% sand.
10 - 15	Moist topsoil, loose, with some clay or silt. Moist, medium dense, with some sand.
20 - 30	Loose, moist topsoil with humus material, mostly sand and silt. Moist to wet clay, soft, low shear strength.
40 - 50	Very loose, dry sandy topsoil. Saturated, very soft clay and silts with very low shear strengths and high plasticity. Wet lateritic clays.

Values of Scale Factor, K, for Different Penetrator Masses:

K	Penetrator Mass (kg)
0.30	0.91
0.35	2.27
0.44	4.54
0.62	9.07
0.76	13.61
0.86	18.14
0.94	22.68
1.00	27.22

Nose Performance Coefficient:

Nose Shape	Nose Caliber[1]	N
Flat	0.0	0.56
Hemisphere	0.5	0.65
Cone	1.0	0.82
Tangent Ogive	1.4	0.82
Tangent Ogive	2.0	0.92
Tangent Ogive	2.4	1.00
Inverse Ogive	2.0	1.03
Cone	2.0	1.08
Tangent Ogive	3.0	1.11
Tangent Ogive	3.5	1.19
Step Cone	3.0	1.28
Biconic	3.0	1.31
Inverse Ogive	3.0	1.32
Cone	3.0	1.33

[1] Ratio of nose length to diameter of nose base

APPENDIX B

CORIOLIS ACCELERATION

The angular velocity, ω, of the rotating platform is the rate of change with respect to time of the angle, θ, between any two radial lines on the platform. ω is defined by:

$$\omega = d\theta/dt \tag{B1}$$

The length of the circular arc traveled by any point on the rotating platform is

$$s = r\theta \tag{B2}$$

The angular velocity of the point on the platform is determined by:

$$ds/dt = rd\theta/dt = r\omega \tag{B3}$$

In a time, t, the point will travel the distance

$$s = r\omega t \tag{B4}$$

along a circular arc. An object moving radially within the plane of rotation will travel in time, t, a distance of

$$r = vt \tag{B5}$$

in the radial direction, while the point on the platform at distance r has traveled the distance s in the same time. Thus,

$$s = (vt)\omega t = \omega vt^2 \tag{B6}$$

This is frequently expressed in terms of the coriolis acceleration by

$$s = (1/2)a_c t^2 \tag{B7}$$

where

$$a_c = 2\omega v \tag{B8}$$

is defined as the coriolis acceleration.

APPENDIX C

PROJECTILE PENETRATION PARAMETERS

Penetration Parameters, Transitional Velocity Regime (after Baker, Westine and Dodge, 1973):

Variable	Symbol	Dimensions
Projectile caliber	s	L
Projectile length	l	L
Projectile nose radius	r	L
Projectile nose angle	α	---
Impact angle	β	---
Projectile density	δ_p	FT^2/L^4
Projectile velocity	v	L/T
Target thickness	h	L
Target density	δ_t	FT^2/L^4
Target temperature	θ_t	θ
Specific heat of target	c_t	$L^2/\theta T^2$
Heat of fusion of target	n_t	L^2/T^2
Ultimate stress of target	σ	F/L^2
Ultimate stress of projectile	S	F/L^2
Other stresses or strengths of target	σ_i	---
Other stresses or strengths of projectile	S_i	---
Strain	ε	---

APPENDIX D

COMPUTER PROGRAM FOR CALCULATING MOUNTING LOCATION OF FIRING ASSEMBLY

Definition of terms:

- R = Radius of centrifuge (feet)
- RO = Distance between center of rotation and end of gun barrel (feet)
- VO = Projectile velocity (feet per second)
- N = G-level
- W = Angular velocity
- A = Increment by which gun angle is increased in iterative process
- RO1 = Distance along radius between center of rotation and end of gun barrel (inches)
- EO1 = Perpendicular distance between centerline of rotor arm and end of gun barrel (inches)
- A2 = Gun angle (degrees)

Program Usage:

The program is intialized for the radius of the centrifuge (line 10), then run separately for each RO value (line 20) of interest. The increment of projectile velocity for which calculations will be performed is specified by the counter I in line 90. An initial projectile velocity VO is specified in line 100. The g-level increment for which calculations will be performed is specified by the counter N in line 110. The program incrementally increases the gun angle, A2, by the value of the increment A specified in line 140. Output consists of: G-level, projectile velocity (feet/second), omega, RO1 (inches), EO1 (inches), and A2 (degrees).

Program Listing:

```
 10 R = 6
 20 RO = 1
 30 LPRINT CHR$(15)
 40 LPRINT "RO = ";RO
 50 LPRINT "---------"
 60 LPRINT
 70 LPRINT "  G-LEVEL   VELOCITY   OMEGA   RO'   EO   ANGLE"
 80 LPRINT "            (FT/SEC)           (IN.)  (IN.) (DEG.)
 90 FOR I = 800 TO 1200 STEP 200
100 VO = I
110 FOR N = 20 TO 120 STEP 20
120 W = SQR(N*32.2/R)
130 A = .1
140 A = A+.001
150 VR = VO*COS(A)
160 VT = VO*SIN(A)
170 VC = W*RO
```

```
180  VB = W*R
190  VA = SQR((VC+VT)^2+VR^2)
200  X = VR/VA
210  A1 = 1.570796-ATN(X/SQR(1-X*X))
220  T = SQR((RO*VR)^2-(VO^2+VC^2+2*VC*VT)*(RO^2-R^2)
230  T = T-RO*VR
240  T = T/(VO^2+VC^2+2*VC*VT)
250  Y = ((RO+VR*T)/R)
260  C = 1.570796-ATN(Y/SQR(1-Y^2))
270  C1 = C-W*T
280  VAY = SIN(A1-C)*VA
290  CC = VAY-VB
300  IF A > 1 GOTO 450
310  IF CC < 0 GOTO 140
320  RO1 = COS(C1)*RO
330  EO1 = SIN(C1)*RO
340  A2 = A-C1
350  P = 180/3.141592654
360  A2 = A2*P
370  RO1 = RO1*12
380  EO1 = EO1*12
390  LPRINT TAB(6) N;
400  LPRINT TAB(19) VO;
410  LPRINT TAB(30) USING "##.###";W;
420  LPRINT TAB(42) USING "##.###";RO1;
430  LPRINT TAB(54) USING "##.###";EO1;
440  LPRINT TAB(66) USING "##.###";A2
450  NEXT N
460  NEXT I
470  LPRINT
500  END
```

APPENDIX E

STRUCTURAL CALCULATIONS FOR CENTRIFUGE TESTS

Structural calculations that were used to determine factors of safety for the centrifuge with the equipment additions and loads anticipated for the projectile penetration tests are shown in this appendix.

Assumptions:

1. G-level at any point on platform:

   a. Maximum g-level of 100 g's at sample bucket platform (1.83 m radial distance from rotor center);
   b. Gun assembly mounted at end of rotor arm platform closest to sample bucket platform (worst case condition).

2. Load of rotor arm platform:

   a. Masses of wiring and electrical connections ignored;
   b. Masses of illustrated components determined by electronic balance; mass of structural beam determined prior to drilling electrical connection holes (worst case condition).

3. Load of rack gear and bar assembly:

   Upper bound mass of components determined by electronic balance; final actual mass will be less following milling of slots and recesses.

4. Load of gun system:

   Upper bound mass of components determined by electronic balance; final actual mass will be less following shortening and smooth-boring of gun barrels.

5. Tension or compression stress on bolts:

   No additional assumptions.

6. Shear stress on bolts:

   No additional assumptions.

7. Strength of bolts:

   a. Minimum bolt diameter = 9.3 mm for nominal 9.5 mm diameter bolts; 9.1 mm diameter used for calculations (worst case condition);

b. Minimum bolt diameter = 6.1 mm for nominal 6.4 mm diameter bolts; 6.1 mm diameter used for calculations (worst case condition);
c. Shear resistance of bolts = 68.95 MPa (worst case condition);
d. Bearing resistance of bolts = 335.085 MPa (worst case condition);
e. Bearing resistance of aluminum = 68.95 MPa (worst case condition).

8. Shear stress on bolts in rack gears:

Shear resistance of bolts = 68.95 MPa (worst case condition).

9. Shear stress on bolts in cross bars:

Shear resistance of bolts = 68.95 MPa (worst case condition).

Masses of Components:

1. Rotor arm platform:

Item	Quantity	Mass (kg)
Top cover plate	1	5.443
Bottom cover plate	1	5.443
Cross beam	2	1.665
Side beam	4	0.921
Front beam	1	2.667

Total assembly mass = 20.567 kg

2. Rack gear and bar assembly:

Item	Quantity	Mass (kg)
Rack gear	2	0.989
Cross bar	4	0.313
Tie bar	3	1.433

Total assembly mass = 7.529 kg

3. Gun assembly:

Item	Quantity	Mass (kg)
Gun	1	1.597
Solenoid	1	0.408
Upper mounting plate	1	1.166
Lower mounting plate	1	4.128

Total assembly mass = 7.299 kg

Load and Factor of Safety Calculations:

1. G-level at any point in platform (Figure E.1):

$G_R = [(\omega^2 R)/g](g) = \omega^2 R$

At mounting surface: $R = 1.65\ m + 0.18\ m = 1.83\ m$

$G_R = 100g$

At any point r: $G_r = G_R(r/R) = (100g/1.83\ m)(r) = 54.64r$

$G_A = 54.64r_A = 54.64 \times 0.692\ m = \underline{37.8g}$

$G_B = 54.64r_B = 54.64 \times 0.984\ m = \underline{53.8g}$

$G_C = 54.64r_C = 54.64 \times 0.762\ m = \underline{41.6g}$

2. Load of rotor arm platform (Figure E.2):

$P_1 = MG_A = 20.567\ kg \times 37.8g \times .00980665$

$= 20.567\ kg \times 37.8 \times 9.80665(m/sec^2) \times 1\ kN/(1000kg \cdot m/sec^2)$

$= \underline{7.624\ kN}$

(note: $1\ g = 9.80665\ m/sec^2$)

3. Load of rack gear and bar assembly (Figure E.3):

$P_2 = MG_C = 7.529\ kg \times 41.6g \times .00980665$

$= \underline{3.072\ kN}$

4. Load of gun assembly (Figure E.4):

$P_3 = MG_B = 7.299\ kg \times 53.8g \times .00980665$

$= \underline{3.851\ kN}$

5. Tension or compression stress on bolts (Figure E.5):

$Moment_{(P2+P3)} = (P_2 + P_3)(e_1)$

$= (3.072\ kN + 3.851\ kN)(0.0254\ m) = \underline{0.176\ kN\text{-}m}$

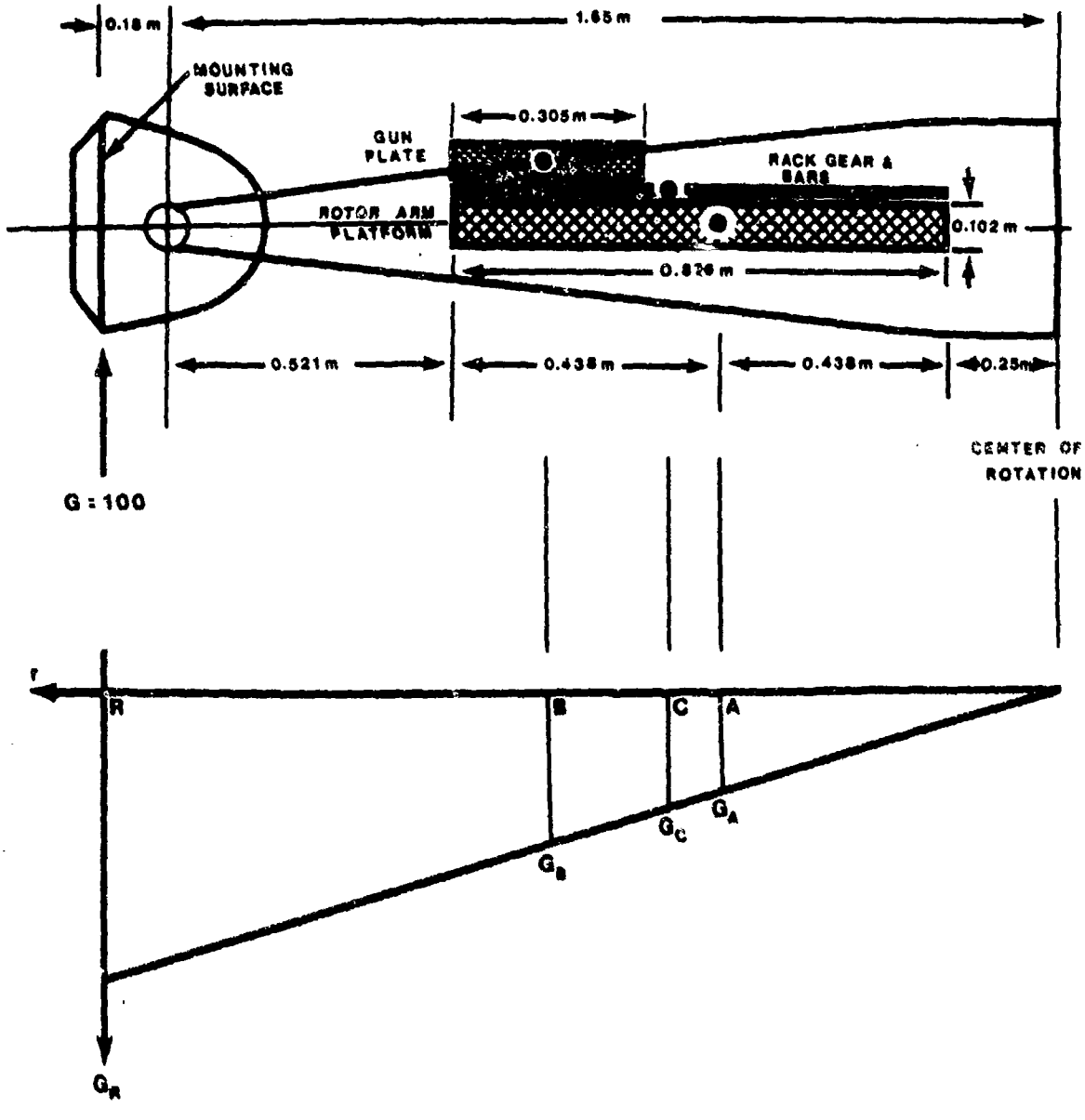

Figure E-1. G-Level At any Point on Platform

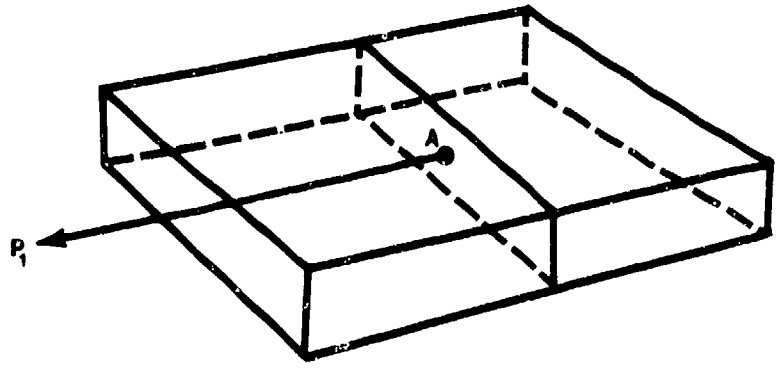

Figure E-2. Load of Rotor Arm Platform

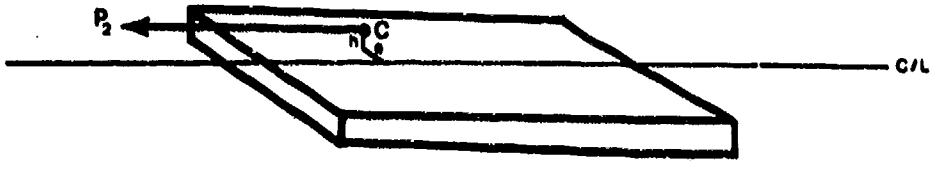

Figure E-3. Load of Rack Gear and Bar Assembly

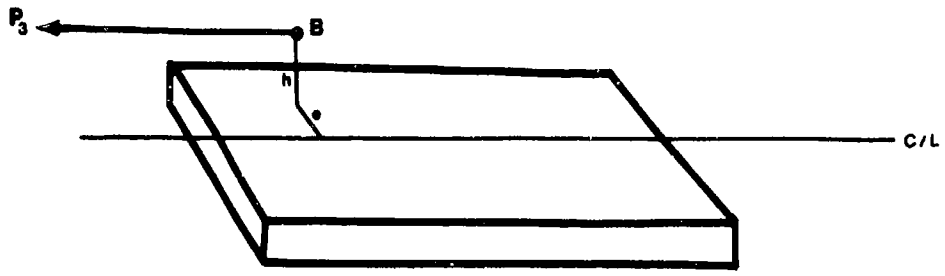

Figure E-4. Load of Gun Assembly

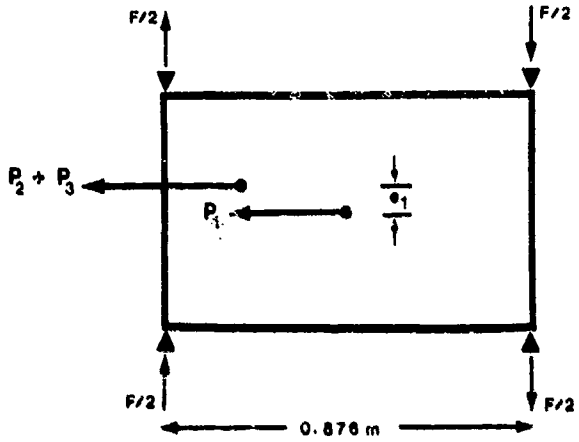

Figure E-5. Tension or Compression Stress on Bolts

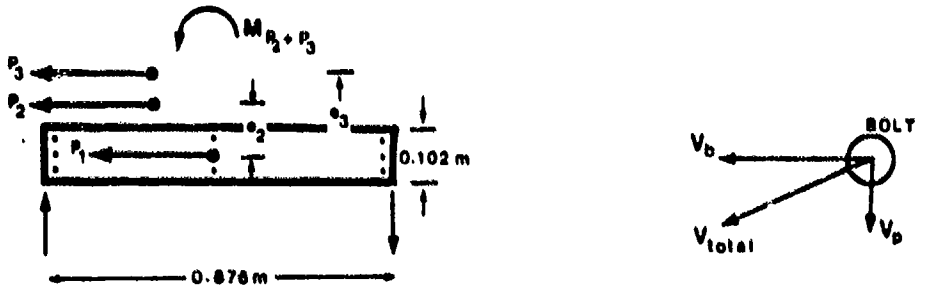

Figure E-6. Shear Stress on Bolts

$F = (0.176 \text{ kN-m})/(0.876 \text{ m}) = \underline{0.201 \text{ kN}}$

For each bolt (six each side): $F_i = F/6 = 0.201 \text{ kN}/6 = \underline{0.034 \text{ kN}}$

6. Shear stress on bolts (Figure E.6):

a) Shear stress due to moments

$\text{Moment}_{P2} = P_2(e_2) = (3.072 \text{ kN})(0.07 \text{ m})$

$= 0.215 \text{ kN-m}$

$\text{Moment}_{P3} = P_3(e_3) = (3.851 \text{ kN})(0.133 \text{ m})$

$= 0.512 \text{ kN-m}$

$\text{Moment}_{(P2+P3)} = M_2 + M_3 = 0.215 \text{ kN-m} + 0.512 \text{ kN-m}$

$= 0.727 \text{ kN-m}$

$V = 0.727 \text{ kN-m}/0.876 \text{ m} = 0.830 \text{ kN}$

$V_b = V/6 = 0.830 \text{ kN}/6 = \underline{0.138 \text{ kN}}$ (for each bolt)

b) Shear stress due to forces

$V_P = (P_1 + P_2 + P_3)/16 = (7.624 \text{ kN} + 3.072 \text{ kN} + 3.851 \text{ kN})/16$

$= 0.909 \text{ kN}$

$V_{total} = (V_P^2 + V_b^2)^{1/2} = ((0.909 \text{ kN})2 + (0.138 \text{ kN})2)1/2$

$= \underline{0.919 \text{ kN}}$

7. Strength of bolts:

a) Shear strength

$\text{Area} = \pi D^2/4 = \pi(6.1 \text{ mm})^2/4 = 29.2 \text{ mm}^2$

$[F_v] = 68.95 \text{ MPa}$

$V_{allow} = [F_v]A = (68.95 \text{ MPa})(29.2 \text{ mm}^2) = 2.013 \text{ kN}$

$F.S. = V_{allow}/V_{total} = (2.013 \text{ kN})/(0.919 \text{ kN}) = \underline{2.2}$

b) Bearing (on bolt)

$[F_b] = 335.085$ MPa

t = 4.57 mm; D = 9.14 mm

$V_{allow} = [Fb]tD = (335.085 \text{ MPa})(4.57 \text{ mm})(9.14 \text{ mm}) = 10.682$ kN

$F.S. = V_{allow}/V_{total} = (10.682 \text{ kN})/(0.919 \text{ kN}) = \underline{11.6}$

c) Bearing (on aluminum)

$[F_a] = 68.95$ MPa

$V_{allow} = [F_a]tD = (68.95 \text{ MPa})(4.57 \text{ mm})(6.1 \text{ mm}) = 1.922$ kN

$F.S. = V_{allow}/V_{total} = (1.922 \text{ kN})/(0.919 \text{ kN}) = \underline{2.1}$

8. Shear stress on bolts in rack gears:

(8) 6.4 mm diameter bolts to fix gear system

$A = \pi(6.1 \text{ mm})^2/4 = 29.2 \text{ mm}^2$

$P_{total} = P_2 + P_3 = 3.072 \text{ kN} + 3.851 \text{ kN} = 6.923$ kN

$V_i = P_{total}/8 = (6.923 \text{ kN})/8 = 0.865$ kN

$V_{allow} = [F_v]A = (68.95 \text{ MPa})(29.2 \text{ mm}^2) = 2.013$ kN

$F.S. = V_{allow}/V_i = (2.013 \text{ kN})/(0.865 \text{ kN}) = \underline{2.3}$

9. Shear stress on bolts in cross bars:

(9) 6.4 mm diameter bolts to fix gear system

$P_{total} = P_2 + P_3 = 6.923$ kN

$V_i = P_{total}/9 = (6.923 \text{ kN})/9 = 0.769$ kN

$V_{allow} = [F_v]A = (68.95 \text{ MPa})(29.2 \text{ mm}^2) = 2.013$ kN

$F.S. = V_{allow}/V_i = (2.013 \text{ kN})/(0.769 \text{ kN}) = \underline{2.6}$

APPENDIX F

Table F-1. PENETRATION TEST DATA - DRY SAND

Test No.	Proj. Mat'l[1]	Proj. Caliber	G Level	Depth (m)	Proj. Velocity[2] (m/s)	Soil Type[3]	Soil Density (Mg/m³)
1	B	22	41.4	.093	304.8	FL	1.61
2	A	22	59.4	.037	304.8	FL	1.62
3	A	22	59.4	.036	304.8	FL	1.63
4	B	30	59.8	.104	304.8	FL	1.62
5	B	44	71.8	.140	304.8	FL	1.62
6	B	30	20.2	.110	304.8	FL	1.63
7	B	30	40.0	.113	304.8	FL	1.61
8	B	30	52.9	.047	304.8	FL	1.83
9	B	44	23.9	.109	304.8	FL	1.83
10	B	44	82.1	.090	304.8	FL	1.82
11	B	44	71.8	.097	304.8	FL	1.83
12	B	35	63.5	.073	304.8	FL	1.83
13	B	30	75.5	.050	304.8	FL	1.83
14	B	35	62.6	.071	304.8	FL	1.83
15	B	30	47.9	.064	304.8	FL	1.83
16	B	22	61.2	.052	304.8	FL	1.83
17	B	44	34.0	.105	304.8	FL	1.83
18	B	44	34.0	.105	304.8	FL	1.84
19	B	30	34.6	.073	304.8	FL	1.83
20	B	22	46.6	.059	304.8	FL	1.82
21	B	35	28.9	.082	304.8	FL	1.82
22	B	22	28.2	.061	304.8	FL	1.82
23	B	22	15.6	.067	304.8	FL	1.84
24	B	35	28.9	.083	304.8	FL	1.82
25	B	35	76.4	.071	304.8	FL	1.82
26	B	44	53.9	.152	304.8	FL	1.61
27	B	30	85.6	.059	304.8	FL	1.83
28	B	44	38.5	.159	304.8	FL	1.61
29	B	22	80.5	.081	304.8	FL	1.63
30	B	22	75.0	.086	304.8	FL	1.62
31	B	35	42.9	.142	304.8	FL	1.61
32	B	44	81.5	.144	304.8	FL	1.61
33	B	30	53.9	.123	304.8	FL	1.60
34	B	44	17.2	.169	304.8	FL	1.62
35	B	22	24.9	.077	304.8	BS	1.61
36	B	44	53.9	.101	304.8	BS	1.59
37	B	44	78.8	.097	304.8	BS	1.61
38	B	22	64.3	.062	304.8	BS	1.60
39	B	22	24.9	.083	304.8	F58	1.64
40	B	44	53.9	.119	304.8	F58	1.64
41	B	44	37.2	.126	304.8	F58	1.66
42	B	44	81.5	.124	304.8	F58	1.64

Test No.	Proj. Mat'l[1]	Proj. Caliber	G Level	Depth (m)	Proj. Velocity[2] (m/s)	Soil Type[3]	Soil Density (Mg/m³)
43	A	44	50.5	.029	304.8	FL	1.85
44	B	44	34.4	.083	304.8	FL	1.83
45	B	44	29.7	.081	304.8	FL	1.83
46	B	30	42.4	.065	304.8	FL	1.82
47	B	30	48.6	.061	304.8	FL	1.82
48	A	30	32.0	.026	304.8	FL	1.83
49	A	44	22.9	.034	304.8	FL	1.82
50	A	44	50.5	.032	304.8	FL	1.83
51	N	44	31.1	.015	304.8	FL	1.83
52	B	44	37.7	.087	304.8	FL	1.83
53	B	30	52.3	.062	304.8	FL	1.82
54	A	44	44.0	.030	304.8	FL	1.83
55	P	44	42.7	.017	304.8	FL	1.83
56	N	44	45.8	.014	304.8	FL	1.83
57	A	44	33.8	.033	304.8	FL	1.83
58	B	30	48.6	.062	304.8	FL	1.83
59	P	30	40.3	.013	304.8	FL	1.83
60	B	30	42.3	.063	304.8	FL	1.83
61	N	44	45.9	.014	304.8	FL	1.83
62	B	30	1.0	.081	294.1	FL	1.83
63	B	30	1.0	.075	212.8	FL	1.83
64	B	35	1.0	.104	313.6	FL	1.83
65	B	35	1.0	.096	254.2	FL	1.83
66	B	35	1.0	.072	193.5	FL	1.83
67	B	44	1.0	.191	221.3	FL	1.62
68	B	44	1.0	.197	300.5	FL	1.62
69	B	44	1.0	.107	308.5	FL	1.83
70	B	44	1.0	.096	124.1	FL	1.83
71	B	44	1.0	.106	262.7	FL	1.83
72	B	44	1.0	.103	174.7	FL	1.83
73	B	44	1.0	.113	308.8	FL	1.83
74	B	44	1.0	.113	313.0	FL	1.83
75	N	22	1.0	.034	274.3	FL	1.62
76	N	22	1.0	.034	280.7	FL	1.62
77	N	22	1.0	.034	313.0	FL	1.62
78	N	30	1.0	.017	244.4	FL	1.83
79	N	30	1.0	.017	237.7	FL	1.83
80	N	44	1.0	.024	159.1	FL	1.83
81	N	44	1.0	.022	152.7	FL	1.83
82	P	22	1.0	.036	297.2	FL	1.62
83	P	22	1.0	.036	255.7	FL	1.62
84	P	30	1.0	.020	228.6	FL	1.83
85	P	44	1.0	.024	158.5	FL	1.83
86	P	44	1.0	.022	163.1	FL	1.82
87	A	22	1.0	.053	279.2	FL	1.62
88	A	22	1.0	.054	285.3	FL	1.62
89	A	22	1.0	.057	310.6	FL	1.62
90	A	30	1.0	.069	272.5	FL	1.62

Test No.	Proj. Mat'l[1]	Proj. Caliber	G Level	Depth (m)	Proj. Velocity[2] (m/s)	Soil Type[3]	Soil Density (Mg/m3)
91	A	30	1.0	.069	311.8	FL	1.63
92	A	30	1.0	.076	301.8	FL	1.61
93	A	30	1.0	.034	296.3	FL	1.83
94	A	30	1.0	.032	240.5	FL	1.83
95	A	30	1.0	.033	267.0	FL	1.83
96	A	30	1.0	.034	290.2	FL	1.83
97	A	30	1.0	.022	96.6	FL	1.83
98	A	44	1.0	.045	122.2	FL	1.83
99	A	44	1.0	.051	177.4	FL	1.83
100	A	44	1.0	.052	260.6	FL	1.83
101	A	44	1.0	.052	266.7	FL	1.83
102	A	44	1.0	.056	312.7	FL	1.83
103	A	44	1.0	.046	209.7	FL	1.83
104	A	44	1.0	.043	179.5	FL	1.82
105	A	44	1.0	.040	188.4	FL	1.83
106	A	44	1.0	.042	166.4	FL	1.83
107	A	44	1.0	.041	166.7	FL	1.83
108	A	44	1.0	.045	211.5	FL	1.83
109	A	44	1.0	.047	229.5	FL	1.83
110	A	44	1.0	.049	286.5	FL	1.83
111	A	44	1.0	.050	310.3	FL	1.83
112	B	22	1.0	.121	306.0	FL	1.62
113	B	22	1.0	.075	296.6	FL	1.83
114	B	22	1.0	.059	191.1	FL	1.83
115	B	22	1.0	.060	233.2	FL	1.83
116	B	22	1.0	.071	246.0	FL	1.83
117	B	22	1.0	.076	313.6	FL	1.83
118	B	30	1.0	.134	292.0	FL	1.62
119	B	30	1.0	.081	313.6	FL	1.83
120	B	44	46.0	.097	304.8	MX	1.94
121	B	44	27.6	.105	304.8	MX	1.94
122	B	44	64.4	.085	304.8	MX	1.94
123	B	44	92.0	.089	304.8	MX	1.94
124	B	44	18.4	.099	304.8	MX	1.94
125	B	44	55.2	.094	304.8	MX	1.94
126	B	44	73.6	.087	304.8	MX	1.94
127	B	44	36.8	.097	304.8	MX	1.94
128	B	44	64.4	.086	304.8	MX	1.94
131	B	44	1.0	.129	313.6	F58	1.70
135	B	44	18.4	.128	304.8	F58	1.70
137	B	44	73.6	.109	304.8	F58	1.70
139	B	44	55.2	.126	304.8	F58	1.70
140	B	44	36.8	.120	304.8	F58	1.71
141	B	44	92.0	.093	304.8	F58	1.69
144	B	44	73.6	.099	304.8	F58	1.70
148	B	44	36.7	.138	304.8	F58	1.66

Test No.	Proj. Mat'l[1]	Proj. Caliber	G Level	Depth (m)	Proj. Velocity[2] (m/s)	Soil Type[3]	Soil Density (Mg/m3)
149	B	44	1.0	.212	285.9	F58	1.63
151	B	44	34.4	.136	304.8	F58	1.63

[1] B = Brass; A = Aluminum; N = Nylon; P = PVC
[2] Velocities estimated for tests at g-levels greater than 1
[3] FL = Ottawa Flintshot sand; F58 = Ottawa F58 Sand; BS = Florida Beach Sand; MX = Soil Blend

Table F-2. PENETRATION TEST DATA[1] - MOIST SAND

Test No.	G Level	Depth (m)	Proj. Velocity[2] (m/s)	Soil Type[3]	Soil Dry Density (Mg/m3)	Moisture Condition[4]
129	1.0	.088	313.0	MX	1.94	S
130	1.0	.096	301.4	MX	1.94	PS
132	1.0	.112	271.6	F58	1.70	PS
133	1.0	.124	297.5	F58	1.71	PS
134	18.4	.128	304.8	F58	1.69	PS
136	73.6	.109	304.8	F58	1.72	PS
138	55.2	.126	304.8	F58	1.70	PS
142	1.0	.111	302.1	F58	1.70	PS
143	1.0	.122	308.8	F58	1.69	S
145	36.8	.106	304.8	F58	1.70	PS
146	36.8	.141	304.8	F58	1.70	S
147	36.1	.159	304.8	F58	1.66	S
150	1.0	.190	303.9	F58	1.63	S
152	35.3	.147	304.8	F58	1.63	S

---

1 All tests conducted using brass 44 caliber projectiles
2 Velocities estimated for tests at g-levels greater than one
3 MX = Soil Blend; F58 = Ottawa F58 sand
4 PS = partially saturated-includes all moisture conditions less than saturated, defined as follows; S = saturated implies to the extent saturation techniques used could achieve

(The reverse of this page is blank.)